

THESIS ON MECHANICAL AND INSTRUMENTAL ENGINEERING E38

**Investigation of the Fatigue Mechanics
Aspects of PM Hardmetals and Cermets**

FJODOR SERGEJEV

TUT

PRESS

TALLINN UNIVERSITY OF TECHNOLOGY
Faculty of Mechanical Engineering
Department of Materials Engineering

**Dissertation was accepted for the defence of Degree of Doctor of
Philosophy in Engineering on November 09, 2007**

Supervisor: Professor Jakob Kübarsepp, Faculty of Mechanical Engineering

Adviser: DSc Heinrich Klaasen, Faculty of Mechanical Engineering

Opponents: Professor Jorn Larsen-Basse, Program Director for Surface
Engineering and Material Design of National Science
Foundation (NSF), Arlington, Virginia, USA.

PhD Ants Lõhmus, University of Tartu, Estonia.

Defence of the thesis: December 27, 2007, at 11:00,
Lecture hall: V-215
Tallinn University of Technology
Ehitajate tee 5, Tallinn

Declaration:

Hereby I declare that this doctoral thesis, my original investigation and
achievement, submitted for the doctoral degree at Tallinn University of
Technology has not been submitted for any academic degree

Copyright: Fjodor Sergejev, 2007
ISSN 1406-4758
ISBN 978-9985-59-751-4
OÜ*INFOTRÜKK*

MASINA- JA APARAADIEHITUS E38

**Pulberkõvasulamite ja -kermiste
väsimusmehaanika aspektide uurimine**

FJODOR SERGEJEV

TTÜ

KIRJASTUS

Simplicity is the ultimate sophistication. *Saying by Leonardo Da Vinci* [1]

I have no special talents. I am only passionately curious. *Saying by Albert Einstein.* [1].

INTRODUCTION

Powder metallurgy materials - cemented carbides (mainly based on tungsten carbide or titanium carbide), also known as hardmetals, ceramic and powder composite materials, are most widely used as tool materials in machining and forming applications as well as materials for wear component because of their excellent hardness-ductility combination. These materials are related to so-called “structurally brittle” materials group.

Until now there is no complete understanding of the material behaviour under complex service conditions where cemented carbides with a heterogeneous structure are subjected to various types of loading and wear. These materials tend to contain natural structural defects: pores, non-metallic inclusions or inhomogeneties etc., and their existence is crucial for most mechanical properties and material selection. The above-mentioned imperfections facilitate fatigue crack initiation, reduce lifetime and decrease cyclic strength, especially at a high number of cycles. It is most difficult to define the number or size of defects due to their variety. Traditional fracture mechanics theories of the evaluation of the effect of defects are based on stress concentration factors and are applicable to defects larger than ~ 1 mm. However, as defect size decreases, these theories become invalid.

The problem of the fatigue strength estimation of wear resistant cemented carbides is of great importance from both a scientific and industrial point of view. Irreversible microscopic changes (micro-crack formation, phase transformation, phase boundary sliding, and pore nucleation during manufacturing and fatigue processes) occur, analogous to the irreversible sliding processes during the fatigue of ductile materials. In addition, different processes caused by crack closure, crack bridging, and friction of opposite crack surfaces have an influence on the fatigue crack growth. Various material parameters such as yield stress (σ_Y), ultimate tensile stress (σ_U), and hardness (HV, HRA or HB), may correlate with fatigue limit (σ_f) or threshold stress intensity factor range (ΔK_{th}).

The presented research is an attempt to enlarge the knowledge concerning time-dependent degradation of composites under alternating stresses and prediction of fatigue strength from limited data. The performance of some TiC-base cermets (prospective for metal forming) in cyclic loading conditions – fatigue, blanking of sheet metal – was analyzed and compared with that of a conventional WC-hardmetal, applicable in metal forming. The results of the mechanical properties (strength, plasticity), fatigue properties, blanking performance and microstructure of cemented carbides are presented.

ACKNOWLEDGEMENTS

I would like to express my deepest gratitude to my supervisor, DSc Jakob Kübarsepp, for his support, guidance and encouragement, who made this work possible. I appreciate his vast knowledge and skill in many areas (e.g., mechanical behaviour of materials, powder metallurgy, metal-forming, pedagogy, organization ability and etc.), and his assistance in writing articles and reports (i.e., grant proposals, scholarship applications and this thesis), which gave me on occasion more strength and generated greater interest for scientific work and teaching activities.

I am grateful for the suggestions, comments, encouragements and contributions from my colleagues and dear friends PhD Irina Preis, PhD Maksim Antonov and DSc Irina Hussainova. Only their enthusiasm and positive energy made it possible to conduct all needed experiments and tests on time, resulted in number of published articles and reports, presented in thesis.

I sincerely appreciate advices of DSc Heinrich Klaasen during scheduling of experiments and preparation of this thesis. His ideas concerning functional testing (blanking), adhesion wear, microstructural characterization (XRD) and wide experience in these fields are the main stimulating factors for conduction of such research.

Many thanks go to my colleagues DEng Jüri Pirso and PhD-student Lauri Kollo from Laboratory of Powder Metallurgy for the explanation of the principles of production technology of powder materials and help with sample preparation.

I also wish to extend my gratitude to PhD Renno Veinthal, PhD-students Mart Saarna and Priidu Peetsalu for their help during conduction of experiments. It was my pleasure of collaboration with senior research scientists Mart Viljus, Valdek Mikli and research scientist Rainer Traksmäa, from Centre of Material Research (TUT), who visualized my test results and allowed to show them to wide auditory.

I am deeply grateful to the staff of Tallinn University of Technology for their shared experience, fruitful and always enjoyable working atmosphere.

This work was supported by Estonian Science Foundation: grants no. 5882, 6163, 6660 and targeted financing project T505 (“Wear resistant materials and wear”). I would like to thank Archimedes Foundation, Doctoral School of “New production technologies and processes” and Tallinn University of Technology for funding and covering my travel and living costs abroad.

Finally, I would like to thank my wife, Natalja, for her love and for being incredibly responsive, supportive and most for all patient. My family and friends, thank you for constant direct and indirect support, persistence, understanding and encouragement at different stages of the present work.

I dedicate this work to my lovely daughter Aleksandra.

CONTENTS

INTRODUCTION	5
ACKNOWLEDGEMENTS	6
CONTENTS	7
LIST OF PUBLICATIONS	9
ABBREVIATIONS, TERMS AND SYMBOLS	11
1 REVIEW OF THE LITERATURE	13
1.1 Characterization of materials mechanical reliability	13
1.1.1 Fatigue testing	14
1.1.2 Fatigue performance prediction approaches	16
1.1.3 Correlation between fatigue properties and microstructure of cemented carbides	20
1.1.4 Fatigue properties of hardmetals and cermets	22
1.2 Fracture mechanics of cemented carbides	25
1.2.1 Fracture mechanics testing methods	25
1.2.2 Linear-elastic fracture mechanics (LEFM)	28
1.2.3 Other approaches	30
1.3 Correlation between fracture mechanics and microstructure	31
1.4 Aims of the study	31
2 EXPERIMENTAL PROGRAM	33
2.1 Materials and testing procedures	33
2.2 Fatigue testing	35
2.2.1 Conventional testing (3 PB)	35
2.2.2 Surface fatigue testing	36
2.3 Durability testing in blanking	37
2.4 Adhesive wear testing	37
2.5 Instrumented indentation testing	38
2.6 Structural-fractographical investigations	38
3 RESULTS AND DISCUSSION	39
3.1 Strength and fatigue properties	39
3.1.1 Weibull analysis	39
3.1.2 Statistical analysis	41

3.1.3 Fatigue strength prediction using Murakami method	42
3.1.4 Surface fatigue life prediction.....	44
3.2 Performance of carbide composites in sheet metal blanking.....	46
3.3 Indentation fracture toughness of carbide composites.....	47
3.4 Microstructural aspects of failure of carbide composites	48
3.4.1 Surface fatigue fractography	48
3.4.2 Fractographical peculiarities of fatigue failure in blanking	50
CONCLUSIONS	53
REFERENCES	55
LIST OF PUBLICATIONS OF AUTHOR	60
ABSTRACT	63
KOKKUVÕTE	65
PUBLICATIONS	67
Paper I.....	67
Paper II.....	73
Paper III	81
Paper IV	95
CURRICULUM VITAE.....	103
ELULOOKIRJELDUS	105

LIST OF PUBLICATIONS

The present dissertation is based on the following papers, which are referred in the text by their Roman numerals I-IV. As some of the recent research have not been published yet, this thesis was somewhat enlarged.

I. Kübarsepp, J., Klaasen, H. and Sergejev, F. Performance of cemented carbides in cyclic loading wear conditions. *Materials Science Forum*, 2007, Vols. 534-536, pp. 1221-1224.

II. Sergejev, F., Preis, I., Klaasen, H., Kübarsepp, J. Murakami approach: Fatigue strength prediction of cemented carbides by considering pores to be equivalent to small defects. *Proceedings of European Congress and Exhibition on Powder Metallurgy*. Prague, Czech Republic, 2005, pp. 335-340.

III. Sergejev, F., Antonov, M. Comparative study on indentation fracture toughness measurements of cemented carbides. *Proceedings of the Estonian Academy of Sciences, Engineering*, 2006, Vol. 12, pp. 388–398.

IV. Sergejev, F., Preis, I., Kübarsepp, J., Antonov, M. Correlation between surface fatigue and microstructural defects of cemented carbides. *Wear* (Article in press. Available online 15 June 2007).

Approbation

International conferences

1. 34th Leeds-Lyon Symposium on Tribology: Tribological contacts and component life. Material transformation, fatigue, crack initiation and propagation, Lyon, France, September 4-7, 2007.
2. ECerS – 10th International Conference of European Ceramic Society, Berlin, Germany, June 17-21, 2007.
3. Euro PM2006 - International Powder Metallurgy Congress and Exhibition, Hard Materials and Diamond Tooling, Ghent, Belgium, October 23-25, 2006.
4. The 15th International Baltic Conference “Engineering Materials & Tribology” BALTMATTRIB - 2006, Tallinn, Estonia, October 5-6, 2006.
5. 2006 POWDER METALLURGY World Congress and Exhibition, PM2006, Busan, Korea, September 24-28, 2006.
6. The 12th Nordic Symposium in Tribology, Nordtrib 2006, Helsingør, Denmark, June 7-9, 2006.
7. The 14th International Baltic Conference “Materials Engineering 2005”, Kaunas, Lithuania, October 6-7, 2005.
8. Euro PM2005 - International Powder Metallurgy Congress and Exhibition, Prague, Czech Republic, October 2-5, 2005.

Authors contribution

The list of publications that are not included into present work is added after references.

The author of this thesis took part in sample preparation routine, was responsible for carrying out of the experiments, collecting, processing and further analysis of experimental data (Paper I-XIV, XVI). The author also took part in discussion on the content (Paper I, XII-XVI) and have compiled several manuscripts (Paper II-V, VI-VIII, XIII). However the intellectual merit which is the result of the framework where the contribution of every author should not be underestimated.

ABBREVIATIONS, TERMS AND SYMBOLS

ASTM – American Standards for Materials Testing

CAD – Computer-Aided Design

CDM – Continuum Damage Mechanics

DIN – Deutsches Institut für Normung e.V. (the German Institute for Standardization)

FCG – Fatigue Crack Growth

FFM – Finite Fracture Mechanics

HIP – Hot Isostatic Pressing

HV – Vickers Hardness

IFT – Indentation Fracture Toughness

LEFM – Linear Elastic Fracture Mechanics

PM – Powder Metallurgy

SEM – Scanning Electron Microscope

Sinter/HIP – Hot Isostatic Pressure Sintering

TUT – Tallinn University of Technology

UH – Universal Hardness

XRD – X-ray Diffraction

$\sqrt{area_{max}}$ - maximum size of the defect area (Murakami's parameter)

ν - Poisson's ratio

$\Delta\sigma_f$ (ΔS_f) – fatigue sensitivity

σ_0 ($S_{b,0}$ or R_{TZ}) – normalized parameter of inert strength (scale parameter for monotonic loads Weibull statistics) or transverse rupture strength

σ_a (S_a) – applied stress amplitude

σ_e (S_e) – endurance limit

σ_f (S_f) – fatigue limit (fatigue strength at 10^7 cycles)

ΔK – stress-intensity-factor range, $\Delta K = K_{max} - K_{min}$

ΔK_{th} – threshold stress intensity factor range (fatigue-crack-growth threshold)

σ_m (S_m) – applied mean stress

σ_N (S_N) – fatigue strength at a specified life

σ_U (S_U) – tensile strength

$\sigma_w (S_w)$ – lower limit (lower bound) of fatigue strength
 $\sigma_Y (S_Y)$ – yield strength
 a – crack length
 C - carbide grains contiguity
 c – surface crack length (half-penny crack)
 d_g – average carbide grain size
 d_{WC} and d_{Co} - phase size, tungsten carbide and cobalt binder grains respectively
 E – elastic limit (Young's modulus)
 G – energy release rate
 G_{Ic} – critical energy release rate in plain strain
h.c.p. – hexagonal close packing
 K – stress-intensity factor
 k_f – fatigue notch factor
 K_{Ic} – plain-strain fracture toughness
 K_{max} and K_{min} – maximum and minimum stress-intensity factor respectively
 k_t – theoretical stress concentration factor (elastic stress concentration factor)
 m – Weibull modulus (shape parameters m_i and m_c – for monotonic and cyclic testing correspondingly)
 N – number of cycles/strokes
 N_f – fatigue life
 $N_{f,0}$ - mean cycle number to failure (scale parameter for cyclic loads of Weibull statistics)
 q – notch sensitivity factor
 R – stress ratio, $R = F_{min}/F_{max}$, if not specified differently in text
 R_{TZ} – transverse rupture strength
vol % - volumetric content
 V_{WC} and V_{Co} - phase volume fraction of carbide matrix and binder respectively
 w_f – fracture energy
wt % - content percent by weight
 γ_s – surface energy
 λ - binder mean free path

1 REVIEW OF THE LITERATURE

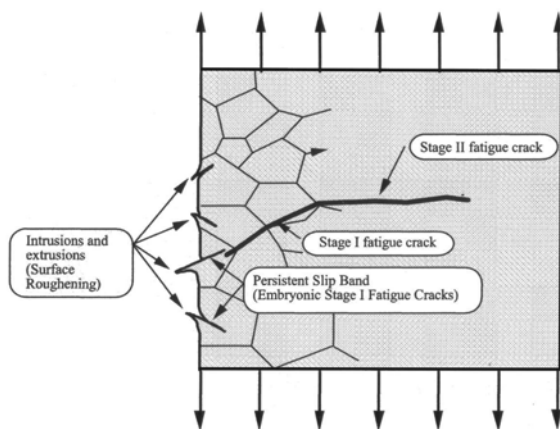
Fatigue testing procedures provide fatigue life prediction and design assurance, but they do not enable life improvement or design optimisation. Explanation of the causes and processes of fatigue can be given by fracture mechanics.

A classical fracture mechanics method disregards materials microstructural aspects as they are based on simplifications: crack itself, or the region where separation has occurred, is regarded as a smooth, continuous surface; the boundary between this surface and regions where separation has occurred, called the crack front, is regarded as a continuous line (generally crack front is a segment of a straight line, ellipse, or circle), and the crack is positioned on a flat plane [2-4]. On the other hand simplicity is the key to popularity of fracture mechanics.

However, for a complete understanding of fatigue fracture (fatigue mechanics), microstructural initiation and growth criteria must be defined and related to macroscopic models as there are some evidence that microstructure plays a major role in microscopic fracture [5-9]. Well known Murakami approach for prediction of the lower bound of the scatter in fatigue strength is the characteristic example of that phenomenon [10], will be discussed in next chapter.

1.1 Characterization of materials mechanical reliability

Fatigue is the progressive, localized, permanent structural change that occurs in materials subjected to fluctuating stresses and strains that may result in cracks or fracture after a sufficient number of fluctuations [11, 12]. In the first stage of the fatigue process the fatigue crack nucleation and crack initiation starts from



cyclic stress. Cyclic growth of the crack (crack propagation), caused by tensile stress and plastic strain, take place in the second stage, see Fig. 1. Finally, in the third stage, sudden fracture of the remaining cross section occurs. The final failure region will typically show evidence of plastic deformation produced just prior to final separation.

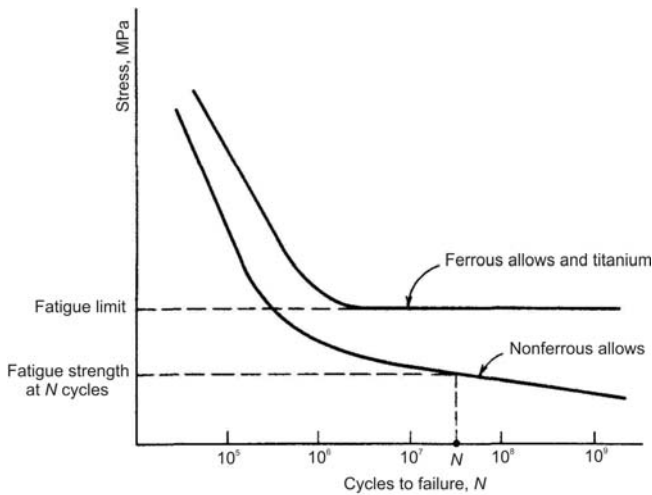
Figure 1. Process of fatigue crack initiation and growth [13].

Significant plastic strains occur during each cycle at high loads. Crack propagates quicker and low numbers of cycles are needed to produce fatigue

failure. Such cyclic behaviour is commonly referred to as *low-cycle fatigue* (LCF, from 1 up to about 10^4 cycles).

The *high-cycle fatigue* (HCF, from 10^4 up to 10^7 cycles) is associated with lower loads and high number of cycles to produce fatigue failure. Fatigue performance at greater number of loads (more than 10^7 cycles) is named *ultra high-cycle fatigue* (UHCF).

To characterize the failure response of nonferrous materials, and of ferrous alloys in the finite-life range, the term *fatigue strength at a specified life*, σ_N or S_N , is used. The term fatigue strength identifies the stress level at which failure will occur at the specified life, number of cycles N . The specification of *fatigue strength* without specifying the corresponding life is meaningless. The



specification of a *fatigue limit* σ_f (S_f) or *endurance limit* σ_e (S_e) always implies infinite life (an infinite number of cycles can be sustained without failure), see Fig. 2. Another term – *fatigue life*, N_f , is used to specify the number of cycles that specimen sustains before failure [12, 14].

Figure 2. Two types of materials responses to cyclic loading [13].

The nonferrous alloys do not exhibit an asymptote, and the curve of stress versus life continues to drop off indefinitely. For such alloys there is no fatigue limit, and failure as a result of cyclic load is only a matter of applying enough cycles. All materials, however, exhibit a relatively flat curve in the long-life range [14]. Observations of WC-Co hardmetal fatigue curves showed absence of any flat regions – the sign of obvious existence of a specific nature of fracture resulting from their production technology [15], see Figs. 6-8 (Chapter 1.1.2 Fatigue performance prediction approaches – S - N curves (Wöhler plots)).

1.1.1 Fatigue testing

Fatigue tests can be classified as crack initiation or crack propagation tests. In crack initiation testing, specimens or parts are subjected to the number of stress cycles required for a fatigue crack to initiate and to subsequently grow large enough to produce failure [11].

In crack propagation testing, fracture mechanics methods are used to determine the crack growth rates of preexisting cracks under cyclic loading.

This chapter will cover only crack initiation fatigue testing methods. Crack propagation testing methods are discussed in Chapter 1.2.1 Fracture mechanics testing methods.

The fatigue life of any specimen or structure is the number of stress (strain) cycles required to cause failure. This number is a function of many variables, including stress level, stress state, cyclic wave form, fatigue environment, and the metallurgical condition of the material.

Cemented carbides are mostly tested by bending (stress-life approach) [16, 17] and indentation techniques (fatigue crack growth approach) [18-20], because of the obvious difficulties in measuring and monitoring strain during testing, see Figs. 3 and 4.

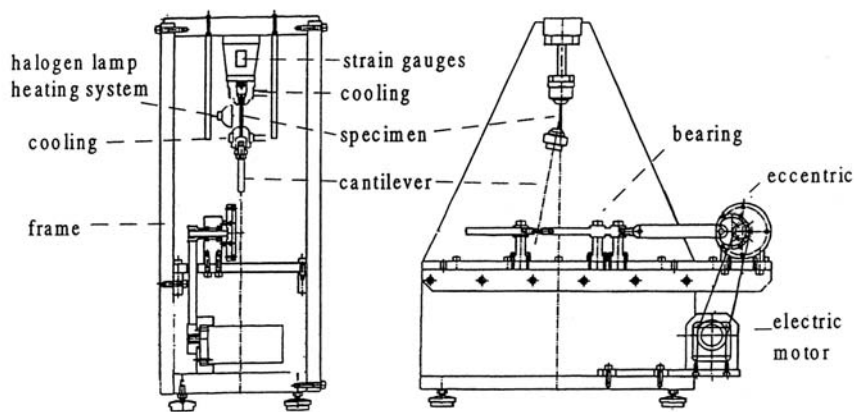


Figure 3. Schematic representation of the apparatus used to investigate the mechanical behaviour of the materials under monotonically increasing and cyclic loads at room temperatures in air [21].

Every approach has own advantages and disadvantages. Testing with 3-point bending (R3a, see Fig. 4) is very time consuming, costly and the scatter of results is undue wide. Four-point bending jig (R4b, see Fig. 4) give no improvement in data scatter. Notched bend testpieces (RN3a and RN4b, see Fig. 4) have several advantages, like: the scatter is considerably reduced; much lower loads required to break testpieces; the strength values obtained are more representative of the intrinsic material strength (because failures from large defects are excluded), but their preparation and notch geometry control is considerably complicated [19].

Indentation techniques are cheap, faster to perform, but less reliable. Residual stresses affect results very much. The magnitude and geometry of residual stress field cannot be always well understood and defined. Cracks emanating from indentation site can intersect and change their geometry, see Fig. 5 [18-20].

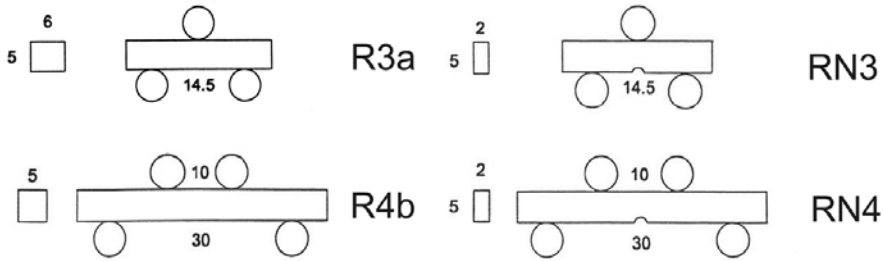


Figure 4. Different bending schemes according to ISO 3327 [17].

Minor changes in the specimen or test conditions can significantly affect fatigue behaviour, making analytical prediction of fatigue limit and life difficult [9].

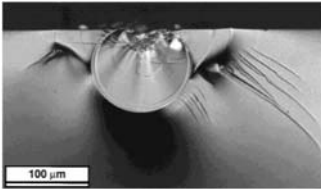


Figure 5. Optical micrograph showing a median crack in SLS glass that has undergone subcritical crack growth under the influence of the applied indentation stresses [18].

1.1.2 Fatigue performance prediction approaches

S-N curves (Wöhler plots)

Several probabilistic approaches can be used for fatigue life prediction and fatigue strength assurance. Oldest and best-known method is to display fatigue data on a plot of cyclic stress level versus number of cycles, or alternatively, on a log-log plot of stress versus life. These plots are called *S-N* curves or Wöhler plots, see Figs. 6 and 7.

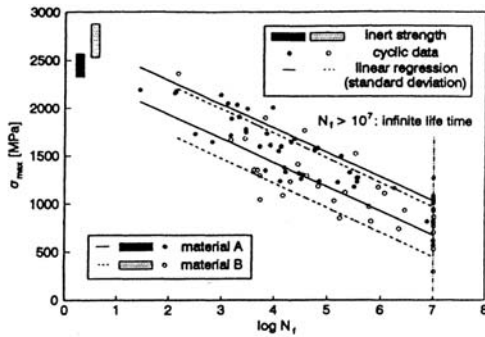


Figure 6. Fatigue ($R=0.1$) of WC-Co hardmetals at room temperature [21].

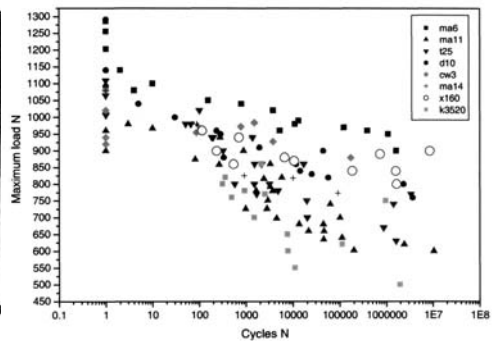


Figure 7. Fatigue ($R=0.1$) of notched test-pieces of various WC-Co hardmetals at room temperature [22].

Alternating stress amplitude σ_a or S_a , mean load σ_m or S_m and other loading characteristics can be plotted against number of cycles, but this do not change the principle of approach. Fatigue properties that can be defined from this data were discussed above. Another materials characteristic that can be derived from *S-N* plots is slope of the fatigue curve. Higher slopes indicate higher

accumulation of the damage during the cyclic loading. This lead to a new term determination - *fatigue sensitivity*, i.e. the intensity in the decrease of strength with an increase of loading cycles (the slope of the curve on an $S-N$ plot). Higher slopes are common for materials with high fatigue sensitivity and vice versa, lower slopes are the sign of lower fatigue sensitivity [Paper I, 23-25].

Stress concentration effect

Fatigue performance is very sensitive to stress concentration. Stress raiser such as a notch or hole significantly reduces fatigue strength. Stress concentration can also arise from surface roughness and metallurgical stress raisers: porosity; inclusions; local overheating during grinding; and decarburization. The effect of stress raisers on fatigue is generally studied by testing specimens containing a notch (usually a V-notch or U-notch, see Figs. 4 and 7) and comparing the $S-N$ curves of notched and unnotched specimens, see Fig. 8 [11, 26].

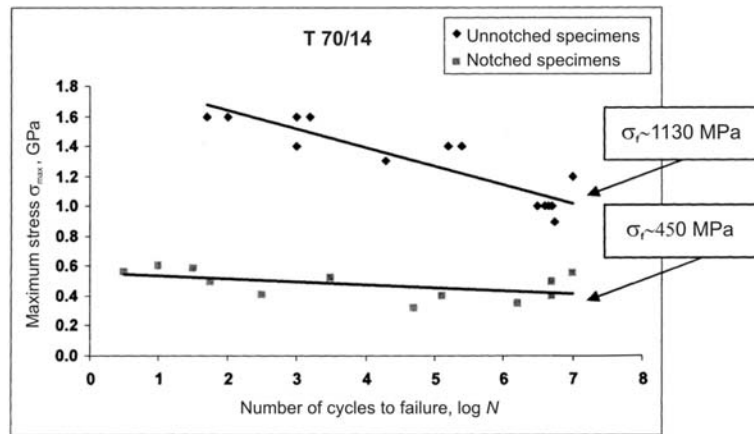


Figure 8. Fatigue strengths of TiC-Fe/Ni cermet (grade T70/14) without and with notches [27]

A useful concept in dealing with notch effect is the *notch sensitivity*, q .

$$q = \frac{k_f - 1}{k_t - 1}, \quad (1)$$

where k_f – fatigue notch factor, $k_f = \frac{\sigma_e}{S_e} = \frac{\sigma_f(Unnotched)}{\sigma_f(Notched)}$;

k_t – elastic stress concentration factor, $k_t = \frac{\sigma}{S} = \frac{\sigma_{max}}{\sigma_{nom}}$.

The value of q between 0 and 1 is a measure of how severely a given member is affected by a notch. If $q=1$, then $k_f=k_t$, material is entirely sensitive to notch, and not sensitive to notch then $k_f=1$ ($q=0$). Both factors k_f and k_t are dependent on notch and specimen geometry. For almost all cases $1 \leq k_f \leq k_t$. Most severe notch carries largest load (Bridgeman effect - local stress state limits shear stress, failure is due to cleavage, not slip) [26].

Mean stress effect

For design purposes, it is more useful to know how the mean stress affects the permissible alternating stress amplitude for a given number of cycles. This usually is accomplished by plotting the allowable stress amplitude for a specific number of cycles as a function of the associated mean stress – *normalized amplitude-mean diagram*, see Figs. 9-10 [11, 14, 28].

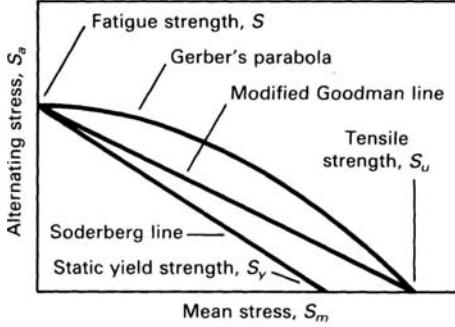


Figure 9. Effect of mean stress on the alternating stress amplitude [11]

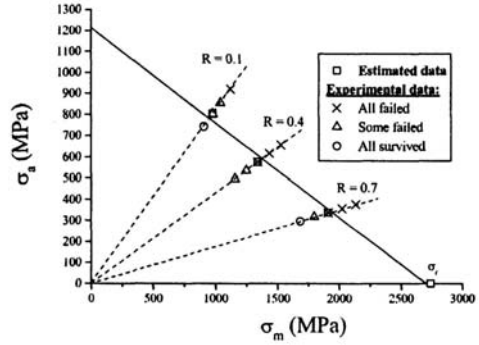


Figure 10. Description through a Goodman-like diagram of mean stress effect on the fatigue of the WC-10 wt % Co hardmetal [28].

Historically, the plot of mean stress has been the object of numerous empirical curve-fitting attempts. The most successful attempts have resulted in four different relationships, see Table 1 [14, 26].

Table 1. Mean stress diagrams curve-fitting equations

Model author	Equation	Designations	Nr.
Goodman's (linear)	$\frac{\sigma_a}{S_e} + \frac{\sigma_m}{S_U} = 1$	S_U – is the materials ultimate tensile strength.	(2)
Gerber's (parabolic)	$\frac{\sigma_a}{S_e} + \left(\frac{\sigma_m}{S_U}\right)^2 = 1$		(3)
Soderberg's (linear)	$\frac{\sigma_a}{S_e} + \frac{\sigma_m}{S_Y} = 1$	S_Y – is the yield strength	(4)
Morrow	$\frac{\sigma_a}{S_e} + \frac{\sigma_m}{\sigma_f} = 1$	σ_f – is the true fracture strength	(5)

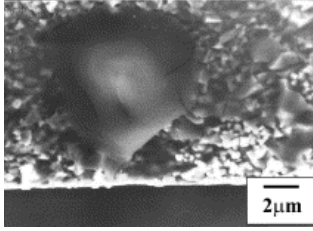
Combined effect of notches and mean stress for a brittle materials during cyclic loading ($\sigma_m \neq 0$) can be estimated by the modified Goodman expression, Eq. 2, to obtain an equivalent completely reversed value for the stress σ at the notch

$$S_e = \frac{k_t S_a}{1 - \frac{k_t S_m}{\sigma_U}}, \quad (6)$$

where $\sigma_a = k_t S_a$ and $\sigma_m = k_t S_m$ - are the stresses at the notch.

Effect of small defects and nonmetallic inclusions

Ceramics and metals in the form used for engineering applications are composed of crystalline grains that are separated by grain boundaries and binder phase. Even within grains the crystals are not perfect, with defects occurring, that have large effects on mechanical behaviour [5, 6, 26]. Besides, presence of the intrinsic structural defects, which act as stress concentrators and crack nuclei (see Fig. 11), are essential for powder metallurgy materials [29].



Summarising these facts the correct definition of a fatigue limit – is the threshold stress for crack propagation and not the critical stress for crack initiation. This definition and a novel quantitative method for inclusion rating and correlations with the fatigue limit were introduced by Yukioka Murakami [10].

Figure 11. SEM micrograph of a subsurface pore discerned as the failure origin of a sample subjected to cyclic loading [28].

He assumed that fatigue strength could be assessed from an evaluation of the square root of the projected area of the largest defect - parameter designated $\sqrt{area_{max}}$, on a plane perpendicular to the maximum principal stress direction. This parameter, contained in a definite volume, can be evaluated using the statistics of extremes of the defects (inclusions) distribution. By applying the method, materials can be classified according to the expected maximum size of the defect (inclusion), namely $\sqrt{area_{max}}$ and accordingly, a prediction of the lower bound of fatigue limit, σ_w , can be made [10]:

$$\sigma_w = \frac{1.43(HV + 120)}{(\sqrt{area_{max}})^{1/6}}. \quad (7)$$

Prediction of the threshold stress intensity factor range, ΔK_{th} , can be made according to

$$\Delta K_{th} = C_1(HV + C_2)(\sqrt{area_{max}})^{1/3}, \quad (8)$$

where C_1 – material independent constant, $C_1=3.3 \times 10^{-3}$;
 C_2 – material independent constant, $C_2=120$.

Theoretically, in the case of $\sqrt{area_{max}} = 0$, then accordingly $\sigma_w = \infty$. However, this never occurs because cracks nucleate along slip bands or grain boundaries as a result of reversed slip in grains, and the fatigue limit of the defect free specimens, σ_w , is finite. Therefore, if the value of σ_w is known in advance, then the size of small defects (non-propagating cracks) can be determined using Eq. 8. Prediction equations 7 and 8 are applicable for defects smaller than 1000 μm , and materials with Vickers hardness number lower than 400 approximately.

1.1.3 Correlation between fatigue properties and microstructure of cemented carbides

The microstructure of hardmetal is commonly characterized by three parameters: the phase volume fraction of carbide matrix (V_{WC}) and binder (V_{Co}); the phase size (d_{WC} and d_{Co} , respectively) and the degree of contact of the individual carbide grains (contiguity, C). All three parameters can be interrelated by theoretical equation [7, 30]

$$d_{Co} = \frac{1}{1-C} \cdot d_{WC} \cdot \frac{V_{Co}}{V_{WC}} \quad (9)$$

There is a thin layer of binder surrounding carbide grains and affecting such properties like, plasticity and ductility [6, 24]. If binder phase is brittle then a good possibility of continuous crack propagation exist [6]. Dependence of WC-Co hardmetal mechanical properties (Vickers hardness - HV and fracture toughness - K_{Ic}) from cobalt binder content and tungsten carbide grain size are shown in Fig. 12 [9].

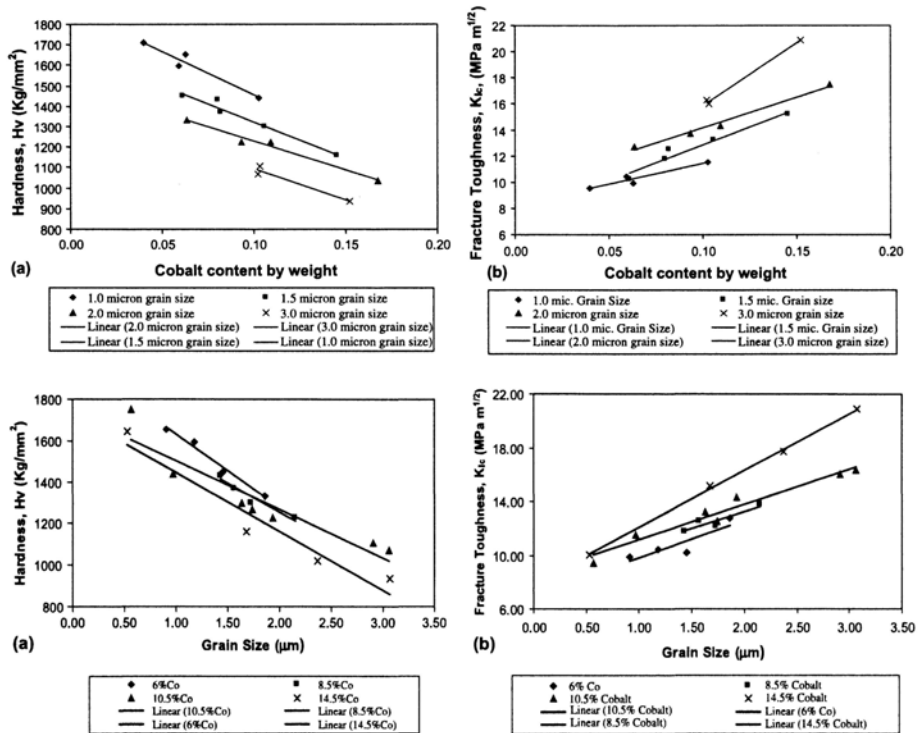
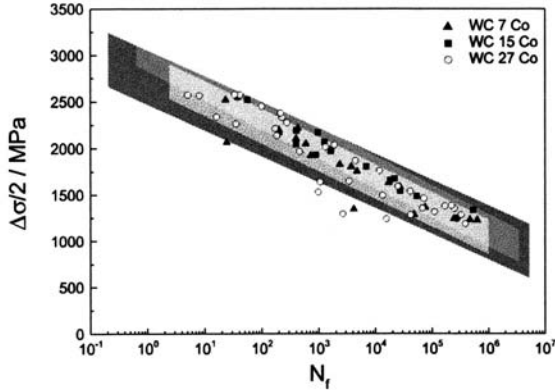


Figure 12. Hardness and fracture toughness as functions of cobalt content and WC grain sizes [9].

The hardness of hardmetals decreases with increase of cobalt binder content (wt %) and WC-grain size (d_{WC}). The effect for fracture toughness is opposite. However, fatigue properties for WC-Co hardmetals with different Co-binder phase content are almost the same, Fig 13. There is an increase in inert strength

for 15 wt % Co, but further enlargement of binder content to 27 wt % Co causes drop of the inert strength.

A decreasing width of the scatter band could be observed with increasing binder content as the overall nature of the compound becomes more metallic. Lower



inert strength can be explained by the loss of rigidity of the material (27 wt % Co), as the hard phase contiguity is no longer given [31]. L. Llanes et al. come over same effect. With decrease of WC carbide grains contiguity C (increase of binder mean free path λ_{Co}) transition from ceramic-like to metallic-like FCG behaviour occurs [31].

Figure 13. Wöhler plots for the WC-Co hardmetals [32].

Examples of typical dislocation configuration in WC grains of WC-Co are shown in Fig. 14. These observations contribute towards an explanation for the ability of WC-Co composite to sustain considerable plastic deformation [7].

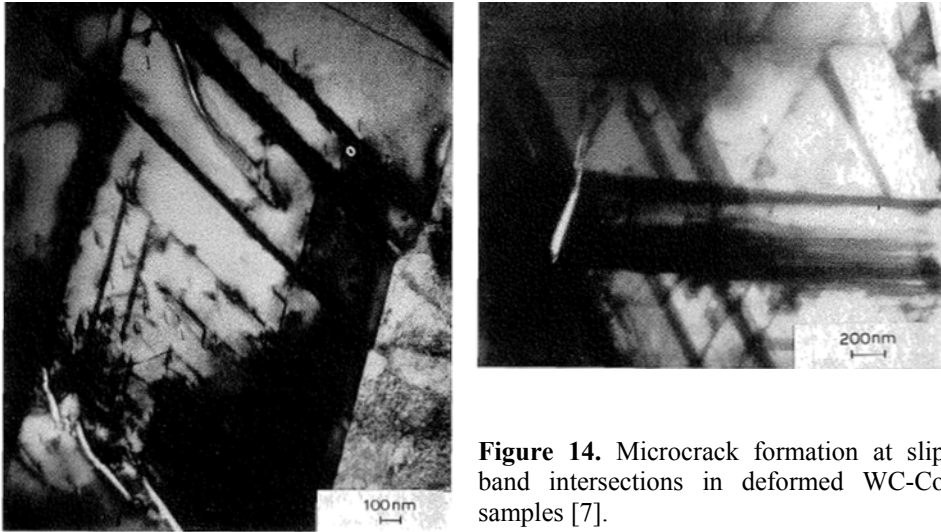
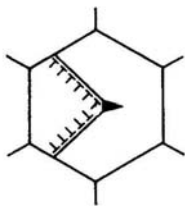


Figure 14. Microcrack formation at slip band intersections in deformed WC-Co samples [7].



This evidence is in a good agreement with crack initiation model proposed by A. H. Cottrell in 1957, see Fig. 15. A crack nucleus is produced by meeting of dislocations in intersecting slip planes [8].

Figure 15. Selected schematic representation of the formation of crack nuclei [8].

The influence of binder content on the fatigue behaviour of WC-Co hardmetals is negligible due to the localization of damage in shear bands in the binder pools and the facilitated crack propagation in the transformed h.c.p.-binder phase or along stacking faults [33].

Where is no yet complete understanding of the influence of the binder content and the grain size of the carbide phase on fatigue properties of TiC-based cermets.

1.1.4 Fatigue properties of hardmetals and cermets

For decades WC-based hardmetals were the ultimate and only well-known material from cemented carbides family. The main mechanical properties and fracture behavior for this group of material are studied by number of brilliant scientists. Their work gives us an opportunity to select hardmetal for needed application with desired properties from very wide range, starting with „classical“ WC-Co (H80T – H03T, from 72.0 up to 96.7 wt% WC), and ending with WC-TiC-TaC-Co (RP10 – RM20), WC-TiC-C-Co (S26T – U20T) and „exotic“ WC-Ni/Cr (TCR30 – TCR10), see Table 2.

Cermets or TiC-based cemented carbides are developing less actively. Only few grades (TiC-Ni/Mo) are investigated enough to be published in engineers and designers handbooks, see Table 3.

Table 2. Fatigue properties and composition of WC-based cemented carbides

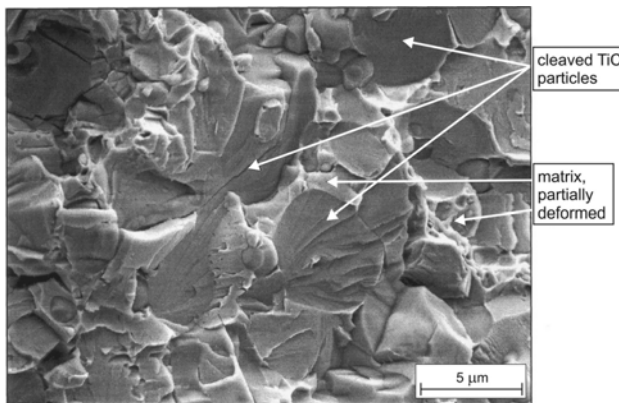
Grade	Composition		Inert bending strength $S_{b,0}$ or R_{TZ} , MPa	Endurance limit S_e , $5 \cdot 10^6$ or 10^7 , MPa	Stress ratio R	Fracture toughness K_{Ic} , MPa·m ^{1/2}	Ref.
	Hard phase, wt%	Binder, wt%					
H4	96.0 WC	4 Co	1400	1050	0.1		[34]
H6	94.0 WC	6 Co	1470	1160			
H8	92.0 WC	8 Co	1510	1210			
Hard metal A	86.5 WC+2.5 TiC+5.0 (Ta,Nb)C	6 Co	2498	960	-1.0		[35]
Hard metal B	82.5 WC+2.0 TiC+3.5 (Ta,Nb)C	12 Co	2734	900			
Hard metal C	86.5 WC+2.5 TiC+5.0 (Ta,Nb)C	4 Co+2 Ni	2547	615			
Cermet A	19.0 WC+30.0 Ti(C,N)+14.0 (Ta,Nb)C+13.0 TiN	10 Co+6 Ni+8 Mo ₂ C	1835	850			
	93.0 WC	7.0 Co	2840	1200	-1.0		[32]
	85.0 WC	15.0 Co	3178	1300			
	73.0 WC	27.0 Co	2887	1170			
	93.0 WC	7.0 CoNiFe	2859	1480			
	85.0 WC	15.0 CoNiFe	3122	980			
	73.0 WC	27.0 CoNiFe	2529	770			
10M	90.0 WC	10.0 Co	2742	1827	0.1	10.4	[28]
				1783	0.4		
				2112	0.7		
RB10	90.0 WC	10.0 Co	2952-3255	2214-2441	0.1	13.4-14.7	[36]
B50T	85.0 WC	15.0 Co	2476-2730	1857-2047		16.2-17.9	
H70T	76.0 WC	24.0 Co	2761-3045	2071-2283		19.1-21.0	
Grade 44	90.0 WC	10.0 Co	4100	1800	-1.0		[25]
Grade 54	90.0 WC	10.0 FeCo	1450	1000			
Grade 57	87.5 WC	12.5 FeCoNi	2800	1800			
Grade 61	90.0 WC	10.0 FeNi	2550	1800			
Grade 62	75.0 WC	25.0 Co	3200	900			
Grade 64	97.0 WC	3.0 Co	2300	1100			

Table 3. Fatigue properties and composition of TiC-based cemented carbides

Grade	Composition		Inert bending strength $S_{b,0}$ or R_{TZ} , (MPa)	Endurance limit S_e $5 \cdot 10^6$ or 10^7 , (MPa)	Stress ratio R	Fracture toughness K_{Ic} , MPa·m ^{1/2}	Ref.
	Hard phase, wt%	Binder, wt%					
RP01	80 TiC	10 Ni+10 Mo	1142-1260	857-945	0.1	8.6-9.5	[36]
P01/P10	80 TiC	8 Ni+12 Mo ₂ C	1181-1302	1248-1376		10.5-11.6	
T30	70 TiC	20 Ni+10 Mo	1600	510	0.1	9.5	[33]

1.2 Fracture mechanics of cemented carbides

Fracture mechanics is a method for predicting failure of structure containing a crack or defect, which depends on experiments and observations to suggest useful representations of the forces that cause the development and extension of cracks from present defect [2, 37, 38]. Fracture mechanics analysis effectively correlates the macroscopic aspects of crack initiation and growth without developing microscopic models for the local fracture processes that depend on the nature of the materials microstructure and the local crack tip stress and deformation history [39].



Micro-fracture mechanics requires a microscopic model for a given fracture mode that designates a local failure criterion and main microstructural characteristics, like grain size, phase and defects distribution, binder free path (binder thickness) [31], carbide contiguity [30, 31, 40], etc.

Figure 16. Fracture surface of Ferro-Titanit (grade WFN), soft annealed [39].

Microstructural failure modes for fatigue (ductile striations, ductile decohesion, brittle cleavage, microvoid and intergranular processes, mixed modes), see Fig. 16, are generally described as microstructurally insensitive [28].

1.2.1 Fracture mechanics testing methods

Fracture mechanics methods are used for crack propagation testing and determination of the crack propagation rates. Fracture toughness is the merit to specify preexisting crack growth resistance for materials.

Similar to fatigue testing there are two main approaches: testing using notched specimens [3, 4, 41], and indentation fracture toughness techniques [42-44].

Various specimen geometries are used (shown in Fig. 17). Crack growth tests are most commonly conducted using zero-to-tension loading, $R=0$, or tension-to-tension loading with a small R value, such as $R=0.1$ [3].

Chevron-notched specimens are the most advanced as they were originally used for determining the fracture toughness of brittle materials, materials unavailable in large scales and materials that are difficult to precrack [41].

Results of crack growth and crack propagation rates testing can be presented in a form of crack length a versus number of cycles N plot, or fatigue crack growth (FCG) rate da/dN against stress intensity range ΔK factor curve.

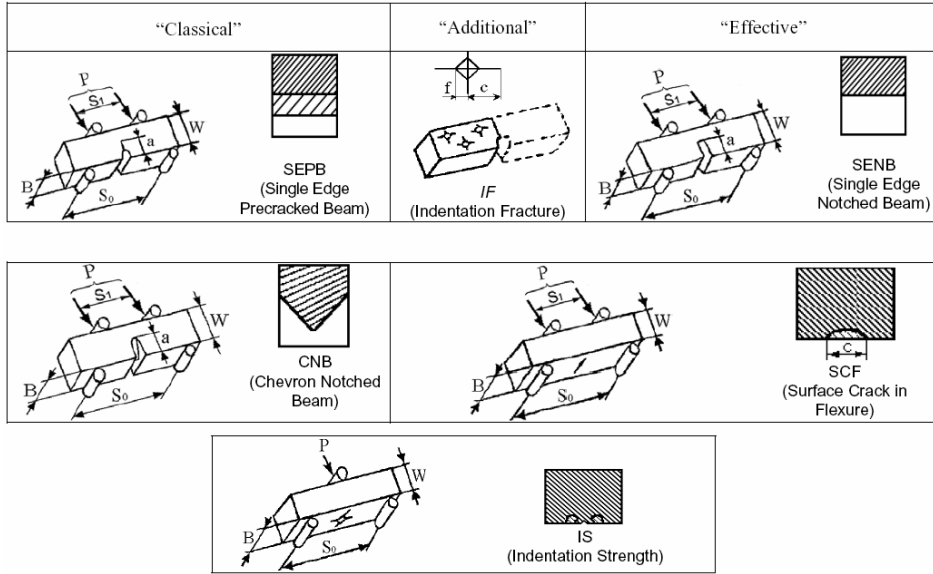
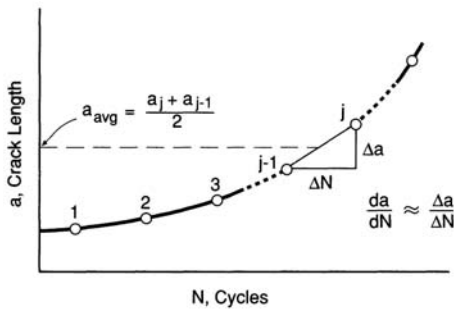


Figure 17. Methods used most often for testing the crack resistance of ceramics [45].



Before starting the test, a precracking must be made. The progress of the crack is recorded as the crack length extension during cyclic loading as shown in Fig. 18.

Figure 18. Crack growth rates obtained from adjacent pairs of a versus N data points [4].

Fatigue crack growth rate plot of WC-10 wt % Co investigated by Y. Torres et al. is presented in Fig. 19. The corresponding stress intensity range values are calculated from the average crack length (a_{avg}) during the interval of loading by

$$\Delta K_j = F \cdot \Delta S \sqrt{\pi a_{avg}} \quad (10)$$

where ΔS – is the stress range;

F – is the function that takes in account the geometry of specimen and notch.

As it is already known for WC-Co hardmetals [44], there is a very large power-law dependence of crack growth rates on ΔK (and K_{max}). This dependence can be quantified by a modified Paris-Erdogan growth relationship of type

$$\frac{da}{dN} = C(K_{max})^m (\Delta K)^n, \quad (11)$$

where C , m and n are constants.

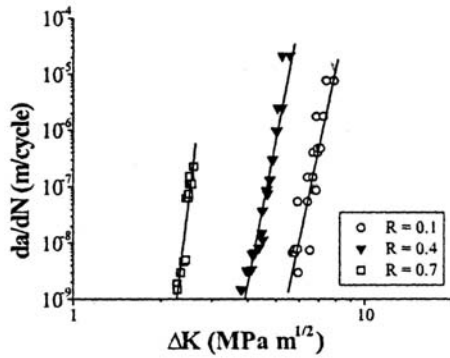
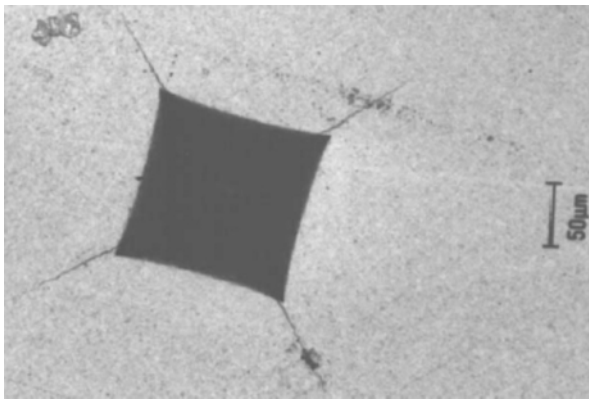


Figure 19. FCG rate as a function of ΔK [44].

More simple technique of Indentation Fracture Toughness (IFT) testing was developed for characterisation of brittle materials, such as glasses and ceramics, using Vickers, Knoop and Berkovich indenters. There is no need to use the specimens with special geometry.



Length of the cracks emanated from the corners of the imprint, as shown in Fig. 20, diagonals of the indentation mark, applied indentation load and main materials mechanical properties (hardness, Young's modulus) must be known to calculate crack growth resistance of tested material.

Figure 20. Optical micrographs of Vickers indentation and induced surface radial cracking in the WC-10 wt % Co [46].

On the basis of the Hill's solution for the expanding spherical cavity problems and an equilibrium relation between the radius of the half-penny crack (c) and a residual crack-opening point force due to the indentation plastic zone the major relationship for estimating or measuring fracture toughness K_c from indentation crack-length data was proposed

$$K_c = \delta \left(\frac{E}{H} \right)^{1/2} \frac{P}{c^{3/2}} \quad (12)$$

where E – is the Young's modulus;

H – is the hardness;

P – is the indentation load;

δ – is the constant dependent only on the geometry of the indenter.

The complexity of the stress field associated with such indentation has let to the emergence of the large number of equations for calculation of IFT of brittle solids [42, 43, Paper III]. It is very difficult to indicate the accuracy associated with the evaluation of IFT because of the existence of a large number of equations, the possibility of encountering different types of crack, and influence of material and testing procedures [44, 47].

1.2.2 Linear-elastic fracture mechanics (LEFM)

For a very sharp crack, presented in an infinitely wide plate that is externally loaded, Inglis [48] first showed that the load is locally amplified by the flaw and depends on the curvature radius of the crack tip, ρ . By approximating ρ to be of the order of the atomic radius, the remote stress at failure σ_f can be found as [3, 4]

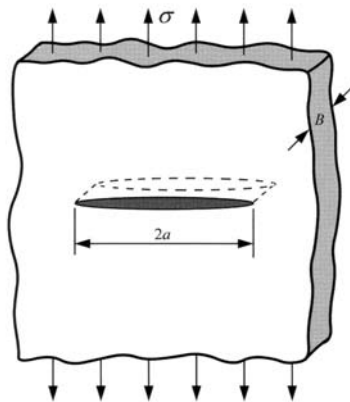
$$\sigma_f = \sqrt{\frac{E\gamma_s}{4a}}, \quad (13)$$

where E – is the Young's modulus;
 γ_s – is the surface energy;
 a – is the half-crack length.

Later Griffith (1920s) [38] proposed his famous energy approach to provide explanation for the fracture initiated by a crack.

Energy balance approach

Using a global energy balance that is based on the first law of thermodynamics, Griffith showed that fracture occurs spontaneously if the energy stored in the structure per unit area of crack advance dA (crack area is equal to $A=2aB$)



exceeds the energy needed to create two new surfaces (the surface energy of the material); and Griffith derived the following expression for the fracture stress σ_f of a semi-infinite two-dimensional plate containing a single side crack perpendicular to the applied stress, see Fig. 21

$$\sigma_f = \sqrt{\frac{2E\gamma_s}{\pi a}}. \quad (14)$$

The Griffith's model is not sensitive to the crack tip curvature radius in an ideally brittle solid [49].

Figure 21. A through-thickness crack in an infinitely wide plate subjected to a remote tensile stress [4].

For solving engineering problems, Irwin [50] proposed the concept of the *energy release rate* G , which is a measure of the energy available for the extension of a unit area of the crack and is defined as the rate of change in elastic potential energy with crack area

$$G = -\frac{d\Pi}{dA}, \quad (15)$$

where Π - is the potential energy of the system, $\Pi = U - F$;
 U - is the strain energy stored in the elastic body;
 F - is the work done by external forces.

For crack showed in Fig. 21, crack extension (fracture) occurs when G reaches a critical value G_c , then the energy release rate or crack driving force and fracture stress can be found as

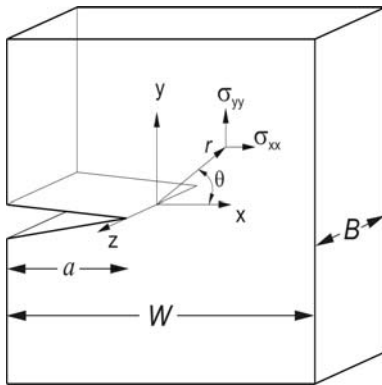
$$G = \frac{\pi\sigma^2 a}{E} = 2w_f = G_c \quad \text{and} \quad \sigma_f = \sqrt{\frac{G_c E}{\pi a}}, \quad (16)$$

where w_f – is the fracture energy, which could include plastic, viscoelastic, or viscoplastic effect, depending on the material.

For ideally brittle material $w_f = \gamma_s$ [4].

Stress approach

In parallel, Westergaard [51], Irwin, Sneddon [52] and Williams [53], derived closed-form expressions for the stresses (stress tensor - σ_{ij}) in a linear elastic cracked body subjected to external forces (see Fig. 22):



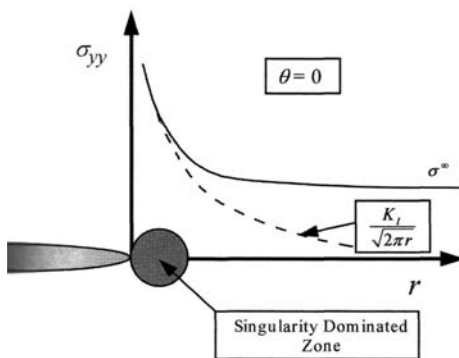
$$\sigma_{ij} = \left(\frac{k}{\sqrt{r}} \right) f_{ij}(\theta), \quad (17)$$

where k – is the constant;
 $f_{ij}(\theta)$ – are the dimensionless angular functions that vary for the different loading modes;
 (r, θ) – are polar coordinates.

Figure 22. Edge crack in a plate subjected to a tensile stress [49].

The major simplification of Eq. 18 is the universal nature of asymptotic stress and displacement fields around the crack tip in linear elastic solid. The dependence in $r^{-1/2}$ is schematically illustrated in Figure 23 for the σ_{yy} stress field component.

The constant k can be replaced by *stress intensity factor* K ($K = k\sqrt{2\pi}$). The



stress intensity factor is usually given with subscript to denote the mode of loading, i.e., K_I , K_{II} , or K_{III} [4]. For any loading mode and cracked body geometry, K defines the crack tip stress intensity by relating the local component of the stress tensor to the applied stress and crack size as

$$\sigma_{ij} = \frac{K}{\sqrt{2\pi r}} f_{ij}(\theta). \quad (18)$$

Figure 23. Stress normal to the crack plane in Mode I [4].

Stress intensity factor K depends linearly on the applied external load σ , on the length of the crack a , and on the geometry of the crack and of the component, and can be expressed by:

$$K = \sigma \sqrt{\pi a} \cdot Y(a/W), \quad (19)$$

where Y – is a dimensionless constant of the relative crack length a/W (W being the distance from the load line to the back-side of the specimen) and depends on the geometry and mode of loading.

The energy release rate and stress intensity factor can be related by combining Eq. 16 and Eq. 19, factor Y is omitted for clarity:

$$G = \frac{K_I^2}{E'}, \quad (20)$$

where $E' = E$ for plane stress, and $E' = \frac{E}{1-\nu^2}$ for plane strain;

ν - is the Poisson's ratio.

As for G , there exists also a critical value of stress intensity factor, K_c , at which crack extension occurs, and can be calculated by

$$K_c = \sqrt{G_c E'} = \sqrt{2\gamma_s E'}. \quad (21)$$

At certain conditions both quantities are a measure of the material toughness, and are independent of specimen size and geometry. When B (Figs. 20 and 21) increases, the toughness decreases until it attains a plateau. In this case, plane strain dominates within the specimen, resulting in a high degree of triaxiality, and the toughness becomes a constant material parameter – the plane strain fracture toughness, K_{Ic} (or similarly, G_{Ic}) [3, 4, 49].

1.2.3 Other approaches

Fatigue damage model based on continuum damage mechanics (CDM) can describe the degradation of material response under cyclic loading and is simulated using equations, which couples damage accumulation and mechanical responses [54].

Another method called FFM method (finite fracture mechanics) [55] allows making predictions when LEFM equations are normally invalid: for short cracks and notches.

Number of methods is directed to the assessment of crack propagation geometries. Crack growth trajectory, plastic zone shape and dimensions can be determined with modified W-criterion approach [56].

Most of recent developments are not yet applied to wide range of brittle materials that makes it difficult to validate predictions results with published data.

1.3 Correlation between fracture mechanics and microstructure

In chapter 1.1.3 the correlation between fatigue properties of cemented carbides and their microstructure was discussed. As it was shown main mechanical properties are greatly affected by the grain size and distribution in the composite material. On the other hand, it is well known that the FCG behaviour of these materials is critically dependent on their microstructure also [57].

Fractographical investigations of WC-Co and TiC-WC-Ni-Co cermets by Ettmayer [58] and Schleinkoffer et al. [21, 59] revealed the microstructural mechanisms of subcritical crack growth during cyclic loading. Ductile binder ligaments are recognized behind the crack tip forming the *multiligament zone*. The ligaments connect two fracture surfaces behind the crack tip and experience a strong plastic deformation. This effect decreases the stress concentration experienced by the crack-tip and increases the crack resistance for propagation (crack tip shielding effect [60]).

The differences between the critical and subcritical crack growth in the fracture surfaces can be observed more clearly for the composites with the higher binder content.

1.4 Aims of the study

Due to the shortage of tungsten and its high price, new ceramic and metal composite grades are to be developed to replace WC-based hardmetals. Many pretending tungsten-free carbides are available. This group of composites is called cermets.

Among them, TiC-based materials are the most promising candidates. Such composites have higher mechanical properties than VC-, TaC- and NbC-cermets, and it is possible to produce TiC-based alloys with smaller carbide grain sizes.

Comparison of TiC-based cermets with WC-Co hardmetals shows their advantages and disadvantages. Titanium carbide based cermets have 1.5-2.0 times lower coefficient of friction as compared to WC-based hardmetals, due to the spherical shape of TiC-grains. Their maximum service temperatures are much higher and their density is 2-3 times lower. However, thermal conductivity is lower and thermal expansion coefficient is ~2 times higher. In general, the transverse rupture strength, fracture toughness, plasticity, Young modulus, endurance limit, and thermal stability are lower. The reprocessing of titanium carbide based cermets is more sophisticated and their wetting during soldering is poor [61].

It seems that hardmetals are almost the most perfect materials for wear applications. Obviously, still, nothing can be perfect. Many investigations have been conducted to extend knowledge about the mechanical degradation of hardmetals. Structural defects are always present in these heterogeneous materials. However, novel technologies allow overcoming these problems. Significant gains in microstructure defects can be limited by the sinter/HIP

technology. Structure densification and reorientation allows obtaining more homogeneous, void free materials [62].

The sinter/HIP technology is obviously preferable over the HIP method, as the sintering process and pressing takes place in the same chamber and in the same atmosphere [29, 62]. In addition, there is no menace of material contamination with hydrogen or oxygen like it happens due to exposition to air in the HIP routine.

The same technology was used to improve structure and mechanical properties of TiC-based cermets [63]. It is one of the objectives of the present research to define fracture behavior of the sinter/HIP-ed TiC-Fe/Ni cermet.

The failures of cemented carbides are in most cases associated with cyclic loading. That is why cermets durability is mainly restricted by fatigue strength. Statistical analysis of the reliability of brittle materials is based on the “weakest-link” concept of the Weibull distribution theory. The same strategy will be used to describe their fatigue characteristics under monotonic and constant amplitude cyclic loading.

A simple statement of facts (fatigue properties, hardness, fracture toughness and etc.) is the easiest task for a researcher. My intention is to predict the reliability of cermets. The Murakami approach is intended to be firstly applied to determine the lower bound of fatigue limit of the studied cemented carbides.

This approach will also be used to predict surface fatigue for TiC-cermets. A new model for the evaluation of surface fatigue life is proposed and verified experimentally. These results are of great importance for practical application of materials under investigation.

A functional testing imitating service condition is planned to be employed to specify the best cermet for blanking operation of sheet metal. Results will be compared with reference hardmetal performance.

A number of additional investigations, like elastic modulus (E) and fracture toughness (IFT), were conducted to fulfil the gaps in the properties for the presented materials.

The fractographic and XRD investigations will be carried out in order to assess the microscale mechanical degradation of a WC-hardmetal and TiC-cermet during monotonic and cyclic loading.

2 EXPERIMENTAL PROGRAM

The importance of fatigue testing and fatigue behaviour prediction for engineering materials is obvious. Tungsten-free cemented carbides are under special attention due to their rare combination of mechanical properties and obvious necessity to enlarge the knowledge about this type of composites.

The main problem concerning testing of cemented carbides is that only few methods are standardized, such as transverse rupture strength evaluation for hardmetals (ISO 3327), determination of flexural strength for advanced technical ceramics (EVS-EN 658-3:2002 and EVS-EN 843-1:2007) and Vickers hardness testing procedures (EVS-EN 23878:2000 - hardmetals and EVS-EN 843-4:2005 – advanced technical ceramics). Fatigue properties at constant amplitude of advanced ceramics (EVS-EN 15156:2006) are specified in uniaxial tension/tension or tension/compression regime. In present investigation the three-point bending scheme was used. Motivation for that will be given later.

Main mechanical properties of tested materials were determined for every batch of specimens to avoid variations in their values. A large enough number of testpieces was tested, according to Weibull statistical analysis requirements: not less than 10 for monotonically increasing loads and more than 35 for cyclic loads for each grade.

Experimental investigations are supported by microscopic and fractographic observations performed on optical and scanning electron microscopes (SEM). Used optical equipment is Zeiss AXIOVERT 25, and SEMs are JEOL JSM840a and HITACHI TM-1000.

Additional X-ray diffraction (XRD) analysis was carried out by the X-ray diffractometer Brooks D5005.

2.1 Materials and testing procedures

Two TiC-based cermets with Fe/Ni binder are under investigation and compared with two WC-Co hardmetals used as reference materials. Main mechanical properties and composition are presented in Table 4.

All hardmetals (grades S13 and H15) and cermet (grade T70/14) testpieces were produced through conventional press and sinter powder metallurgy according to ASTM B406 at the Powder Metallurgy Laboratory of the Tallinn University of Technology. Second cermet (grade ST75/14) specimens were fabricated with use of sinter/HIP technology in the same laboratory.

The specimens were prepared to the following dimensions (width × height × length): for monotonic (R_{TZ}) and cyclic loading – $(5.0\pm 0.3) \times (5.0\pm 0.3) \times 17$ mm; for XRD-study - $(5.0\pm 0.3) \times (5.0\pm 0.3) \times 35$ mm and for surface fatigue testing - $(5.0\pm 0.3) \times (13.5\pm 1.3) \times 22$ mm.

Specimens were ground to a surface finish of about $R_a=1.5 \mu\text{m}$ for WC-based hardmetals and $R_a=2.5 \mu\text{m}$ for TiC-based cermets on four sides (for more details see Paper III).

Table 4. Composition, structural characteristics and main mechanical properties of carbide composites

Grade	H15	S13	T70/14	ST75/14
Composition and microstructure				
WC content, wt%	85	87	-	-
TiC content, wt%	-	-	70	75
Binder composition and content, wt%	15 wt % Co	13 wt % Co	Fe/14 wt % Ni	Fe/14 wt % Ni
Average carbide grain size d_g , μm	2.0	1.5	2.2	2.2
Mechanical properties				
Transverse rupture strength R_{TZ} , GPa	2900	2810	2110	2420
Vickers hardness H_V	1170	1340	1270	1400
Young's modulus E , GPa	560	590	410	420
Poisson ratio	0.23	0.23	0.23	0.23
Additional properties				
Density ρ , g/cm^3	13.90	13.70	5.65	5.46
*Binder microhardness HV	325	325	410	410
**Fracture toughness K_{Ic} , $\text{MPa}\cdot\text{m}^{1/2}$	17.0	14.0	18.0	16.0
Porosity, vol%	<0.2	<0.2	<0.2	<0.2

* - used for prediction of fatigue limit by Murakami approach

** - measured by conventional technique [64, 65], with exception for T75/14 grade (IFT)

The elasticity modulus (E) of ST75/14 cermet was calculated according to the ISO 14577-1:2002 standard (Metallic materials – Instrumented indentation test for hardness and materials parameters) using universal hardness (UH) tester Zwick Z2.5 apparatus.

The microstructures of tested materials are shown in Fig. 24. The WC-grains are lighter and Co-binder is darker. For cermets in opposite, the TiC-grains are darker and Fe/Ni-binder is lighter. The shape of carbides is different also. Tungsten carbide grains are angular, and titanium carbide grains are rounded, with no sharp corners.

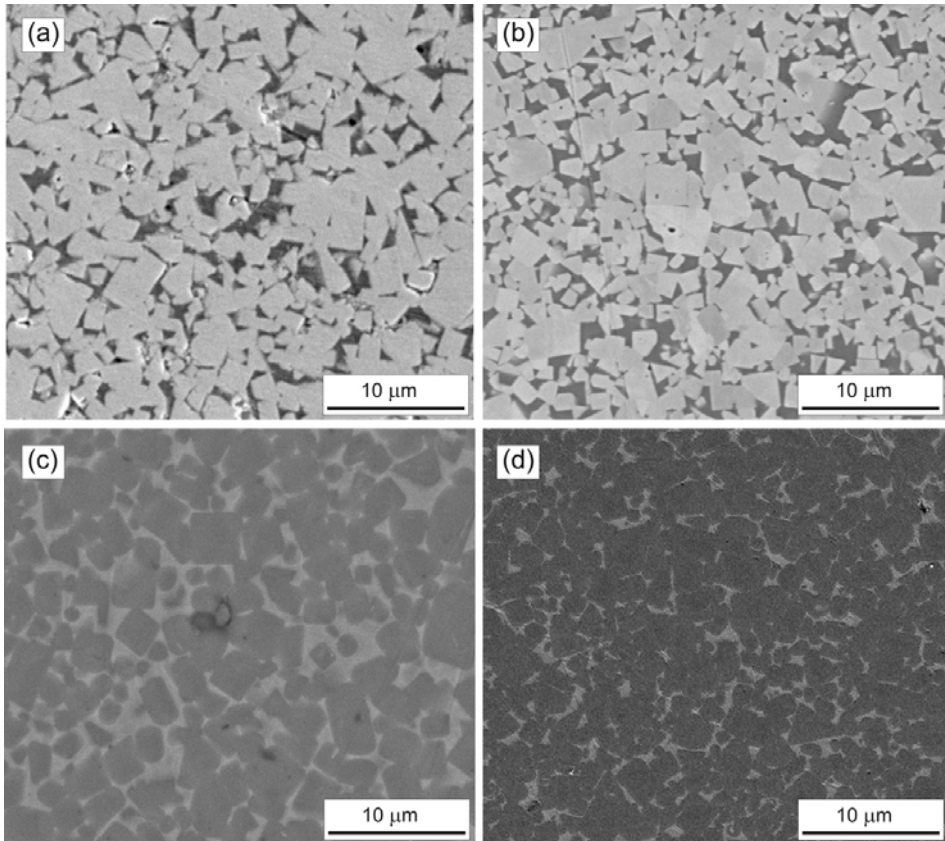


Figure 24. Microstructures of tested hardmetals and cermets: (a) H15 hardmetal; (b) S13 hardmetal; (c) T70/14 cermet and (d) ST75/14 cermet

2.2 Fatigue testing

Two types of fatigue tests were conducted. Conventional fatigue testing of prismatic specimens was carried out on fatigue testing centre with incorporation of three-point bending scheme (3 PB).

Surface fatigue tests are made with use of rotary bending equipment.

All fatigue tests were conducted at room temperature (approx. 21 ± 2 °C) in air and humidity of $40 \pm 5\%$ RH.

2.2.1 Conventional testing (3 PB)

The three-point bending scheme was used in present work because it was my intention to: save material (smaller specimens are tested); present comparison of fatigue data from previous studies [33, 66] where tests were carried out on the same device (3PB); follow the advices of B. Roebuck for testing of hardmetals and cermets [17].

Fatigue strengths were obtained at a specified life of the 10^7 loading cycles. The loading amplitude was constant for every test.

Three-point bending device (3PB) used in experiments, with span between supports equal to 14.5 mm and supports diameters of 5 mm (10 mm for upper part), is shown in Fig. 25. Ball or bearing support is used to exclude specimen's installation mismatches. Applied load is always normal to the specimen. Fracture occurs in the medium third between the supports of the device.

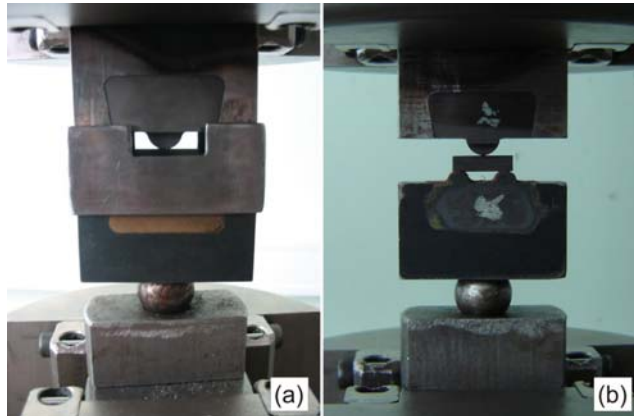


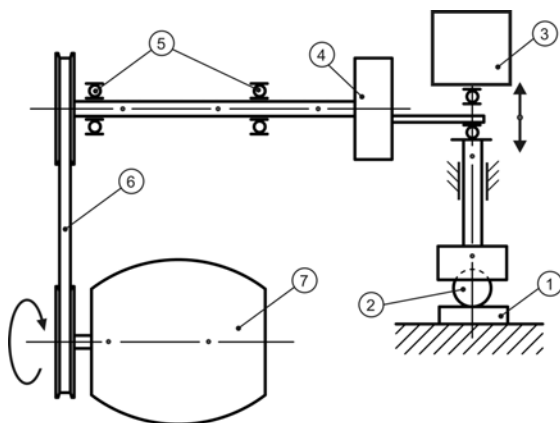
Figure 25. Three-point bending device: (a) with protective cartridge and (b) without protective cartridge.

Fatigue testing with three-point bending (3 PB) was carried out on dynamic testing system INSTRON 8516. Main controlled parameters are: loading scheme (amplitude, stress ratio); loading frequency; specimen deflection. The stress ratio was the same in all-testing sequences, $R=0.1$. The loading frequency varied from 1 up to 35 Hz. The rate of applied force did not exceed 1 kNs^{-1} .

Used fatigue testing scheme and specimen dimensions are not standardized yet.

2.2.2 Surface fatigue testing

Surface fatigue was studied with incorporation of the modified classical rotation bending equipment (single-end rotating cantilever testing machine), see Fig. 26. The frequency of loading cycles was equal to 25 Hz (driven by electromotor with 1500 rpm). The number of loading cycles was controlled automatically.



The used ball indenters were made of WC-6 wt% Co (H6) hardmetal, with diameters ranging from 11.5 up to 12.4 mm. The deformation of the indenters is not the object of the study of this work.

Figure 26. Scheme for surface fatigue testing: 1 – testpiece; 2 – indenter (ball); 3 – weight; 4 – eccentricity device; 5 – bearings; 6 – driving belt; 7 – electric motor.

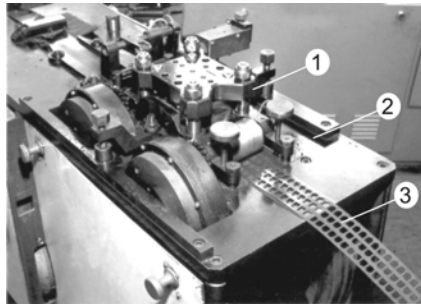
Load was applied along vertical axis of testing apparatus, by axis normal to specimen, and was equal to 20 N for every studied material. Surface fatigue life is limited to the maximum of $2 \cdot 10^6$ cycles.

The micrographical investigation is performed to recognize the surface fracture behaviour of studied materials.

This rig is engineered in TUT. The theoretical background for that method is described in Paper IV. At the present moment limited number of test data does not allow making major conclusions for all studied materials described in this thesis, but some conclusions are given in results and discussion section for H15 and ST75/14 grades.

2.3 Durability testing in blanking

Functional tests, or durability testing in blanking, were performed with use of a 3-position die mounted on an automatic press for the blanking of grooves in the 0.5 mm thick electro-technical sheet steel (HV=150), see Fig. 27. Lower dies inserts (blanking dies) and upper dies (blanking punches) were produced from studied materials.



The wear of blanking tool (dies and punches) was evaluated by the measurement of side wear ΔD (increase in diameter of die cutting edge contour) after intermediate service time of $0.5 \cdot 10^6$ strokes.

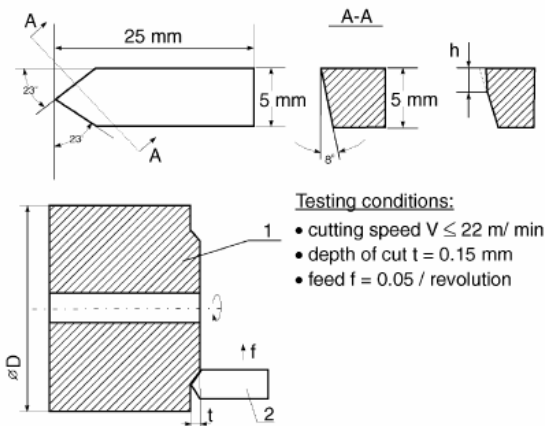
The wear of blanking tool (dies and punches) was evaluated by the measurement of side wear ΔD (increase in diameter of die cutting edge contour) after intermediate service time of $0.5 \cdot 10^6$ strokes.

Figure 27. Durability testing of carbides composites: 1 – blanking die; 2 – the mechanical press body and 3 – the sheet steel [23].

Experimental results are complement to those performed and published previously [23, Paper I].

2.4 Adhesive wear testing

A special method was used for adhesive wear tests, see Fig. 28. Turning of mild steel, with Vickers hardness of 160 HV, at low speed



with Vickers hardness of 160 HV, at low speed ($v_{\text{average}} \approx 15.46 \text{ m} \cdot \text{min}^{-1}$). This method is found to be most appropriate to describe the contact behaviour of carbide composites during sliding, very similar to that of blanking conditions [23, 67, 68].

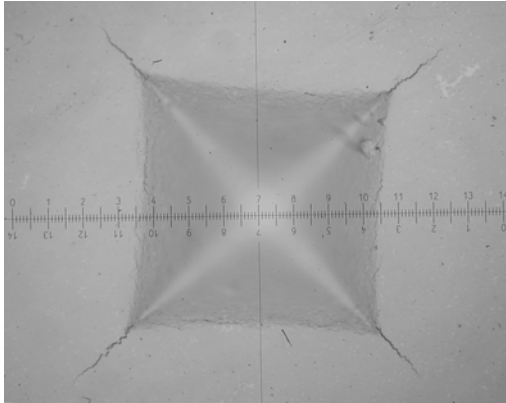
Figure 28. The adhesive-wear testing conditions and the geometry of specimens: 1 – blank or billet; 2 – specimen [23].

The adhesive wear resistance L_1 was evaluated as the distance of cutting path when the height h of wear land at tool (specimen) cutting edge (nose) exceeds 1 mm in length.

A fair correlation between blanking performance and adhesive wear resistance of hardmetals and cermets is observed [67, 69].

2.5 Instrumented indentation testing

The instrumented indentation testing technique was used for determination fracture toughness of tested cemented carbides. The typical imprint produced by indentation of Vickers pyramid is presented in Fig. 29.



A comparative investigation for determination of indentation fracture toughness (IFT) was carried out to define emanating crack type and to find a reliable calculation technique for studied materials (see Paper III)

An attempt to develop universal equation for cemented carbide is made also.

Figure 29. The photograph of indentation imprint for cermet grade ST75/14 (magnification x50).

The results of instrumented indentation (and depth sensing) tests are found to be in good correlation if compared with those determined by conventional testing methods (see Table 7).

2.6 Structural-fractographical investigations

Resistance of cemented carbides to fatigue damage is related to their ability to absorb fracture energy (elastic strain energy storing at crack tips during repeated loading) by means of plastic straining. As we know, the fracture (plastic deformation) starts in the ductile binder phase, but a lot of fractured carbide grains, with signs of fatigue striations, pointing on the fact of possible plasticity of even very hard TiC-grains.

It means that fracture resistance of cemented carbides depends on the plasticity of both binder and carbide phases.

Fractographical investigations allow to trace crack propagation paths and to define fracture mechanisms. The XRD analysis is used for qualifying changes in fine structure – increase in density of dislocation network and dispersity of micrograins – as a result of local plastic strain. Changes in both carbide phases of WC [001] and TiC [200] were determined.

3 RESULTS AND DISCUSSION

3.1 Strength and fatigue properties

Large scatter of test data is typical for cemented carbides. This is why transverse rupture strength and durability of tested materials are analysed and assessed statistically, using standard methods.

Prediction of the lower bound of fatigue strength is also made using Murakami method and statistics of extremes.

3.1.1 Weibull analysis

Statistical nature of material strength derives from the fact that the strength is limited by the distribution of the most severe defects i.e., the strength-determining flaws. The initial strength can be described only by statistical distribution because flaws are generated both by processing and by in-service use (handling).

Weibull statistics has been commonly used to characterize the statistical variation in the fracture strength of brittle materials such as ceramics, and composites [70, 71]. The evaluation of the Weibull parameters σ_0 (corresponding to the fracture stress with a failure probability of 63.2 %), m_i (shape parameter for monotonic loads), $N_{f,0}$ (scale parameter for cyclic loads, corresponding to the mean cycle number to failure), m_c (for cyclic loads) are usually evaluated using maximum likelihood (ML) method (ENV 843-5:1996 or EVS-EN 843-5:2007). It is recommended to use ML method as it leads to the highest estimation precision of the parameters. However, the LR method was used due to its simplicity. Although, the ML method results are more often in an overestimation of the Weibull parameters than underestimation, and hence results are in a lower safety than the LR method in reliability prediction [70-74]. Results of statistical analysis for studied materials are shown in Figs. 30-32.

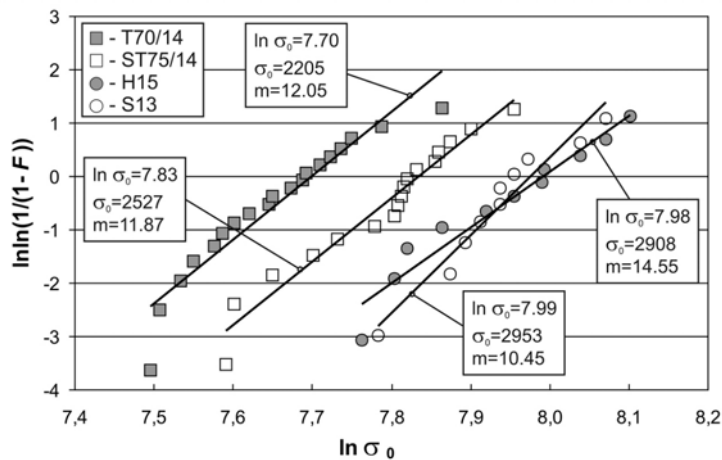


Figure 30. Weibull plot for the inert strength σ_0 of hardmetals and cermets submitted to monotonic loads.

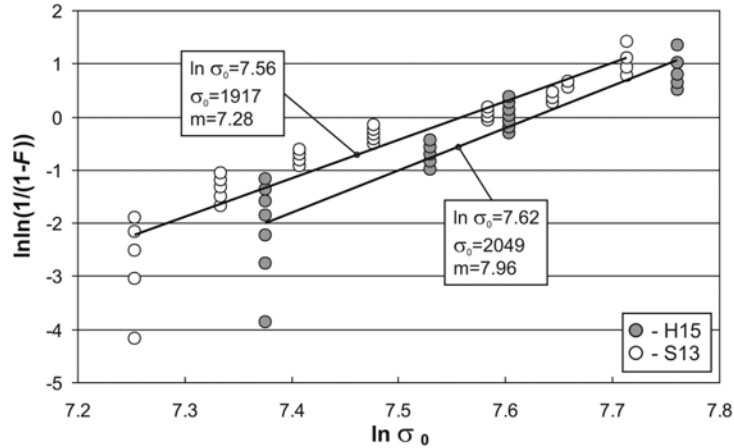


Figure 31. Weibull plot for the inert strength σ_0 of hardmetals after submitting to cyclic loads.

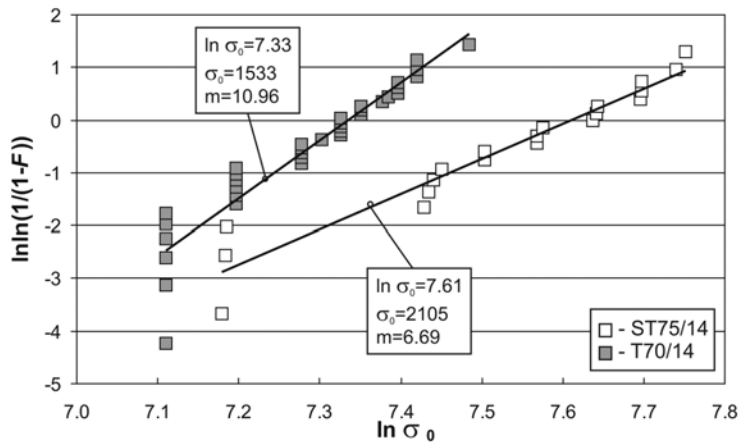


Figure 32. Weibull plot for the inert strength σ_0 of cermets after submitting to cyclic loads.

Calculated Weibull parameters for monotonously increasing and cyclic loads are presented in Table 5.

Table 5. Weibull parameters obtained for studied hardmetals and cermets.

Grade	Monotonic loads		Cyclic loads				
	m_i	σ_0	m_i	σ_0	m_c	σ_f	$N_{f,0}$
H15	10.45	2952	7.96	2049	0.83	1677	~ 1757000
S13	14.55	2908	7.28	1917	0.81	1510	~ 445000
T70/14	12.05	2205	10.96	1561	0.92	1428	~ 648000
ST75/14	11.87	2527	6.69	2105	0.51	1675	~ 1284000

Weibull analysis results are compared with those of Loshak et al. [15], Kursawe et al. [32] and number of work by Schleinkofer-Sockel group [21, 24, 35, 74].

Parameters m_i , σ_0 and m_c received in present experiments are in good agreement with those obtained by 3PB tests and evaluated using ML method [15, Papers XIV-XVI]. Other reference investigators have used a reversed cantilever bending scheme with stress ratio of -1, but the same tendencies of decrease for m_i and m_c with increase of binder content are clearly visible. Strength parameters values tend to be greater for hardmetals with higher binder content.

3.1.2 Statistical analysis

Fatigue testing results for hardmetals and cermets are presented in form of $S-N$ curves (Wöhler plots) with indication of inert strengths (transverse rupture strengths) obtained by monotonic loading and standard deviation bounds received with use of linear regression (LR) analysis, see Figs. 33 and 34 correspondingly.

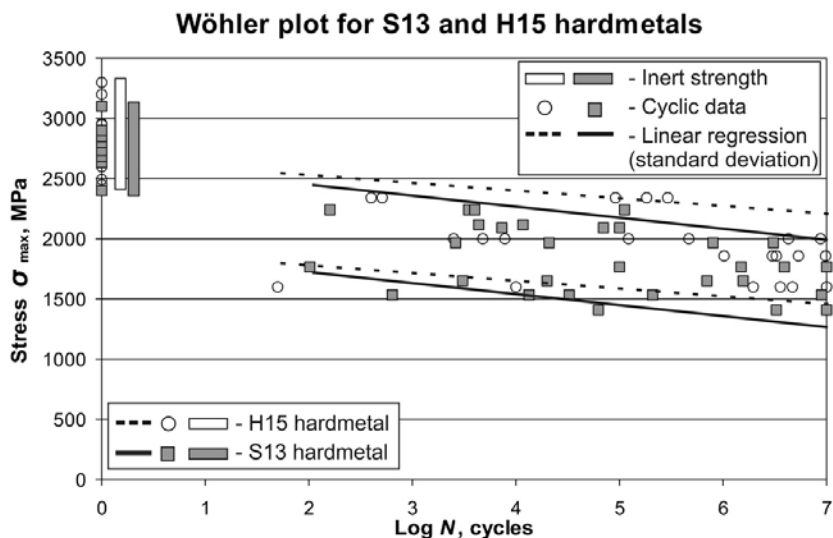


Figure 33. Wöhler plot of the cycles to failure N for different cyclic stress amplitudes σ_{max} for hardmetals S13 and H15. Inert strengths σ_0 of materials are given for comparison.

Fatigue strength average values for H15 is ~ 1750 MPa and for S13 - ~ 1600 MPa, and the lower bounds are ~ 1370 and ~ 1230 MPa respectively. For additional fatigue data for hardmetals and cermets see Papers IX and XVI.

Clear tendency of the fatigue sensitivity decrease (decrease of the fatigue curve slope) for hardmetals with higher binder content can be observed, as it was noted by previous investigators [31, 32, 35]. The scatter of data does not vary significantly as the composition and mechanical properties of tested hardmetals are almost the same.

Fatigue strength average values for T70/14 is ~ 1380 MPa and for ST75/14 - ~ 1715 MPa, and the lower bounds are ~ 1170 and ~ 1455 MPa respectively. Fatigue sensitivity decreases comply with higher binder content for T70/14 over ST75/14, as it was seen for hardmetals also.

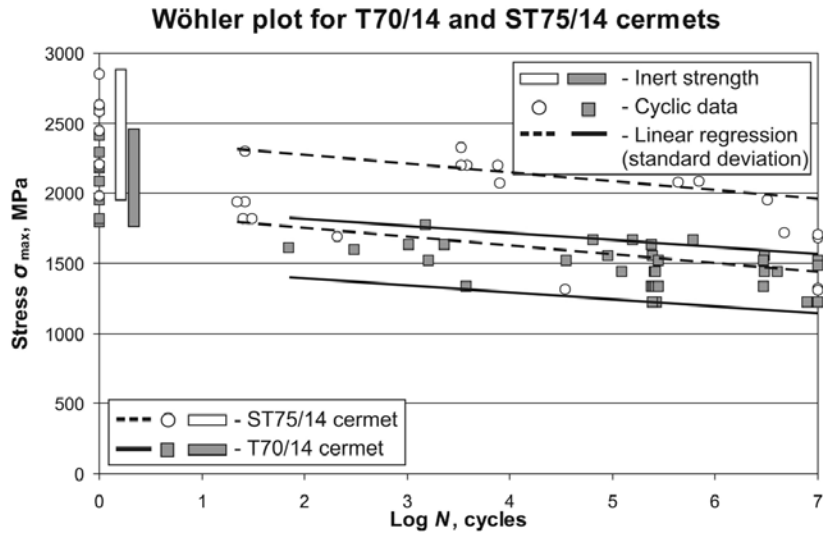


Figure 34. Wöhler plot of the cycles to failure N for different cyclic stress amplitudes σ_{max} for cermets T70/14 and ST75/14. Inert strengths σ_0 of materials are given for comparison.

The scatter of fatigue data for cermets is much narrower than that of hardmetals as the overall nature of the compound behavior becomes more metallic [30, 33].

3.1.3 Fatigue strength prediction using Murakami method

The Murakami approach explains the phenomenon of non-propagating behaviour of fatigue cracks (including short cracks) and gives a quantitative measure for assessment of their maximum size. Results of fatigue tests show that the critical maximum defect size (or non-propagating crack size) is equal to the size of carbide grain (Fig. 35), though there is some scatter in defect size (see Paper IX for materials H15, T70/14 and T60/8).

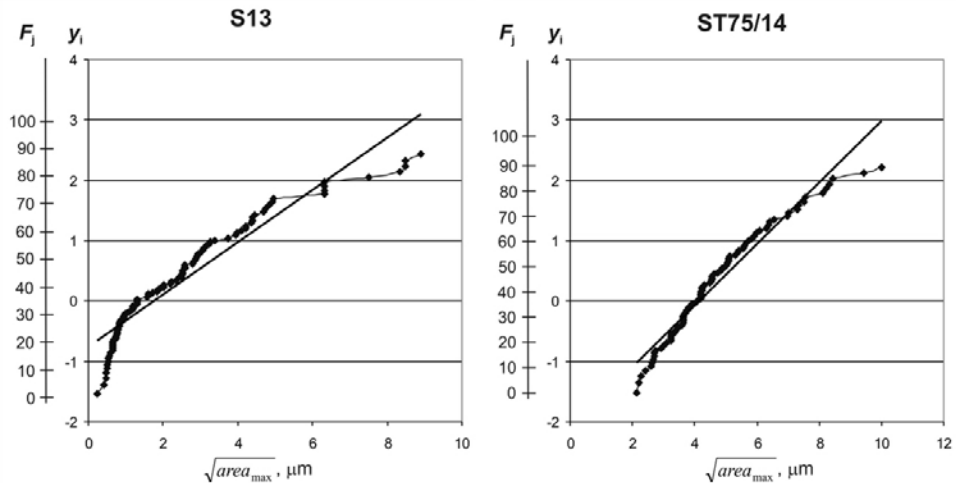


Figure 35. Prediction of the maximum pores size from the statistics of extremes graphs for S13 (left) and ST75/14 (right).

The F_i is the cumulative distribution function (%) and y_i is the reduced variates - are the parameters of statistics of extreme used for inclusion rating method. Pores with minimum size of $\sim 1.8 \mu\text{m}$ for S13 and $\sim 3.9 \mu\text{m}$ for ST75/14 and larger are the main fatigue life limitation factors. To increase fatigue performance of cemented carbides we need to get rid of pores larger than that critical values and exclude possibility of small pore clusters formation, see Figs 36-37.

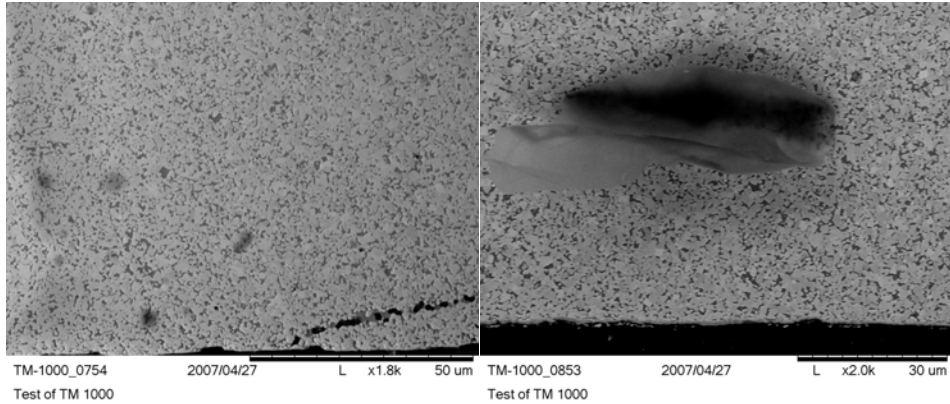


Figure 36. Clusters of small pores (left) and binder pools (right) could be found in S13 hardmetal.

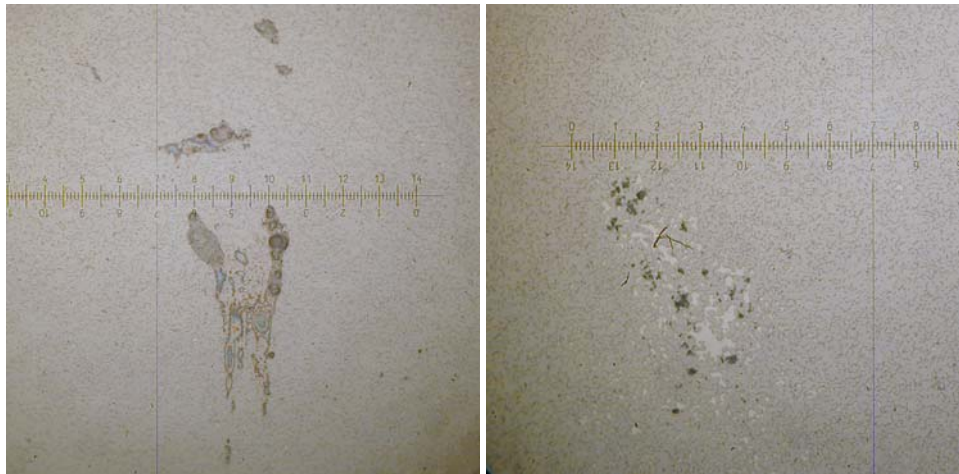


Figure 37. Clusters of small pores (left) and binder pools (right) could be found in ST75/14 cermet (x50).

Major constraint of this approach is that for materials with $HV \geq 400$ there is no linear correlation between fatigue limit and Vickers hardness. This means that prediction is not accurate in this case. Since it is well established that mechanical degradation under cyclic loading in WC-Co hardmetals starts in the cobalt binder phase [50], and taking into account the fractographical examinations of the previously studied materials [33, 49], also currently studied

materials approve this fact, I have used microhardness of binder phase for prediction of fatigue strength (see Paper II).

An important conclusion can be made. Fatigue strength prediction does not depend on microstructure of binder phase (martensite, bainite or austenite for Fe/Ni binder), or heat treatment.

Results of defects inspection and calculation of the lower bound of scatter of fatigue strength are shown in Table 6.

Table 6. Defects inspection items for S13 hardmetal and ST75/14 cermet with predicted lower bound of fatigue strength (S – is the area of prediction, T – return period)

Grade	Prediction of $\sqrt{area_{max}}$			Prediction of lower bound of the scatter of the fatigue strength σ_w , MPa		
	S , mm ²	T	$\sqrt{area_{max}}$, μm	for surface defects	for defects just below surface	for interior defects
S13	1	140.1	29.1	1150	1130	1250
	10	1401.4	42.1	1080	1060	1180
	100	14014.4	55.0	1030	1020	1130
ST75/14	1	6.9	10.1	1630	1610	1780
	10	69.8	17.6	1480	1460	1620
	100	697.8	24.9	1400	1380	1530

Comparison of experimental fatigue strength values and predicted ones using Murakami approach has shown that they are in good agreement with fatigue strength received by conventional fatigue testing of specimens with square section of 5×5 mm² ($S=25$ mm²): for S13 lowest fatigue strength value is equal to 1155 MPa and for ST75/14 - 1430 MPa.

3.1.4 Surface fatigue life prediction

The formation of characteristic deformation site during surface fatigue testing was revealed. Three zones can be identified (Fig. 38): A – central round zone of severe deformation; B – collar zone of binder extrusion, and finally C – slightly deformed transition collar zone.

In *zone A* the binder is almost totally absent as it was squeezed out during deformation. Carbide grains are in contact with each other and some binder can be found only between large grains.

The traces of binder extrusion are visible in *zone B*. Binder then transmitted to the ball, and as it rotates during loading, then is carried away from testpiece. Large surface and subsurface pores are exposed and packed with binder particles.

The deformation in *zone C* is very small due to the change of load magnitude with the increase of indenter penetration depth (and deformation site diameter enlargement).

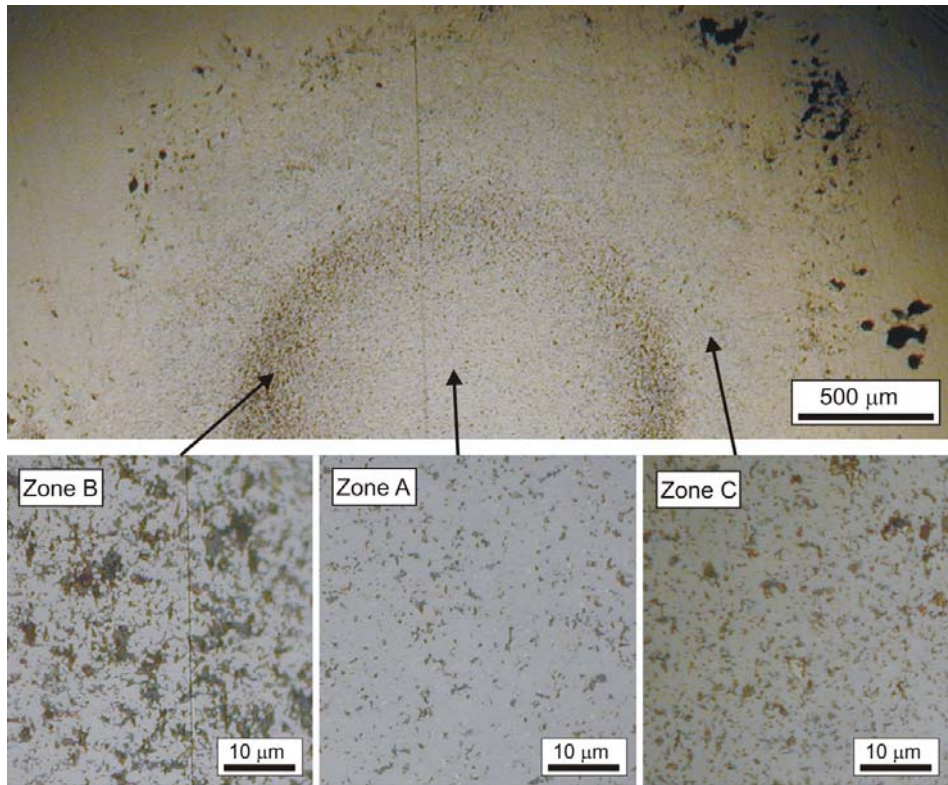


Figure 38. The deformation of H15 hardmetal produced by surface fatigue testing.

The affected zone depth is found to be of about 60 μm in the centre of indentation crater.

Surface fatigue testing results for H15 hardmetal and ST75/14 cermet are presented in form of *S-N* curves, where maximum applied stress is derived from applied load to area of indent ratio, see Fig. 39.

Results are in good agreement with that of 3 PB fatigue testing.

We can see the same trends here also. The slope of *S-N* curve of TiC-based cermet is lower and data scatter is narrower if compared to WC-Co hardmetal. Surface fatigue strength at $2 \cdot 10^6$ cycles for both materials is almost the same.

Maximum applied stress is equal to 1440 MPa and 1120 MPa for H15 and ST75/14 correspondently. Although, the compression strength of H15 is about 4000 MPa and for ST75/14 is 3500 MPa, these values are sufficient to deform composites surfaces plastically. On the graph test data is brought to correlation with bending fatigue testing data.

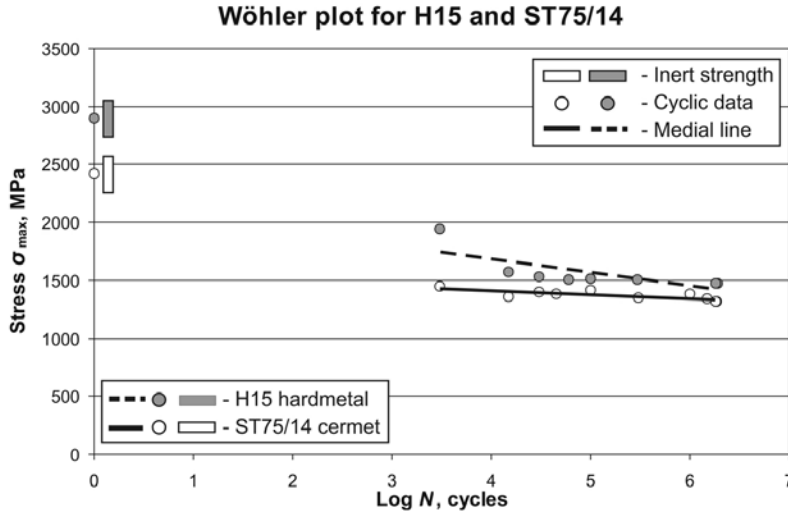
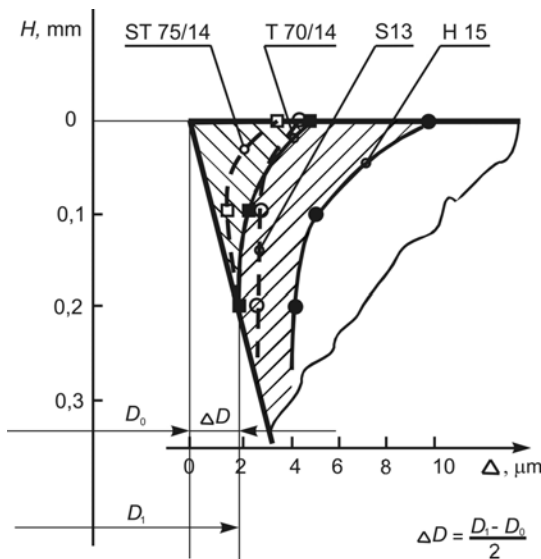


Figure 39. The Wöhler plot for surface fatigue of H15 and T70/14 composites.

The inert strength values indicated on the graph are calculated from applied load to area of indenter ratio and brought to correlation with bending fatigue testing data. For used ball indenter radiuses the real inert strength in surface fatigue testing is equal to ~1400 MPa and 1190 MPa for H15 and ST75/14 respectively.

3.2 Performance of carbide composites in sheet metal blanking

A comparison of wear contours of cutting edges (and side wear ΔD) of tools



(blanking dies) from carbide composites is presented in Fig. 40. Superiority of the TiC-based cermets with Fe/Ni binders over an ordinary WC-Co hardmetals (grades S13 and H15) refer to better adhesive wear resistances of these materials (see Paper I, for comparison to T60/8 grade).

Blanking performance was evaluated as a number of strokes (N) divided by side wear (ΔD) of a blanking die tools.

Figure 40. Wear contours of cutting edges of dies from different cemented carbides.

There exists a correlation between blanking performance, adhesive wear resistance as it was proved earlier [23, 68, 69] and fatigue sensitivity as shown in Fig. 41. This correlation may also be referred to Vickers hardness of studied materials.

Fatigue sensitivity ΔS_f was used as a merit of the material degradation during cyclic loading. It can be characterized by the decrease of fatigue strength with increase of loading cycles (the slope of S - N curve on the Wöhler plot). Here fatigue sensitivity was evaluated as difference of fatigue strengths S_f at 10^3 (S_{f3}) and 10^7 cycles (S_{f7}) by equation $\Delta S_f = S_{f7} - S_{f3}$. Cermets with lower fatigue sensitivity show higher performance in blanking.

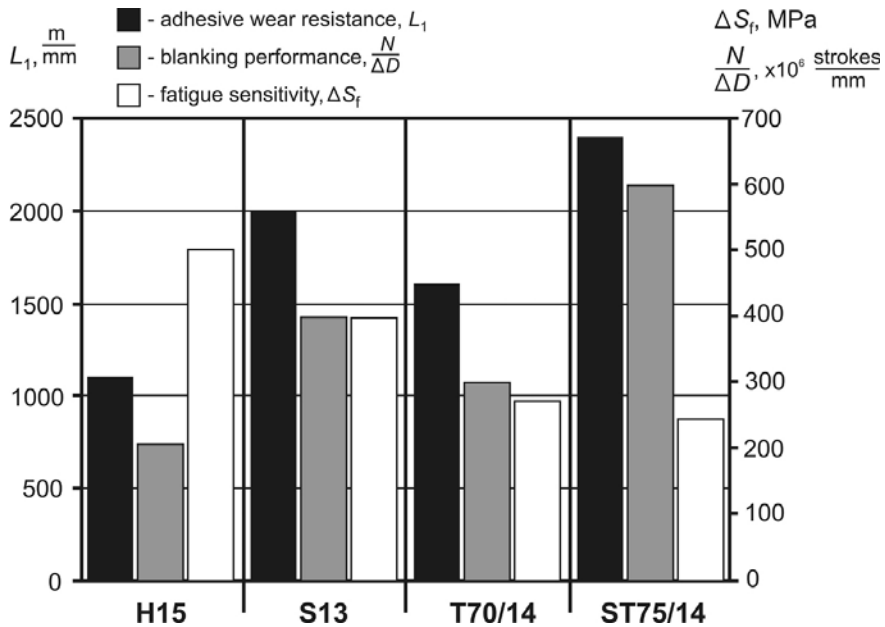


Figure 41. Blanking performance, adhesive wear resistance and fatigue sensitivity correlation graph.

The explanation for that phenomenon is fully dependent on composition and microstructure. As it was stated previously [Papers VI, 75] the improvement of cyclic loading degradation resistance of cemented carbides can be achieved by increase of the energy absorbing ability of binder and/or carbide phases.

Based on the results of XRD analysis it can be concluded that the fracture of carbide composites during cyclic loading propagates in their carbide phase and is preceded by local plastic strain. This means that the ability of carbide composite to undergo plastic strain, that is, its ability to absorb fracture energy by local plasticity, depends on the plasticity of both ductile binder and the carbide phases. The superiority of TiC-based cermets in relation to WC-hardmetals appears to be a result of their higher resistance to adhesive wear and fatigue damage (see Paper I).

3.3 Indentation fracture toughness of carbide composites

The sizes of cracks emanated from corners of indentation imprint are measured from photographs. From graph of diagonal crack length versus applied load the slope of c - P curve is found to be $2/5$ for studied materials. Then the coefficient

δ can be obtained from medial line equation (see Paper V). This method is universal, but sufficient number of tests must be performed (at least 5 for 3 different loads), and cracks are to be recognized.

Using Eqs. 10 and 12, with substitution of coefficient δ , the K_{IcIFT} and stress intensity range ΔK can be defined for tested materials. Results of calculations are presented in Table 7.

Table 7. Fatigue crack growth parameters for tested materials

Grade	Constant δ	K_{IcIFT} , MPa·m ^{1/2}	ΔK , MPa·m ^{1/2}	da/dN, mm/cycle
H15	0.025	18.2	6.7	$8.4 \cdot 10^{-7}$
S13	0.024	14.4	6.0	$1.4 \cdot 10^{-6}$
T70/14	0.030	17.6	6.2	$1.3 \cdot 10^{-6}$
ST75/14	0.046	16.8	5.1	$8.1 \cdot 10^{-7}$

The results are in good agreement with previously published data [44].

The fatigue crack growth rates are obtained from fractographical investigations. Distance between striations which can be found from fractured carbide grains is measured and then crack growth rates are calculated [76].

3.4 Microstructural aspects of failure of carbide composites

Fatigue fracture of cemented carbides is well investigated and documented [7, 28, 32, 35, 60]. Main fracture mechanisms are revealed in numerous studies [31, 34, 59,]. Fracture predominantly starts in the binder phase, proceeded with cobalt binder transformation and followed with trans- and intergranular carbide grains fractures. The same behaviour is observed in TiC-Fe/Ni cermets [33], with the exception of binder phase transformation.

Sinter/HIP technology did affect the ST75/14 cermet as it was expected. The statistical analysis of defects distribution (see Fig. 35) shows much smaller values if compared with T70/14 (Paper IX). However, the critical defect size is still equal to average grain size. The fracture behaviour is similar to that of T7014 cermet.

3.4.1 Surface fatigue fractography

The fractographical investigation of deformed surface in perpendicular plane to loading direction exposed a number of transgranular (cleavage, Wallner lines) and intergranular fractures of carbide grains or traces of brittle and evidences of fatigue fractures (striations), see Figs. 42 and 43.

Large WC-grains are crushed to the smaller pieces, and then smaller grains extrude binder from the deformation site. Sufficient contact forces enable elastic fracture of grains and in time process advances into the depth of the material (Fig. 42). Unfractured large grains are pushed together and form carbide skeleton. During loading they oscillate provoking fatigue fracture to occur.

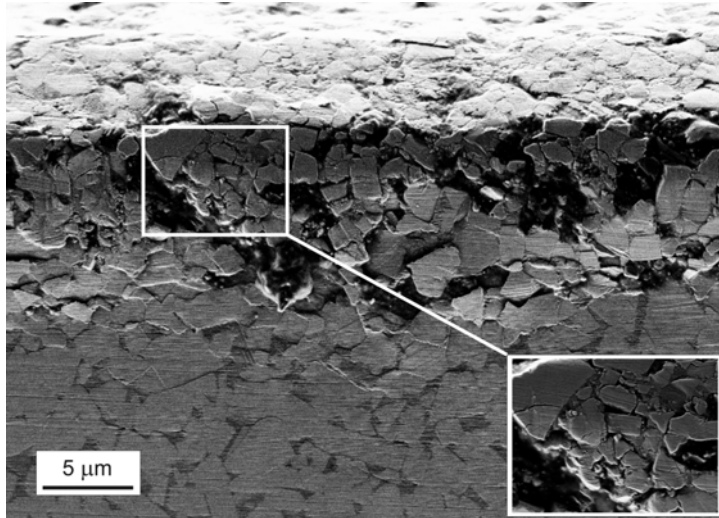


Figure 42. The subsurface degradation of hardmetal H15 microstructure.

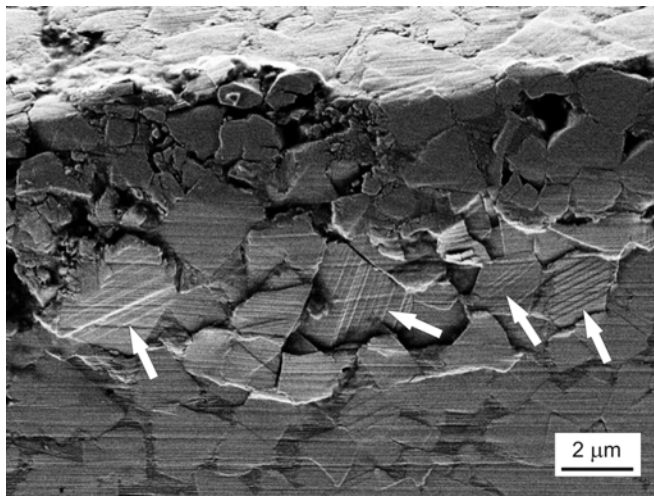


Figure 43. SEM micrograph of H15 subsurface with fatigue striations observed in WC phase (marked with arrows).

Delamination is clearly visible (Fig. 43). In the affected zone the grains are separated from lower layers. Obtained debris can be easily removed from testpiece surface. And still it is not clear what kind of failure criterion can be specified for surface fatigue because the number of small cracks is large and final fracture can occur at any time.

3.4.2 Fractographical peculiarities of fatigue failure in blanking

The XRD study revealed the ability of “brittle” carbide phase to absorb fracture energy by local plastic strain (Paper I).

XRD-trials performed in present study (on composites tested in monotonic and cyclic loadings in fatigue testing) revealed alterations in their diffractograms (decrease in intensities and in broadness of lines of X-ray reflections from carbides) referring to changes in fine structure resulted from local plastic strain (Figs. 44 and 45).

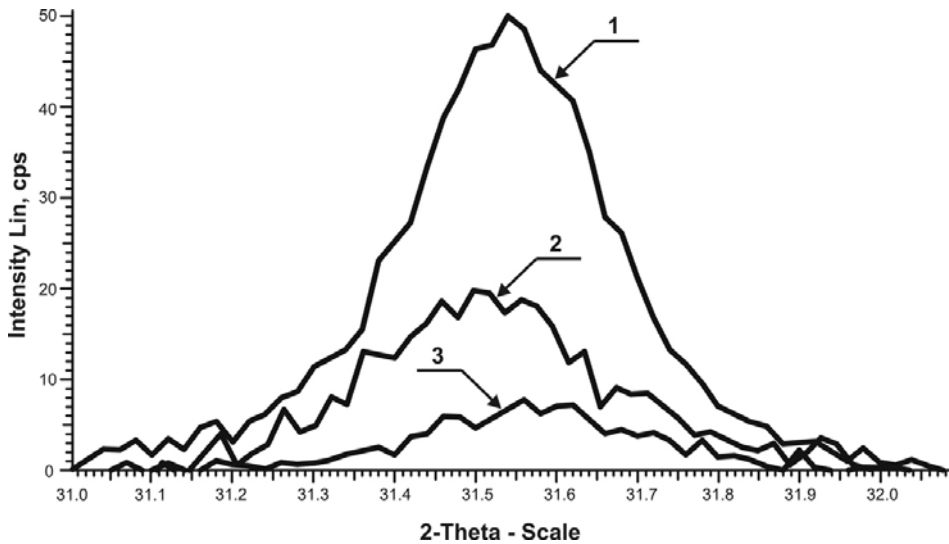


Figure 44. XRD patterns (diffractograms) of carbide phase of WC-hardmetal: 1 – before testing (etalon); 2 – fractured hardmetal during cyclic loading; 3 – fractured hardmetal during monotonic loading.

Decrease of intensities is the merit of static distortions (atoms distortions, movements of dislocations) of the carbide grains. In our case the drop of intensity is bigger for WC-phase (from initial state of 50 cps till 20 cps for cyclic loading, and till 7 cps for monotonic), resulting in higher fatigue sensitivity.

For the TiC-phase the change of intensities is much smaller. The cyclic loading defined with drop from initial 80 cps till 60, and till 40 for monotonic loading correspondingly, see Fig. 45.

Greater broadness of lines allows presuming presence of microstresses aimed to the direction of plastic stress. In TiC grains it is more uniform and slightly larger. Broadness is oriented to the direction of main stress (resulted in plastic straining).

The intensity in embrittlement (decrease in plasticity) is more expressed in WC phase than in TiC grains. The higher resistance of a composite to embrittlement during cyclic loading result in its lower fatigue sensitivity (higher resistance to fatigue damage).

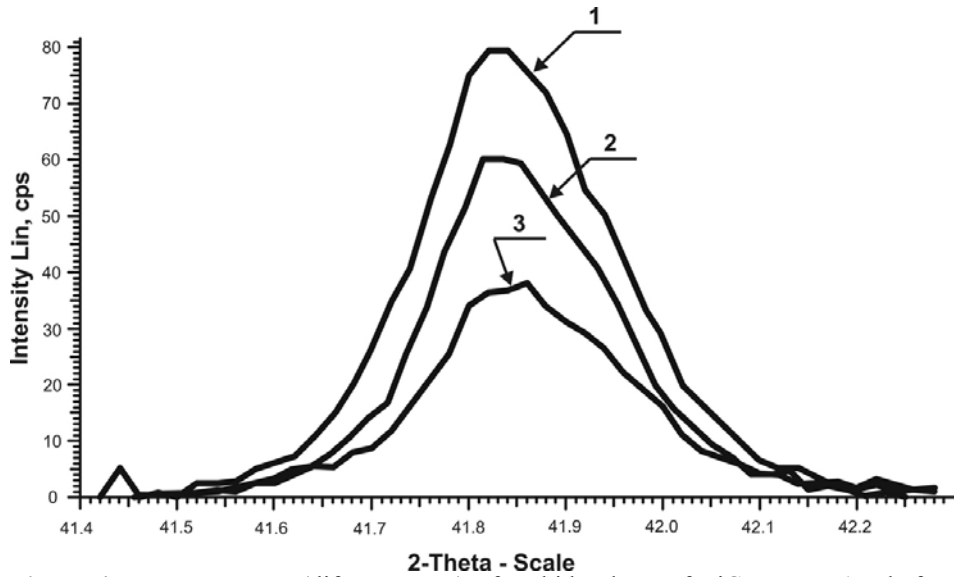


Figure 45. XRD patterns (diffractograms) of carbide phase of TiC-cermet: 1 – before testing (etalon); 2 – fractured hardmetal during cyclic loading; 3 – fractured hardmetal during monotonic loading.

Higher rate of decrease in plasticity during cyclic loading of tungsten carbide exceeds that of titanium carbide and increases the fatigue sensitivity of the WC-based composite.

CONCLUSIONS

The main conclusions of the present thesis are as follows:

1. The fatigue behaviour of WC- and TiC-based carbide composites under various loading conditions was studied;
2. It was proven that the fatigue phenomenon of heterogeneous materials is based on the fact that both phases (hard ceramic particles and ductile binder) are involved in the fracture process, although failure starts mainly in the binder;
3. Strength and reliability assessment of hardmetals and cermets is complicated and usually refers to statistical methods. The “weakest-link” concept (Weibull distribution theory) is the most effective method for brittle materials. Weibull analysis displays a drastic dependence of the composites properties (R_{TZ} , σ_f , $N_{f,0}$) on the binder phase content and composition;
4. The grades H15 hardmetal and ST75/14 cermet have the higher fatigue limits as compared with S13 hardmetal and T70/14 cermet. The scatter of fatigue data is wider for materials with lower binder content. Composites with higher binder content behave as ductile “metallic” materials and lower binder content leads to brittle fracture;
5. The functional testing conducted in blanking of sheet metal provided evidence of relatively better performance of TiC-Fe/Ni cermets as compared to WC-Co hardmetal. The results are related to microstructure, adhesive wear resistance and fatigue performance. The blanking performance of the carbide composite is controlled by its adhesive wear resistance and fatigue sensitivity (slope of $S-N$ curve);
6. The results of adhesion wear resistance testing also demonstrated better resistance of TiC-based cermets as compared to conventional WC-based hardmetal at the same level of hardness. The more spherical shape of TiC carbide grains may be the reason for that;
7. Predictions of the lower bound of fatigue limits are made. The Murakami approach was firstly applied to TiC-Fe/Ni cermets. Calculation results are in good agreement with fatigue testing results. The critical size $\sqrt{area_{max}}$ of microstructural defect (pore, non-metallic inclusion, inhomogeneity) can also be determined by this technique, being equal to average carbide grain sizes for the studied materials;
8. A technique for surface fatigue testing was elaborated and presented in a recent study. The method is proved experimentally to be efficient for surface fatigue life (N_f) prediction. Severe subsurface microstructural degradations (grains cleavage, striations, binder extrusion) were observed by the fractographic examination. For the studied H15 and ST75/14 grades the surface fatigue testing results showed excellent convergence

with experimental data received from standard fatigue tests. Surface fatigue and standard fatigue curves displayed the same slopes for the corresponding material (fatigue sensitivities). Further testing should be done to make it possible to draw major conclusions on that matter;

9. In cyclic loading the plasticity of composite phases (in particular carbide phase) decreases. Rate of decrease in plasticity (embrittlement) during cyclic loading of tungsten carbide exceeds that of titanium carbide. The lesser decrease in plasticity reduces the fatigue sensitivity of the carbide composite.

REFERENCES

1. *The on-line library of famous knowledge quotations, quotes and sayings from famous people.* <http://famousquotes365.com/>
2. **Irwin, G. R.** *Fracture Mechanics*, in ASM handbook. Ninth ed., Vol. 8. USA: American Society for Metals, 1985 pp. 437-464.
3. **Knott, J. F.** *Fundamentals of Fracture Mechanics*. Butterworths, London, 1973.
4. **Anderson, T. L.** *Fracture Mechanics. Fundamentals and Applications*. CRC Press, Taylor&Francis Group, New York, 2005.
5. **Gerberich, W. W.** *Microstructure and Fracture*, in ASM handbook. Ninth ed., Vol. 8. USA: American Society for Metals, 1985 pp. 476-492.
6. **Van Vlack, L. H.** *Materials Science for Engineers*. Addison-Wesley Publishing Company, Atomizdat, 1975 (in Russian).
7. **Roebuck, B., Almond, E. A.** Deformation and fracture processes and the physical metallurgy of the WC-Co hardmetals. *International Materials Reviews*, 1988, 33, pp. 90-110.
8. **Kocañda, S.** *Fatigue failure of metals*. Sijthoff & Noordhoff International Publishers, Warsaw, 1978.
9. **Fang, Z. Z.** Correlation of transverse rupture strength of WC-Co with hardness. *International Journal of Refractory Metals & Hard Materials*, 2005, 23, pp. 119-127.
10. **Murakami, Y.** *Metal fatigue: Effects of Small Defects and Nonmetallic Inclusions*. UK: Elsevier Science Ltd., 2002.
11. **Czyryca, E. J., Utah, D. A., Cullen, W. H., Majno, L. C., Meyer, R. A., Ritchie, R. O., Stentz, R. H., Williams, R.** *Fatigue Testing*, in ASM handbook. Ninth ed., Vol. 8. USA: American Society for Metals, 1985 pp. 361-436.
12. ASTM E 1823-96 (2002) Standard Terminology Relating to Fatigue and Fracture Testing.
13. **Lawrence, F. V.** *Mechanisms of fatigue crack initiation and growth*. www.mechse.uiuc.edu/media/pdfs/about/research/fcp/2%20Mechanisms.pdf.
14. **Collins, J. A., Daniewicz, S. R.** *Failure Modes: Performance and Service Requirements for metals*, in Handbook of materials selection. New York: John Wiley & Sons, 2002 pp. 705-773.
15. **Loshak, M.** *Strength and durability of hardmetals*. Naukova Dumka, Kiev, 1984 (in Russian).

16. EVS-EN 15156:2006. Advanced technical ceramics - Ceramic composites. Mechanical properties at room temperature - Determination of fatigue properties at constant amplitude.
17. **Roebuck, B.** *Bend strength tests for hardmetals*. VAMAS Technical Report, part 1 and 2. UK: National Physical Laboratory, 1996.
18. **Sglavo, V. M., Green, D. J.** Indentation Determination of Fatigue Limits in Silicate Glasses. *Journal of American Ceramic Society*, 1999, 82, pp. 1269–74.
19. **Mudhopadhyay, A. K.** Indentation fatigue in silicon nitride, alumina and silicon carbide ceramics. *Bulletin of Material Science*, 2001, 24, pp. 105–109.
20. **Guiberteau, F., Padture, N. P., Cai, H., Lawn, B. R.** Indentation fatigue. A simple cyclic Hertzian test for measuring damage accumulation in polycrystalline ceramics. *Philosophical Magazine. A*, 1993, 68, pp. 1003-1016.
21. **Shleinkofer, U., Sockel, H., Schlund, P., Görting, K., Heinrich, W.** Behaviour of hardmetals and cermets under cyclic mechanical loads. *Materials Science and Engineering. A*, 1995, 194, pp. 1-8.
22. **Roebuck, B., Maderud, C. J., Morrell, R.** Elevated temperature fatigue testing of hardmetals using notched testpieces. *International Journal of Refractory Metals & Hard Materials*, 2008, 26, pp. 19-27.
23. **Klaasen, H., Kübarsepp, J.** Wear of advanced cemented carbides for metalforming tool materials. *Wear*, 2004, 256, pp. 846-853.
24. **Shleinkofer, U., Sockel, H., Görting, K., Heinrich, W.** Fatigue of hard metals and cermets – new results and a better understanding. *International Journal of Refractory Metals & Hard Materials*. 1997, 15, pp. 103-112.
25. **Sailer, T., Herr, M., Sockel, H.-G., Schulte, R., Feld, H., Prakash, L. J.** Microstructure and mechanical properties of ultrafine-grained hardmetals. *International Journal of Refractory Metals & Hard Materials*. 2001, 19, pp. 553-559.
26. **Dowling, N. E.** *Mechanical Behavior of Materials: Engineering Methods for Deformation, Fracture, and Fatigue*. Second edition. Prentice-Hall, Inc., New Jersey, 1999.
27. **Smirnov, A.** *Fatigue notch sensitivity of cemented carbides*. Thesis for the degree of Master of Science in Engineering. Tallinn, 2007.
28. **Torres, Y., Anglada, M., Llanes, L.** Fatigue mechanics of WC-Co cemented carbides. *International Journal of Refractory Metals & Hard Materials*, 2001, 19, pp. 341-348.
29. **Schatt, W., Wieters, K.-P.** *Powder Metallurgy: Processing and Materials*. European Powder Metallurgy Association, UK, 1997.

30. **Golovchan, V. T., Litoshenko, N. V.** On the contiguity of carbide phase in WC-Co hardmetals. *International Journal of Refractory Metals & Hard Materials*, 2003, 21, pp. 241–244.
31. **Llanes, L., Torres, Y., Anglada, M.** On the fatigue crack growth behavior of WC-Co cemented carbides: kinetics description, microstructural effects and fatigue sensitivity. *Acta Materialia*, 2002, 50, pp. 2381-2393.
32. **Kursawe, S., Pott, Ph., Sockel, H.-G., Heinrich, W., Wolf, M.** On the influence of binder content and binder composition on the mechanical properties of hardmetals. *International Journal of Refractory Metals & Hard Materials*, 2001, 19, pp. 335-340.
33. **Preis, I.** *Fatigue performance and mechanical reliability of cemented carbides*. Thesis for the degree of Doctor of Philosophy in Engineering. Tallinn, 2004.
34. **Kreimer, H.** *Strength of hardmetals*. Metallurgiya, Moscow, 1971 (in Russian).
35. **Shleinkofer, U., Sockel, H., Görtig, K., Heinrich, W.** Fatigue of hard metals and cermets. *Materials Science and Engineering. A*, 1996, 209, pp. 313-317.
36. CES Selector Version 4.6.1. Granta Design Ltd., Cambridge, 2006.
37. http://en.wikipedia.org/wiki/Fracture_mechanics.
38. **Griffith, A. A.** The phenomena of rupture and flow in solids. *Philosophical Transactions of the Royal Society of London*, 1921, A 221, pp. 163-198.
39. **Foller, M., Meier, H.** A new investigation on mechanical properties of ferro-titanit. *Proceedings of 6th International Conference on Tooling*, Karlstad, Sweden, 2002 pp. 1-15.
40. **Ritchie, R. O.** *Micro-Fracture Mechanics*, in ASM handbook. Ninth ed., Vol. 8. USA: American Society for Metals, 1985 pp. 465-468.
41. **Sherman, D. H.** *Fracture toughness testing using Chevron-notched specimens*, in ASM handbook. Ninth ed., Vol. 8. USA: American Society for Metals, 1985 pp. 469-475.
42. **Ray, K. K., Dutta, A. K.** Comparative study on indentation fracture toughness evaluations of soda-lime-silica glass. *British Ceramic Transactions*, 1999, 98, pp. 165-171.
43. **Li, Z., Ghosh, A., Kobayashi, A. S., Bradt, R. C.** Indentation fracture toughness of sintered silicon carbide in the Palmqvist crack regime. *Journal of American Ceramic Society*, 1989, 72, pp. 904–911.
44. **Torres, Y., Casellas, D., Anglada, M., Llanes, L.** Fracture toughness evaluation of hardmetals: influence of testing procedure. *International Journal of Refractory Metals & Hard Materials*, 2001, 19, pp. 27–34.

45. **Gogotsi, G. A.** Crack resistance of modern ceramics and ceramic composites. I. SEVNB-method. *Powder Metallurgy and Metal Ceramics*, 2004, 43, pp. 371-382.
46. **Rosa, L. G., Amaral, P. M., Anjinho, C., Fernandes, J. C., Shohoji, N.** Fracture toughness of solar-sintered WC with Co additive. *Ceramics International*, 2002, 28, pp. 345-348.
47. **Schubert, W. D., Neumeister, H., Kingler, G., Lux, B.** Hardness to toughness relationship of fine-grained WC-Co hardmetals. *International Journal of Refractory Metals & Hard Materials*, 1998, 16, pp. 133-142.
48. **Inglis, C. E.** Stresses in the plate due to the presence of crack and sharp corners. *Transactions of the Institute of Naval Architects*, 1913, 55, pp. 163-198.
49. **Tchenguisse Miserez, G. A.** *Fracture and toughening of high volume fraction ceramic particle reinforced metals*. Thesis for the degree of Doctor in Science. Lausanne, 2003.
50. **Irwin, G. R.** Analysis of stresses and strains near the end of a crack traversing a plate. *Journal of Applied Mechanics*, 1957, 24, pp. 361-364.
51. **Westgaard, H. M.** Bearing pressures and crack. *Journal of Applied Mechanics*, 1939, 6, pp. 49-53.
52. **Sneddon, I. N.** The distribution of stress in the neighbourhood of the crack in an elastic solid. Proceedings of the Royal Society of London, 1946, A 187, pp. 229-260.
53. **Williams, M. L.** On the stress distribution at the base of a stationary crack. *Journal of Applied Mechanics*, 1957, 24, pp. 109-114.
54. **Fish, J., Yu, Q.** Computational mechanics of fatigue and life predictions for composite materials and structures. *Computer Methods in Applied Mechanics and Engineering*, 2002, 191, pp. 4827-4849.
55. **Taylor, D., Cornetti, P., Pugno, N.** The fracture mechanics of finite crack extension. *Engineering Fracture Mechanics*, 2005, 72, pp. 1021-1038.
56. **Wasiluk, B., Hoshide, T.** The fracture process in elastic-plastic materials under biaxial cyclic loading. *International Journal of Fatigue*, 2003, 25, pp. 221-229.
57. **Torres, Y., Sarin, V. K., Anglada, M., Llanes, L.** Loading mode effects on the fracture toughness and fatigue crack growth resistance of WC-Co cemented carbides. *Scripta Materialia*, 2005, 52, pp. 1087-1091.
58. **Ettmayer, P.** Hardmetals and cermets. *Annual Reviews of Materials Science*, 1989, 19, pp. 145-164.

59. **Shleinkofer, U., Sockel, H.-G., Görtig, K., Heinrich, W.** Microstructural processes during subcritical crack growth in hard metals and cermets under cyclic loads. *Materials Science and Engineering. A*, 1996, 209, pp. 103-110.
60. **Kotoul, M.** Shielding model of fracture in WC-Co. *Materials Science and Engineering. A*, 1997, 234-236, pp. 119-122.
61. **Kübarsepp, J.** *Hard metals with steel binder*. Valgus, Tallinn, 1991 (in Russian).
62. **Upadhyaya, G. S.** *Cemented tungsten carbides: Production, Properties and Testing*. USA: Noyes Publications, 1998.
63. **Klaasen, H., Kollo, L., Kübarsepp, J.** Mechanical properties and wear performance of compression sintered TiC based cermets. *Powder Metallurgy*, 2007, 50, pp. 23-27.
64. **Hussainova, I.** Microstructure and erosive wear in ceramic-based composites. *Wear*, 2005, 258, pp. 357-365.
65. **Pirso, J., Viljus, M., Letunovitš, S.** Friction and dry sliding wear behaviour of cermets. *Wear*, 2006, 260, pp. 815-824.
66. **Sergejev, F.** Thesis for the degree of Master of Science in Engineering. Tallinn, 2003.
67. **Kübarsepp, J., Klaasen, H., Pirso, J.** Behaviour of TiC-based cermets in different wear conditions. *Wear*, 2001, 249, pp. 229-234.
68. **Klaasen, H., Kübarsepp, J.** Structure sensitivity of wear resistance of hardmetals. *International Journal of Refractory Metals and Hard Materials*, 1995, 15, pp. 89-94.
69. **Klaasen, H., Kübarsepp, J., Eigi, R.** Peculiarities of hardmetals wear in blanking of sheet metal. *Tribology International*, 2006, 39, pp. 303-309.
70. **Wu, D., Zhou, J., Li, Y.** Methods for estimating Weibull parameters for brittle materials. *Journal of Materials Science*. 2006, 41, pp. 5630-5638.
71. **Wu, D., Li, G., Jiang, H., Li, Y.** Improved estimation of Weibull parameters with the linear regression method. *Journal of American Ceramic Society*, 2004, 87, pp. 1799–1802.
72. **Wu, D., Zhou, J., Li, Y.** Unbiased estimation of Weibull parameters with linear regression method. *Journal of the European Ceramic Society*, 2006, 26, pp. 1099–1105.
73. **Song, L., Wu, D., Li, Y.** Optimal probability estimators for determining Weibull parameters. *Journal of Materials Science Letters*. 2003, 22, pp. 1651-1653.
74. **Shleinkofer, U., Sockel, H.-G., Schlund, P., Kindermann, P., Schulte, R., Werner, J., Görtig, K., Heinrich, W.** Limited fatigue lives of uncoated and

coated hardmetals under cyclic loads. *Proceedings of European Conference on Advances in Hard Materials Production*. Stockholm, Sweden, 1996 pp. 239-246.

75. **Lisovsky, A. F.** Some speculations on an increase of WC-Co cemented carbide service life under dynamic loads. *International Journal of Refractory Metals & Hard Materials*. 2003, 21, pp. 63-67.

76. **Hershko, E., Mandelker, N., Gheorghiu, G., Sheinkopf, H., Cohen, I., Levy, O.** Assessment of fatigue striation counting accuracy using high resolution scanning electron microscope. *Engineering Failure Analysis*, 2008, 15, pp. 20-27.

LIST OF PUBLICATIONS OF AUTHOR

(not included in the thesis)

V. Sergejev, F., Preis, I., Hussainova, I., Kübarsepp, J. Fatigue mechanics of TiC-based cemented carbides. *Proceedings of the Institution of Mechanical Engineers, Part J: Journal of Engineering Tribology* (accepted for publication).

VI. Klaasen, H., Kübarsepp, J., Preis, I., Sergejev, F., Traksmaa, R. Blanking performance and fatigue endurance of carbide composites. *Proceedings of 10th International Conference of European Ceramic Society*. Berlin, Germany, 2007 (in press).

VII. Sergejev, F., Kübarsepp, J., Preis, I. Application of the Murakami approach for prediction of surface fatigue of cemented carbides. *Proceedings of 2006 Powder Metallurgy World Congress*. Busan, Korea, Part 1, 2006, pp. 633-634.

VIII. Sergejev, F., Preis, I., Kübarsepp, J., Klaasen, H. Cemented carbides surface fatigue prediction using Murakami approach. *Proceedings of European Congress and Exhibition on Powder Metallurgy*. Ghent, Belgium, 2006, pp. 61-66.

IX. Preis, I., Marquis, G., Sergejev, F. Estimation of the endurance limit of cemented carbides based on pore size. *Proceedings of 9th International Fatigue Congress 2006*. Atlanta, USA, 2006.

X. Sergejev, F. Comparative study on indentation fracture toughness measurements of cermets and hardmetals. *Proceedings of European Congress and Exhibition on Powder Metallurgy*. Ghent, Belgium, 2006, pp. 43-48.

XI. Klaasen, H., Kübarsepp, J., Preis, I., Sergejev, F. Fatigue performance of cemented carbides. *Proceedings of European Congress and Exhibition on Powder Metallurgy*. Prague, Czech Republic, 2005, pp. 323-328.

XII. Klaasen, H., Kübarsepp, J., Preis, I., Sergejev, F., Traksmaa, R. Performance of cemented carbides in cyclic loading conditions. *Materials Science (Medžiagotyra)*, 2006, 12, pp. 144-146.

- XIII. Sergejev, F., Preis, I., Klaasen, H. Prediction of fatigue strength of cemented carbides based on Murakami approach. *Proceedings of the 14th International Baltic Conference Materials Engineering 2005*. Kaunas, Lithuania, 2005, p. 42-44.
- XIV. Preis, I., Sergejev, F. Microstructural aspects of fatigue mechanics of hardmetals and cermets. *Macchine Utensili* (2004) July, pp. 66-70.
- XV. Preis, I., Sergejev, F. Failure of brittle materials: Test methods and Weibull modulus. *Proceedings of the 3rd Youth Symposium on Experimental Solid Mechanics*. Porretta Terme (Bologna), Italy, 2004, pp. 115-117.
- XVI. Preis, I., Sergejev, F. Microstructural aspects of fatigue mechanics of hard metals and cermets. *Proceedings of the 2nd Youth Symposium on Experimental Solid Mechanics*. Milano Marittima (Rovenna), Italy, 2003, pp. 123-124.

ABSTRACT

Hardmetals and cermets are widely used as tool materials in machining and forming applications as well as materials for wear components because of their excellent combination of mechanical properties. Time-dependent mechanical degradation of these heterogeneous materials containing natural microstructural defects (pores, non-metallic inclusions or inhomogeneities and etc.) occurs at complex service conditions.

The aims of the present work are to conduct fatigue strength predictions from limited data and to study novel TiC-based cermets (prospective for metal forming) to substitute conventional tungsten based hardmetals. The Murakami prediction approach applied is based on the correlation of various material parameters, such as yield stress (σ_Y), hardness (HV, HRA or HB) with fatigue limit (σ_f) and preexisting crack growth resistance (K_{Ic}).

The theoretical model of surface fatigue prediction is proposed and it is proved experimentally. Fractographical investigations revealed traces of deformation and the size of affected subsurface zone.

Prediction results are in good agreement with fatigue properties received by conventional testing. The performance of some TiC-Fe/Ni cermets in cyclic loading conditions – fatigue, blanking of sheet metal – was analyzed and compared with that of a conventional WC-hardmetal applicable in metal forming. The results of microstructure investigation of cemented carbides are also presented.

Keywords: hardmetals, cermets, fatigue properties, surface fatigue, mechanical reliability, blanking performance.

KOKKUVÕTE

Pulbermetallurgia teel valmistatud kõvasulamid ja kermised on tuntud oma omaduste kõvaduse-sitkuse hea kombinatsiooniga. Neist valmistatakse lõike-, surve- ja stantsimistöötlemise tööriistamaterjale. Kallite WC-Co kõvasulamite kasutamine on põhjendatud kümneid kordi pikema püsivusaja tõttu. Keerulised tsüklilised koormamisskeemid tingivad selliste heterogeensete materjalide mehaanilist degradeerimist.

Kõvasulamite ja kermiste väsimusomaduste prognoosimine (ettearvutamine) on raskendatud neis mikrostruktuursete defektide (poorid, võõrad lisandid, mittemetalsed ühendid jne.) olemasolu tõttu. Kaasaegsed tehnoloogiad ei võimalda valmistada defektita pulbermaterjale, kuid paagutus samaaegse isostaatilise kuumpressimisega (sinter/HIP) vähendab kõvasulamite ja kermiste poorsust ja tõstab nende töökindluskarakteristikuid.

Käesoleva töö eesmärgid:

1. Uurida TiC-baasil kermiste mehaanilisi omadusi, eelkõige väsimustugevust ning funktsionaalsed omadusi lehtmaterjali stantsimisel.
2. Kohandada kõvasulamite ja kermiste väsimusomaduste prognoosimise meetodikat kasutades selleks teraste jaoks väljatöötatud meetodikat nn. Murakami meetodit.
3. Uurida võimalusi pindväsimuse prognoosimiseks (ettearvutamiseks). Pindväsimus on oluline eelkõige stantsimise tööriistamaterjalide püsivuse suurendamiseks.
4. Viia läbi karbiidkomposiitide mikrostruktuurseid uuringuid leidmaks seoseid mikrostruktuursete defektide ja väsimusomaduste vahel. Uurida purunemismehhanismi tsüklilise (väsimus, stantsimine) koormamise tingimustes ja sinter/HIP tehnoloogia mõju sellele.

Töö eksperimentaalses osas uuriti WC- ja TiC-baasil karbiidkomposiitide väsimust ning pindväsimust. Väsimuskatsetes rakendati kolmepunktilist paindeskeemi. Määrati WC-Co ja TiC-Fe/Ni komposiitide paindetugevused ja hinnati Weibulli statistika abil.

Purunenud katsekehi uuriti SEM-ga, et selgitada välja mikrostruktuursete defektide jaotused ja suurused. Statistiliselt analüüsitud andmeid kasutati Murakami meetodikas (mikrostruktuursete defektide kriitiliste suuruste leidmine).

Pindväsimuse prognoosimise teoreetiline meetodika baseerub purunemis- ja kontaktmehaanika arvutusmeetoditel. Katsemasin on konstrueeritud ja valmistatud TTÜ-s. Katsete tulemused kinnitavad teooria õigsust.

Teostati funktsionaalsed katsed stantsimissoorituse ja adhesioonkulumiskindluse määramiseks. Katsete tulemused on heas korrelatsioonis

väsimuskatsetuste tulemustedega. Teostati röntgenstruktuursed (XRD) uuringud seose leidmiseks kõvasulamite ja kermiste töövõime ja struktuuri vahel. Selgitati välja materjalide purunemismehhanismi erisused ja iseloom tsüklilisel ja monotoonsel koormamisel.

Peamised järeldused on alljärgnevad:

1. Staatiliste testimise tulemustest on näha, et kõvasulamites ja kermistes sideaine sisaldus määrab paindetugevuse ja purunemise iseloomu. Üks trend kehtib mõlema materjali jaoks – mida suurem on sideaine sisaldus, seda metalsem on komposiidi käitumine purunemisel. Sideaine mahulised sisaldused on kõvasulamites S13 ja H15 umbes samad kui kermistes T70/14 ja ST75/14 vastavalt;
2. Sideaine sisaldus avaldab mõju väsimusomadustele. Ta määrab nii väsimustugevuse kui ka väsimuskõvera kalde. Suurema sideaine sisalduse juures on väsimustugevus suurem, kalle ja sellest tulenevalt ka väsimustundlikus ja tulemuste hajuvused on väiksemad. Nii sugune käitumine on iseloomulik nii kõvasulamitele kui ka kermistele. Siin tuleb arvestada sellega et ST75/14 on valmistatud sinter/HIP tehnoloogia abil;
3. Esmakordselt on TiC-basil kermiste jaoks väsimustugevuse alampiiri ettearvutamisel on kasutatud Murakami meetodit. Tulemused on kooskõlas kolmepunktiliste väsimuskatsete tulemustega;
4. Pindväsimusel materjalide käitumise suundumused on samad kui väsimusel kolmepunktilise paindega. Sideaine sisaldus määrab kõvasulamite ja kermiste pindväsimuse omadused;
5. Funktsionaalsete testide tulemused lihtsustamisel on võimalik seostada materjali käitumisega väsimuse ja adhesioonkulumise tingimustes. Suurema töövõimega kermetit (ST75/14) iseloomustab kõrgem vastupanu adhesioonkulumisele ja väiksem väsimustundlikus;
6. Tsüklilistel koormustel karbiidkomposiitide faaside (sh karbiidne faas) plastsus väheneb. Plastsuse vähenemine (hapruse suurenemine) tsüklilistel koormustel monotoonse koormamisega värreldes on iseloomulikum volframkarbiidkõvasulamitele titaankarbiidkermistega võrreldes.

Märksõnad: kõvasulamid; kermised; väsimus omadused; pindväsimus; mehaaniline usaldusväärsus; stantsimissooritus.

PUBLICATIONS

Paper I

J. Kübarsepp, H. Klaasen and F. Sergejev.

Performance of cemented carbides in cyclic loading wear conditions. *Materials Science Forum* 2007, Vols. 534-536, pp. 1221-1224.

Performance of Cemented Carbides in Cyclic Loading Wear Conditions

J. Kübarsepp^a, H. Klaasen^b and F. Sergejev^c

Department of Materials Engineering, Tallinn University of Technology,

Ehitajate tee 5, 19086, Tallinn, ESTONIA

^{a,b} e-mail: jakob.kubarsepp@ttu.ee

^c e-mail: fjodor.sergejev@ttu.ee

Keywords: hardmetal, cermet, cemented carbide, wear, fatigue, blanking performance

Abstract. The present study describes the wear and mechanical behaviour of some carbide composites (TiC-base cermets and WC-base hardmetals) in cyclic loading applications (blanking of sheet metal). Adhesive wear as well as fatigue endurance were tested, followed by XRD measurements. The results show that the blanking performance of a carbide composite is dependent on its level of resistance to adhesion wear and fatigue sensitivity. XRD measurement revealed that fatigue damage is preceded by plastic strain in both the ductile binder and the brittle carbide phase.

Introduction

Tungsten-base hardmetals are the most widely used wear resistant composites because of their excellent combination of wear resistance and strength [1]. TiC-base cermets (tungsten-free hardmetals) have proved to be very useful in certain applications because of their fair specific strength and meritous physical properties [2, 3].

This paper focuses on the mechanical and tribological behavior of some advanced TiC-base cermets in terms of their performance as tool materials for cyclic loading (blanking) applications. Another important aim is to identify any correlation that might exist between blanking performance on the one hand and fatigue endurance and adhesive wear resistance on the other hand.

Experimental Procedure

Table 1 shows the advanced TiC-base cermets, the performance of which was tested in complicated wear conditions (in relation to ordinary WC-hardmetal H15).

Table 1. Structural characteristics, hardness HV and transverse rupture strength R_{TZ} of composites

No	Grade	Carbide [wt%]	Binder composition, structure	HV [GPa]	R_{TZ} [GPa]
1	H15	85	Co(W)	1.15	2.9
2	T70/14	70	Fe+14Ni steel, austenite	1.25	2.2
3	T60/8	60	Fe+8Ni steel, martensite-bainite	1.20	2.3

The durability test procedure was similar to that of in service functional procedures – blanking of grooves into electrotechnical sheet steel (thickness $t = 0.5$ mm, proof stress $R_{co,2} = 1600$ N/mm²) in a 3-position (reinforced with alloys – in Table 1) die. Durability was evaluated by the side wear Δ of the dies after the intermediate service time of 0.5×10^6 strokes [4]. Fatigue tests resembled those for the bending fatigue – fatigue of specimens 5x5x15 mm under repeated (frequency 35 Hz) transverse bending load [5]. The wear performance of alloys was studied in the cutting adhesive

wear conditions [3], where the wear resistance L_1 was determined as the length of the cutting path (by turning mild steel at low speed) when wear track at the tool (specimen) nose reaches $h = 1\text{mm}$.

After the above tests were completed, XRD studies were performed on the diffractometer Bruker D5005. A decrease in the intensity ΔI of the X-ray reflection lines from carbides (as a measure of local plastic strain) was determined.

Results and Discussion

In the case of the functional tests, the wear contours of cutting edges (and side wear Δ) of carbide tools refer to an obvious superiority of the TiC-cermet with Ni-steel binders (grade T70/14) over an ordinary WC-base hardmetal (grade H15) (Fig.1) and TiC-cermet (grade T60/8).

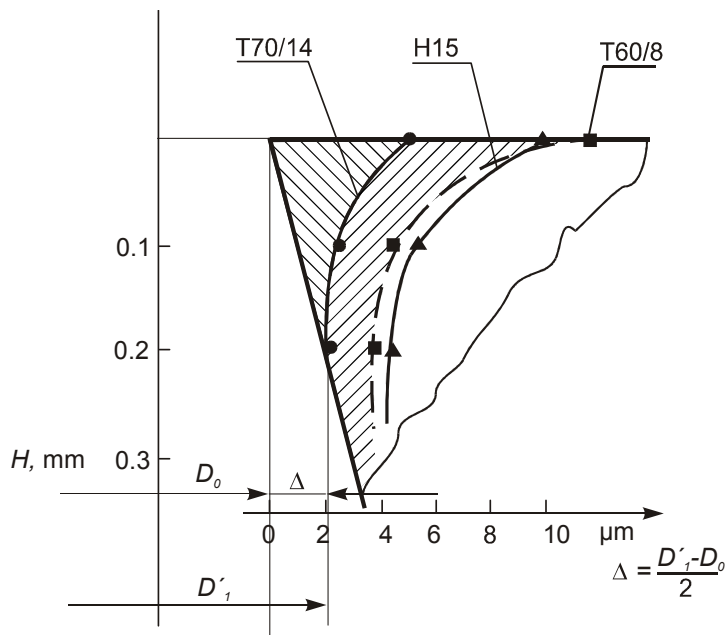


Fig.1. Wear contours of cutting edge of dies from different cemented carbides

The results of adhesive wear trials (wear curves $h - L$, Fig.2) confirms the superiority of grade T70/14 over H15 and T60/8.

From the results of the fatigue tests (Wöhler curves), we can make an unusual observation in connection with H15 in the behavior of grade T70/14 characterized by lower fatigue sensitivity (Fig. 3). The fatigue sensitivity of an alloy is indicated by the decrease in the intensity in the fatigue strength, ΔS_m , with increasing loading cycles, N (the slope of its Wöhler curve).

The results of the present study (Figs.1–3 and Table 2) show that there exist a positive correlation between cemented carbide blanking performance and its fatigue sensitivity (factor $\Delta S = S_{m7} - S_{m3}$) and adhesive wear resistance L_1 .

In addition, SEM results show that the plastic strain (onset of failure) of cemented carbides in the case of static and cyclic loading starts and that it takes place mainly in the ductile binder [6, 7]. Based on the results of XRD studies (Table 3) it can be concluded that the fracture of carbide composites during cyclic loading propagates in their carbide phase and is preceded by local plastic strain. This means that the ability of a carbide composite to undergo plastic strain, that is, its ability to absorb fracture energy by local plastic strain, depends on the plasticity of both the ductile binder and the “brittle” carbide-phase. The results in Table 3 show that the ability of the carbide phase to undergo local plastic strain depends on the loading mode. Cyclic loading results in a decrease of carbide ability to strain plastically in relation to monotonic loading (measures $c = I_o/I_c$ and $m = I_o/I_m$).

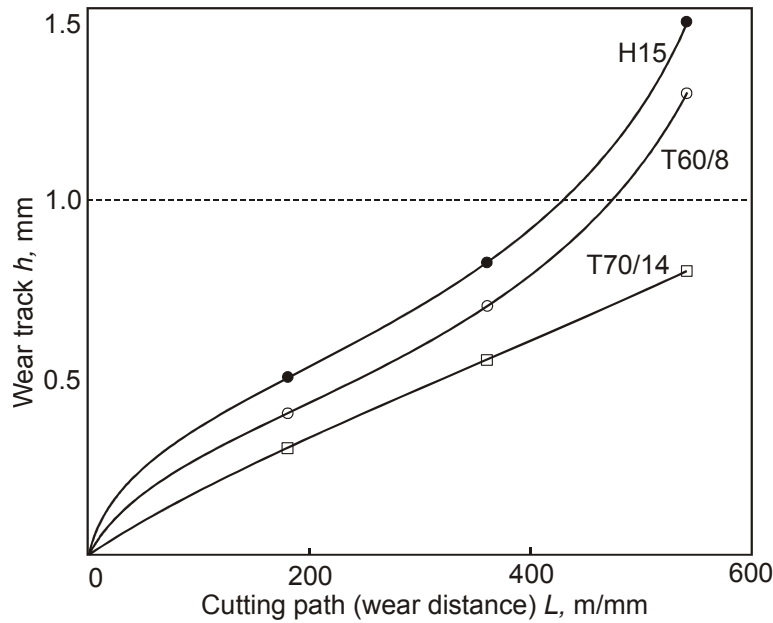


Fig.2. Wear kinetics (curves) of carbide composites

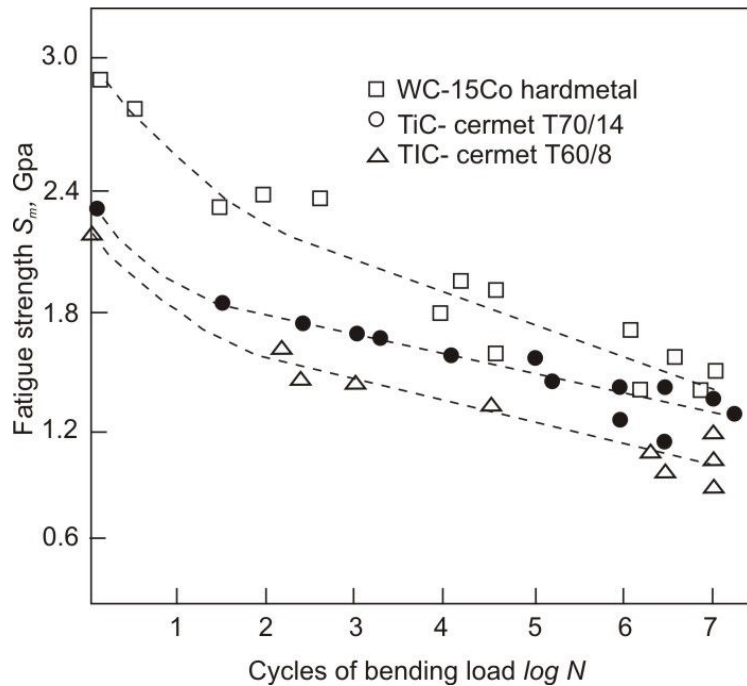


Fig.3. Wöhler curves of carbide composites

Table 2. Performance characteristics of carbide composites: N/Δ -blanking performance, ΔS – fatigue sensitivity ($\Delta S = S_{m7} - S_{m3}$, where S_{m7} and S_{m3} – fatigue strength at 10^7 and 10^3 loading cycles, respectively), L_1 – adhesive wear resistance, R_{TZ} – transverse rupture strength, HV – hardness.

Grade	HV [GPa]	R_{TZ} [GPa]	$N/\Delta \cdot 10^6$ [strokes/mm]	ΔS [GPa]	L_1 [m/mm]
T70/14	1.25	2.2	180	0.35	590
H15	1.15	2.9	120	0.55	430

The extent of embrittlement is distinct for both carbides – WC and TiC. It can be seen that the plasticity of TiC in monotonic loading is less than that of WC ($m_{TiC} < m_{WC}$). However, in the cyclic loading conditions, TiC in cermet shows similar level of plasticity with that of WC. It means that

rate of decrease in plasticity (embrittlement) during the cycling loading of tungsten carbide (measure m/c) exceeds that of titanium carbide (4.0 versus 1.5 as shown in Table 3).

A higher resistance of composite phases (binder and carbide) due to decrease in plasticity in the cyclic loading conditions appears to result in a higher resistance of the composite to fatigue damage (lower fatigue sensitivity, lower slope of Wöhler curve). The superiority (higher blanking performance) of the advanced TiC-base cermet T70/14 in relation to the ordinary WC-hardmetal appears to be a result of its higher resistances to adhesive wear and fatigue damage.

Table 3. Decrease in the intensity of lines of X-ray reflections from the carbide phase of cemented carbides tested: I_o , I_m , I_c – intensities before and after monotonic (m) and cyclic (c) loadings, respectively

Grade	Carbide, line	Intensity, Lin [Cps]			Decrease in intensity		Embrittlement m/c
		I_o	I_m	I_c	$m = \frac{I_o}{I_m}$	$c = \frac{I_o}{I_c}$	
H15	WC, [001]	51	8	32	6.4	1.6	4.0
T70/14	TiC, [200]	78	37	57	2.1	1.4	1.5

Conclusions

Based on the results of our experiments, the following conclusions could be drawn.

- The blanking performance of a carbide composite is controlled by its adhesive wear resistance and fatigue sensitivity (slope of Wöhler curve).
- Surface failures of a carbide composite in the cyclic loading wear conditions (blanking and fatigue) start in the binder and propagate in the carbide phase, and are preceded by local plastic strain that can be observed in both the ductile binder and the brittle carbide.
- In cyclic loading, the plasticity of composites phases (in particular carbide phase) decreases.
- The lesser decrease in plasticity that occur in the carbide composite phases reduces the fatigue sensitivity of the composite.

References

- [1] K.J.Brookes: *World Dictionary and Handbook of Hardmetals and Hard Materials*, (International Carbide data, London, UK,1996).
- [2] M. Foller and H. Mayer, in: *Proc. 6th Int. Conf. on Tooling*, Karlstadt, Sept., (2002), p.180-220.
- [3] H.Klaasen and J.Kübarsepp: *Int. J.Refract. Met. Hard Mater. Vol 15 (1997)*, pp. 89 – 96.
- [4] H.Klaasen and J.Kübarsepp: *WEAR Vol. 256 (2004)*, pp.846-854.
- [5] H.Klaasen, J.Kübarsepp and I.Preis, in: *Proc. European Conf. "Hard Materials and Diamond Tooling 2002*(European Powder Metallurgy Assoc., UK, 2002), pp.240 -246.
- [6] H.Reshetnyak (H.Klaasen) and J.Kübarsepp: *Powder Metallurgy, Vol.41/3 (1998)*, pp.211-216.
- [7] H.Schleinkofer, H.Sockel and K.Görting: *Int. J.Refract. Met.Hard Mater. Vol.15 (1997)*, pp. 103-112.

Paper II

Sergejev, F., Preis, I., Klaasen, H., Kübarsepp, J.

Murakami approach: Fatigue strength prediction of cemented carbides by considering pores to be equivalent to small defects. *Proceedings of European Congress and Exhibition on Powder Metallurgy*. Prague, Czech Republic, 2005, pp. 335-340.

Murakami Approach: Fatigue Strength Prediction of Cemented Carbides by Considering Pores to be Equivalent to Small Defects

Fjodor Sergejev*, Irina Preis, Heinrich Klaasen, Jakob Kübarsepp

Tallinn University of Technology, 19086 Tallinn, Ehitajate tee 5, Estonia

** Corresponding author. Tel.: +372-620-33-55; fax.: +372-620-31-96. E-mail address: Fjodor.Sergejev@ttu.ee (F. Sergejev)*

Abstract: A lot of investigations have been conducted to clarify fatigue mechanisms and to identify the crucial controlling factors of this process. High structure sensitivity of fatigue, relevance of binder strength (its structure and composition) on fatigue properties of PM materials is widely known. Appearance of structural defects and inhomogeneities, such as pores, non-metallic inclusions and etc. is marginal for material selection. The new technique developed by Y. Murakami for the prediction of lower bound of the fatigue limit of materials was firstly applied for WC-Co hardmetal (H15) and TiC-based cermets (T60/8 and T70/14). The fatigue properties were correctly predicted by considering the maximum occurring pore size using the statistics of extremes. The Vicker's hardness of binders (as main responsible for the fracture mechanism) and geometrical parameter of maximum area of structural defect were assumed to be the basis of such calculations. The results of this procedure showed excellent convergence with experimental data received from previous testing procedures of fatigue tests.

Keywords: hardmetals; cermets; fatigue limit; Murakami model (extreme value statistics); microstructure; Vicker's hardness.

1. INTRODUCTION

Prediction of the materials fatigue limit from limited information is the main aim for many researchers. Various material parameters such as yield stress (σ_Y), ultimate tensile stress (σ_U), and hardness (HV, HRA or HB), may be correlated with fatigue limit (σ_f) or threshold stress intensity factor range (ΔK_{th}) [1-5]. These investigations avouch high structure sensitivity of fatigue of cemented carbides ("structurally brittle" materials). Irreversible microscopic changes (micro-crack formation, phase transformation, phase boundary sliding and pore nucleation during manufacturing and fatigue processes) occur, analogous to the irreversible sliding processes during the fatigue of ductile materials. In addition different processes, caused by crack closure, crack bridging, and friction of opposite crack surfaces, have an influence on the fatigue crack growth.

The main goal of present study is to find coalescence between fatigue properties and structure of materials, because structural defects are essential for PM materials. Structural defects and inhomogeneities can appear in shape of pore, non-metallic inclusion, chemical composition, surface and natural defects, and etc. It is most difficult to define defects number or size due to their variety. Traditional theories of defects effect evaluation are based on stress concentration factors and are applicable to defects larger than ~1 mm. However, as defect size decreases, these theories become invalid [6-8].

In present work Murakami method was applied for the first time for hardmetals and cermets to evaluate quantitatively the effects of defects on the fatigue strength and threshold stress intensity factor. The estimate of this prediction has been done by analyzing the pore

sizes using the statistics of extremes. The results of equating the lower band of scatter of endurance limit (σ_n) and threshold stress intensity factor range (ΔK_{th}) on the basis of binder Vicker's hardness (HV) and geometric parameter \sqrt{area}_{max} showed its excellent convergence with experimental data received from both testing procedures standard fatigue tests and accelerated fatigue ones [1, 9, 10].

2. MATERIALS AND DEFECTS RATING PROCEDURE

The Murakami method (1983) was applied to make prediction of maximum inclusion size and lower limit (σ_n) of the fatigue strength and threshold stress intensity factor range (ΔK_{th}) for WC-Co hardmetal (H15) and TiC-based cermets with Fe/Ni steel binder (T60/8 and T70/14). Mechanical properties and composition of tested cemented carbides (at ambient temperature) are given in Table 1.

Material	H15	T70/14	T60/8
WC content, wt%	85	-	-
TiC content, wt%	-	70	60
Binder composition and structure	Co	Fe/14wt% Ni austenite	Fe/8wt% Ni martensite
Carbide average grain size, μm	2,1	2,0-2,4	2,2
Hardness, HRA	87,5	88,5	87,5
Transverse rupture strength, R_{TZ} (GPa)	2,7	2,4	2,2
Young's modulus, E (GPa)	600	410	-
Hardness of binder, HV	175	366,5	293

Table 1. General data and mechanical properties of tested materials [9-13]

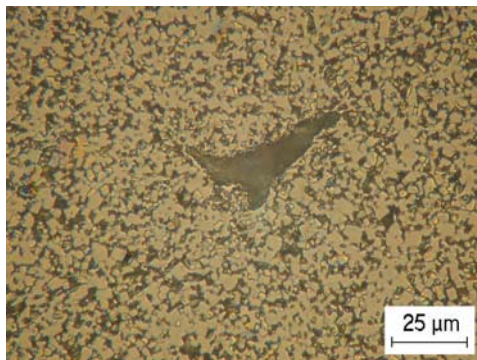


Fig. 1. Sample of SEM images of the inspection area for hardmetal H15

Specimens were produced through conventional press and sinter powder metallurgy by Laboratory of Powder Metallurgy of Tallinn University of Technology (according to ASTM B406). After standard and accelerated fatigue tests (3PB – three point bending schema, R3a) were performed a section perpendicular to the maximum normal stress was cut from the specimen and examined with scanning electron microscope (SEM).

SEM pictures of the inspection areas were made on JEOL JSM840a apparatus, see Fig. 1.

Defects areas were measured by means of transporting the SEM images of samples into AutoCAD interface (see Figs. 2), and resulted in the calculation and rating of the size of the defect areas.

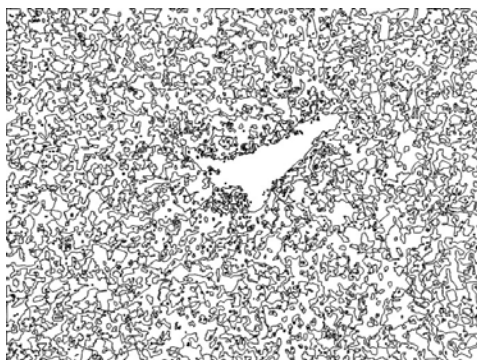
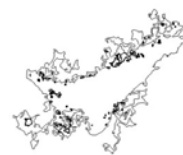


Fig. 2. Images of area of defects imported to AutoCAD for the defect area calculation (X1000)



Prediction of the lower bound of fatigue limit and evaluation of threshold stress intensity factor range were conducted with acceptance that hardness (Vicker's hardness - HV) of binder is main responsible fracture characteristic

Vicker's hardness of binder was measured on Bühler Micromet 2001 apparatus.

Finally, results of lower limit of fatigue strength prediction were compared with previous experimental data received from both testing procedure of standard fatigue tests and accelerated fatigue ones.

Calculations of threshold stress intensity factor range were collated with computations of ΔK_{th} according to model proposed by Torres, Anglada and Llanes [2, 5].

3. RESULTS AND DISCUSSIONS

3.1 Prediction of the lower limit of the fatigue strength

Arrangement of defects regarding free surface is: on the surface, just below surface and interior (invisible). Equations proposed by Murakami are [1]:

for surface defect

$$\sigma_w = 1,43(HV + 120)/(\sqrt{area_{max}})^{1/6}, \quad (1)$$

for defect just below surface

$$\sigma_w = 1,41(HV + 120)/(\sqrt{area_{max}})^{1/6}, \quad (2)$$

for interior defect

$$\sigma_w = 1,56(HV + 120)/(\sqrt{area_{max}})^{1/6}, \quad (3)$$

where HV – Vicker's hardness, kgf/mm^2 ;

$\sqrt{area_{max}}$ - square root of the maximum size defect area, μm .

Defects inspection items are shown in Tables 2-4 for hardmetal H15, cermets T60/8 and T70/14 correspondingly.

Maximum defects distribution		
$\sqrt{area_{max}} = a \cdot y + b = 33,006y + 55,665$		
Prediction of $\sqrt{area_{max}}$		
*S (mm^2)	T	$\sqrt{area_{max}}$ (μm)
1	7,44	119,552
10	74,41	197,682
100	744,01	273,883
Prediction of lower bound of the scatter of the fatigue strength		
for surface defects, MPa	for defects just below surface, MPa	for interior defects, MPa
$\sigma_{f1}=598$	$\sigma_{f1}=590$	$\sigma_{f1}=652$
$\sigma_{f10}=550$	$\sigma_{f10}=542$	$\sigma_{f10}=600$
$\sigma_{f100}=521$	$\sigma_{f100}=513$	$\sigma_{f100}=568$

* - the area of prediction

Table 2. Defects inspection items for H15 hardmetal

Maximum defects distribution		
$\sqrt{area}_{max} = a \cdot y + b = 35,232y + 9,392$		
Prediction of \sqrt{area}_{max}		
*S (mm ²)	T	\sqrt{area}_{max} (μm)
1	1542,44	268,023
10	15424,44	349,158
100	154244,47	430,283
Prediction of lower bound of the scatter of the fatigue strength		
for surface defects, MPa	for defects just below surface, MPa	for interior defects, MPa
$\sigma_{f1}=735$	$\sigma_{f1}=725$	$\sigma_{f1}=802$
$\sigma_{f10}=703$	$\sigma_{f10}=693$	$\sigma_{f10}=767$
$\sigma_{f100}=679$	$\sigma_{f100}=670$	$\sigma_{f100}=741$

* - the area of prediction

Table 3. Defects inspection items for T60/8 cermet

Maximum defects distribution		
$\sqrt{area}_{max} = a \cdot y + b = 74,516y - 5,765$		
Prediction of \sqrt{area}_{max}		
*S (mm ²)	T	\sqrt{area}_{max} (μm)
1	1542,44	541,244
10	15424,44	712,846
100	154244,47	884,428
Prediction of lower bound of the scatter of the fatigue strength		
for surface defects, MPa	for defects just below surface, MPa	for interior defects, MPa
$\sigma_{f1}=771$	$\sigma_{f1}=760$	$\sigma_{f1}=841$
$\sigma_{f10}=736$	$\sigma_{f10}=726$	$\sigma_{f10}=803$
$\sigma_{f100}=710$	$\sigma_{f100}=700$	$\sigma_{f100}=775$

* - the area of prediction

Table 4. Defects inspection items for T70/14 cermet

The results of equating the lower bound of scatter of fatigue strength (H15 - $\sigma_{w1} \approx 590$ MPa; T60/8 - $\sigma_{w1} \approx 725$ MPa; T70/14 - $\sigma_{w1} \approx 760$ MPa) showed its excellent convergence with experimental data received from both the standard (H15 - $\sigma_{f,min} \approx 720$ MPa; T60/8 - $\sigma_{f,min} \approx 815$ MPa; T70/14 - $\sigma_{f,min} \approx 900$ MPa) and accelerated (H15 - $\sigma_f \approx 500$ MPa; T60/8 - $\sigma_f \approx 620$ MPa; T70/14 - $\sigma_f \approx 550$ MPa) testing procedures [9, 10, 12-14].

3.2 Evaluation of threshold stress intensity factor range

Materials having higher Vicker's hardness show higher values of threshold stress intensity factor ΔK_{th} . However, the trends cannot be expressed in a simple form, such as $\Delta K_{th} \propto HV$. Murakami proposed following equation [1]:

$$\Delta K_{th} = C_1(HV + C_2)(\sqrt{area}_{max})^{1/3}, \quad (4)$$

where C_1 – material independent constant, $C_1 = 3,3 \times 10^{-3}$;

C_2 – material independent constant, $C_2 = 120$;

Results of calculations are compared with threshold characteristics (K_{th}) quantified by equation proposed by Y. Torres, M. Anglada and L. Llanes, 2001, are given in table 5.

Tested grades	Fracture toughness, K_{IC} ($\text{MPa}\cdot\text{m}^{-1/2}$)	Threshold stress intensity factor, K_{th} ($\text{MPa}\cdot\text{m}^{-1/2}$)	Threshold stress intensity factor range, ΔK_{th} ($\text{MPa}\cdot\text{m}^{-1/2}$)
H15	17,0	9,6	7,5
T60/8	14,1	7,9	9,9
T70/14	17,5	11,9	14,8

Table 5. Threshold characteristics of examined materials [2, 11, 14]

4. CONCLUSIONS

1. The new technique developed by Murakami (1983) for the prediction of the lower bound of endurance limit of WC-based hardmetal (H15 - 85wt% WC and 15wt %Co) and TiC-based cermet (T60/8 – 60wt %TiC and Fe/8wt% Ni and T70/14 – 70wt %TiC and Fe/14wt% Ni) was applied.
2. The results of inclusion rating and correlations with the fatigue limit procedures showed excellent convergence with experimental data received from both testing procedure of standard fatigue tests and accelerated fatigue ones.
3. Threshold stress intensity factor range (ΔK_{th}) values calculated by equations proposed by Murakami are in agreement with results received from previous works.
4. A good correlation between the proposed geometrical parameter \sqrt{area}_{max} and lower limit of the fatigue strength and threshold stress intensity factor range of hardmetals and cermets has been demonstrated. Applied method is suggested as a reliable measure of the resistance of hardmetals to fracture, for material selection as well as for quality assurance.

Acknowledgments

This work was supported by the Estonian Ministry of Education and Science and the Estonian Science Foundation grant T-505.

REFERENCES

1. Fatigue of metals. Y. Murakami, Elsevier Science Ltd., London, UK, 2002.
2. **Torres, Y., Anglada, M., Llanes, L.** Fatigue mechanics of WC-Co cemented carbides *International Journal of Refractory Metals and Hard Materials* 19 2001: pp. 341 – 348.
3. Fatigue of materials. S. Suresh, Cambridge University Press,. 1991.
4. Strength and durability of hardmetals. M. Loshak, Naukova Dumka, Kiev, 1984 (in Russian).
5. **Llanes, L., Torres, Y., Anglada, M.** On the fatigue crack growth behavior of WC-Co cemented carbides: kinetics description, microstructural effects and fatigue sensitivity *Acta Materialia* 50 2002: pp. 2381 – 2393.
6. **Shleinkofer, U., Sockel, H.-G., Götling, K., Heinrich, W.** Fatigue of hardmetals and cermets – new results and better understanding *International Journal of Refractory Metals and Hard Materials* 15 1997: pp. 103 – 112.
7. **Shleinkofer, U., Sockel, H.-G., Götling, K., Heinrich, W.** Microstructural processes during subcritical crack growth in hard metals and cermets under cyclic loads *Materials Science and Engineering* A209 1996: pp. 103 – 110.
8. **Shleinkofer, U., Sockel, H.-G., Götling, K., Schlund, P., Heinrich, W.** Behaviour of hard metals and cermets under cyclic mechanical loads *Materials Science and Engineering* A194 1995: pp. 1 – 8.

9. Fatigue performance and mechanical reliability of cemented carbides. I. Preis, Dissertation for the degree of Doctor of Philosophy in Engineering, TUT Press, 2004.
10. **Preis, I.** Statistical strength of brittle materials: test methods and Weibull modulus. *Proceedings of 3rd International Conference of DAAM*, Tallinn, Estonian Republic. 2002: pp. 205 – 208.
11. **Reshetnyak, H., Kübarsepp, J.** Resistance of hardmetals to fracture *Powder Metallurgy*, Vol. 41 1998: pp. 211 – 216.
12. **Klaasen, H., Kübarsepp, J., Preis, I.** Wear behaviour, durability and cyclic strength of TiC-based cermets *Materials Science and Technology*, 20 2004: pp. 1006 – 1010.
13. **Klaasen, H., Kübarsepp, J., Preis, I.** Toughness and durability of cemented carbides *Proceedings of the International Conference on deformation and fracture of structural PM materials, September 2002*, Košice, Slovak Republic. – IMR SAS – European Powder Metallurgy Association, Vol. 1 2002: pp. 77 – 83.
14. Fatigue behavior of powder metallurgy heterogeneous materials. F. Sergejev, Thesis for the degree of Master of Science in Engineering, TUT Press, 2003.

Paper III

Fjodor Sergejev and Maksim Antonov.

Comparative study on indentation fracture toughness measurements of cemented carbides. *Proceedings of the Estonian Academy of Sciences, Engineering*, 2006, Vol. 12, pp. 388–398.

Comparative study on indentation fracture toughness measurements of cemented carbides

Fjodor Sergejev and Maksim Antonov

Department of Materials Engineering, Tallinn University of Technology, Ehitajate tee 5, 19086 Tallinn, Estonia; Fjodor.Sergejev@ttu.ee

Received 2 June 2006, in revised form 10 November 2006

Abstract. Majority of the fracture toughness studies of metallic materials typically use the Chevron notch technique, compact specimens and round notched tensile specimens. These methods require considerable time for sample preparation and for the notch geometry control. Only a few of them can be applied for cemented carbides due to the very high brittleness of the hard phase. This is why various indentation fracture toughness (IFT) techniques have been developed [^{1,2}], which are more rapid and simple. Indentation toughness measurements results depend critically on the assumption about the crack type (Palmqvist or median/radial cracks), on the equations used for the calculation of fracture toughness and on the material-dependent and material-independent constants [³]. In the present work a comparative study of IFT calculation methods was carried out to find a reliable technique for studied materials (WC-Co, TiC-Fe/Ni). Several IFT equations for ceramic materials, recommended by standards and publications, were used for the evaluation of the fracture toughness and compared with published conventional fracture toughness data [^{4,5}]. Only few of the equations give reliable estimation of the fracture toughness of cemented carbides.

Key words: cermets, hardmetals, fracture toughness, indentation, Palmqvist crack, Vickers hardness.

1. INTRODUCTION

In discussions on the hardness and toughness of hardmetals (WC-based) and cermets (TiC-based), it is always assumed that the higher the hardness of the composite material, the lower the fracture toughness, and vice versa. Although this principle is valid in general, a lot of specific aspects must be considered.

The measurements of fracture toughness of cemented carbide are complicated because of very high brittleness of these materials. Sample preparation is time-consuming and expensive. Methods, based on single edge notched beam (SENB, ASTM STP 1419), single edge precracked beam (SEPB, ISO 15732), the single

edge V-notched beam (SEVNB, CEN/TS 14425-5:2004), Chevron notched beam, surface crack in flexure (CNB and SCF, ASTM C1421-01b) and other conventional techniques require very precise notch geometry control. Results crucially depend on the surface preparation and on the state of residual stresses.

On the other hand, the indentation fracture toughness technique is much easier to conduct. There is no need for the preparation of the specimens with special geometry and complex notches. Method involves measurements of the lengths of the cracks, which emanate from the corners of Vickers indentation diagonals, of the applied indentation load and of a few material properties such as elasticity modulus and Poisson's ratio. This method is basically used for the measurement of mechanical properties of glasses and ceramics.

The main restrictive factor of the adaptation of IFT for cemented carbides is very high hardness of WC-Co and TiC-Fe/Ni cermets. These materials tend to crack only at elevated loads. This complicates cracks length measurements and makes hardly possible to define the crack formation model [^{6,7}] (Fig. 1). These difficulties led to deviations in the calculation results.

In this paper we compare different IFT measurement methods for cemented carbides.

2. EXPERIMENTAL PROCEDURE

Mechanical properties and composition of the studied materials are listed in Table 1. All cemented carbides were produced with conventional press and sinter powder metallurgy according to ASTM B406 at the Powder Metallurgy Laboratory of the Tallinn University of Technology. The cemented carbide specimens were prepared to the following dimensions (width \times height \times length): WC-Co grade – $(5.0 \pm 0.3) \times (5.0 \pm 0.3) \times 19$ and TiC-based ones – $(5.0 \pm 0.3) \times (5.0 \pm 0.3) \times 16$, mm³. Specimens were ground to a surface finish of about 1.5 μ m for WC-Co hardmetals and 2.5 μ m for TiC-base cermets on four sides (measured along 8 mm of the specimen by the Surtronic 3+ apparatus, using CR filter). Opposite ground faces were parallel within 0.03 mm.

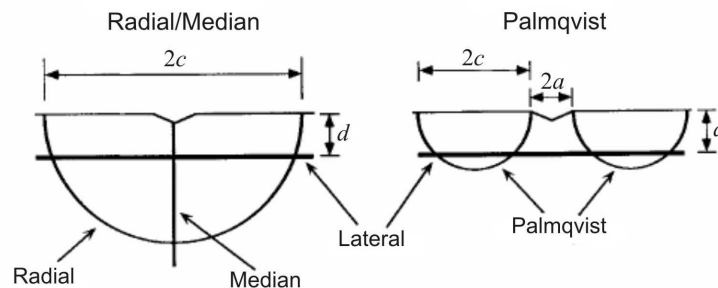


Fig. 1. Principal scheme of the indentation crack geometry.

Table 1. Mechanical properties of the tested materials

Grade	Carbide, wt%	Binder composition, structure	Poisson's ratio	Vickers hardness, H_V	Elasticity modulus E , GPa
WC10	90	Co(W)	0.23*	1310	551
WC15	85	Co(W)	0.23*	1126	508
TiC70/14	70	Fe + 14Ni steel, austenite	0.23*	1268	398
TiC60/8	60	Fe + 8Ni steel, martensite-bainite	0.22*	1122	423

Values marked * are estimates. Source: CES 2005 Edupack.

Hardness and IFT tests were carried out on the INDENTEC 5030 SKV at 5 different loads P between 2.5 and 50 kgf at an indentation duration 10 s. Additional universal hardness tests were produced on the Zwick Z2.5 apparatus at loads of 10, 30 and 50 kgf for the evaluation of the elasticity modulus E . Elasticity modulus was calculated according to the ISO 14577-1:2002 standard (Metallic materials – Instrumented indentation test for hardness and materials parameters).

The values of average indentation diagonals (Fig. 2) were obtained from at least six readings at each load level. The lengthening of cracks was observed with the increase of the applied indentation load (Fig. 3). Estimates of fracture toughness values were made at two different load P levels of 30 and 50 kgf for WC10, WC15 and T60/8 cemented carbides, and at 5 load levels 2.5, 5.0, 10.0, 30.0 and 50.0 kgf for the T70/14 cermet. Optical investigation has shown that maximum available magnitude of the microscope ($\times 100$) was not sufficient for crack length measurement in hardmetals WC10 and WC15 at loads lower than 30.0 kgf. Some expressions for the determination of fracture toughness have limited applicability.

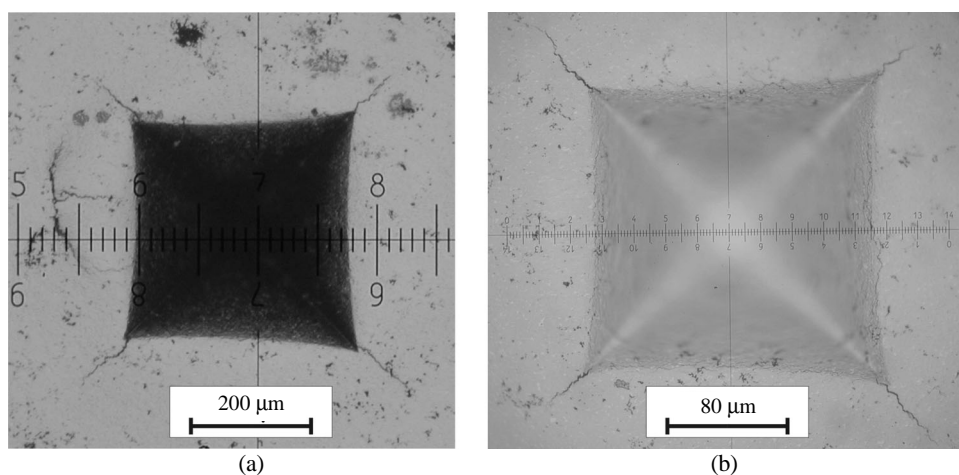


Fig. 2. Photographs of Vickers indentations of the T70/14-70 wt% TiC (a) and Fe-14 wt% Ni cermets.

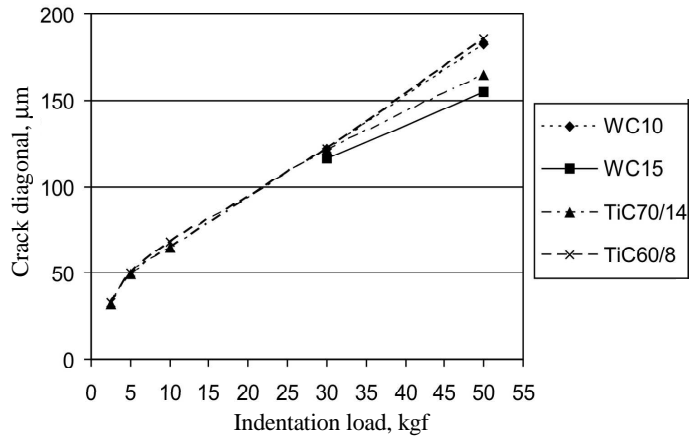


Fig. 3. Dependence of the crack diagonal length on the indentation load.

3. RESULTS AND DISCUSSION

For IFT calculations it is recommended to take into account the true (load-independent) hardness of the material [1,8]. It is well known that the apparent hardness decreases with the increase of the indentation load and approaches a constant value at a relatively high load level (Fig. 4). Measured Vickers hardness

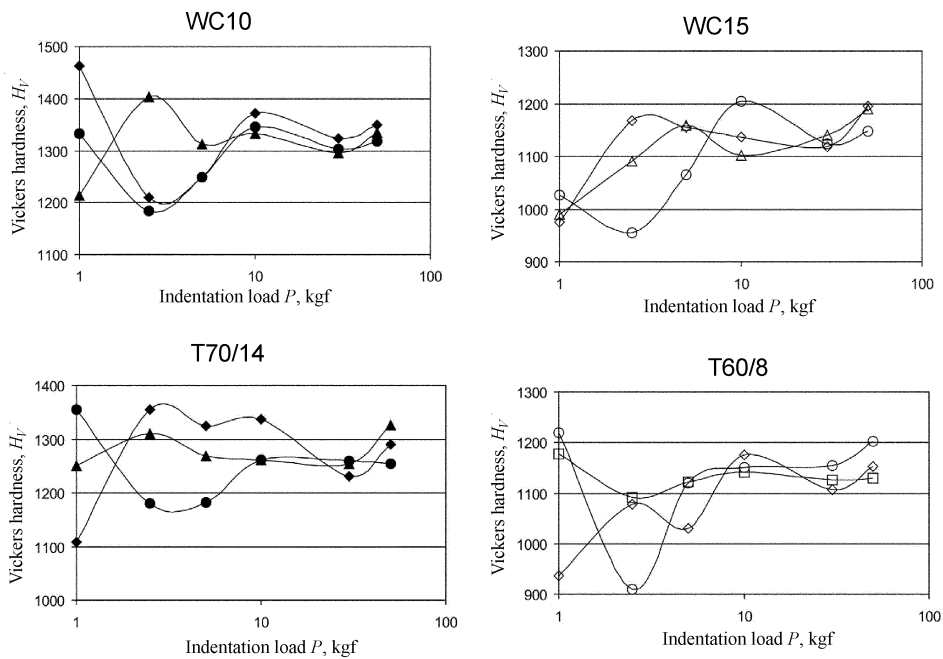


Fig. 4. Dependence of the Vickers hardness on the indentation load for tested cermets.

H_V was used in calculations. Equations for fracture toughness calculation were obtained in three different ways. The first way considers Palmqvist cracks as semi-elliptical cracks or uses the two-dimensional through-crack model (Table 2). The second way considers median cracks, based on the half-penny-shaped-crack model. The third way is based on curve-fitting technique.

Table 2. Equations for calculation of fracture toughness (K_{Ic}) values from Vickers indentation crack systems

Eq. No.	Equation	Ref.
Palmqvist crack system		
1	$K_c = 0.0515 \frac{P}{c^{3/2}}$	[9]
2	$K_c = 0.079 \frac{P}{a^{3/2}} \log\left(4.5 \frac{a}{c}\right)$	[10]
3	$K_c = 0.035 \left(\frac{l}{a}\right)^{-1/2} \left(\frac{H_V}{E\Phi}\right)^{-2/5} \left(\frac{H_V a^{1/2}}{\Phi}\right)$	[11]
4	$K_c = 0.048 \left(\frac{l}{a}\right)^{-1/2} \left(\frac{H_V}{E\Phi}\right)^{-2/5} \left(\frac{H_V a^{1/2}}{\Phi}\right)$	[12]
Median crack system		
5	$K_c = 0.0726 \frac{P}{c^{3/2}}$	[9]
6	$K_c = 0.0752 \frac{P}{c^{3/2}}$	[13]
7	$K_c = 0.129 \left(\frac{c}{a}\right)^{-3/2} \left(\frac{H_V}{E\Phi}\right)^{-2/5} \left(\frac{H_V a^{1/2}}{\Phi}\right)$	[11]
8	$K_c = 0.014 \left(\frac{E}{H_V}\right)^{1/2} \left(\frac{P}{c^{3/2}}\right)$	[14]
9	$K_c = 0.016 \left(\frac{E}{H_V}\right)^{1/2} \left(\frac{P}{c^{3/2}}\right)$	[15]
10	$K_c = 0.0725 \left(\frac{P}{c^{3/2}}\right)$	[16]

Table 2. Continued

Eq. No.	Equation	Ref.
Curve fitting technique		
11	$K_C = 0.055 \log \left(8.4 \frac{a}{c} \right) \left(\frac{H_V}{E\Phi} \right)^{-2/5} \left(\frac{H_V a^{1/2}}{\Phi} \right)$	[17]
12	$K_C = (H_V a^{1/2}) \left(\frac{E}{H_V} \right)^{2/5} 10^y,$ $y = -1.59 - 0.34x - 2.02x^2 + 11.23x^3 - 24.97x^4 + 15.32x^5, \quad x = \log \left(\frac{c}{a} \right)$	[18]
13	$K_C = 0.142 \left(\frac{H_V}{E\Phi} \right)^{-2/5} \left(\frac{H_V a^{1/2}}{\Phi} \right) \left(\frac{c}{a} \right)^{-1.56}$	[19]
14	$K_C = 0.0089 \left(\frac{E}{H_V} \right)^{2/5} \left(\frac{P}{a \cdot c^{1/2}} \right)$	[11]
15	$K_C = 0.0889 \left(\frac{H_V \cdot P}{\sum_{i=1}^4 c_i} \right)^{1/2}$	[20]
16	$K_C = 0.4636 \frac{P}{a^{3/2}} \left(\frac{E}{H_V} \right)^{2/5} 10^F,$ $F = -1.59 - 0.34B - 2.02B^2 + 11.23B^3 - 24.97B^4 + 16.32B^5,$ $B = \log \left(\frac{c}{a} \right)$	[18]
17	$K_C = 0.018 \left(\frac{E}{H_V} \right)^{1/2} \left(\frac{P}{c^{3/2}} \right)$	[21]

Φ is a constant, $\Phi \cong 3$.

Comparison of IFT values for WC10 hardmetal (at loads of 30 and 50 kgf) and for TiC70/14 cermet (at loads from 2.5 to 50 kgf), calculated using Eqs. (1)–(17) are shown in Figs. 5 and 6, respectively. Fracture toughness K_{Ic} varies from 10.247 to 30.394 MPa·m^{1/2} for WC10 and from 5.387 to 31.44 MPa·m^{1/2} for TiC70/14. From these results it is obvious that IFT depends on the indentation load (Figs. 7 and 8).

A comparison of the obtained data with the published one is shown in Table 3. Results of the indentation fracture toughness measurement and calculation for WC15 hardmetal and TiC60/8 cermet are very similar to those of WC10 and TiC70/14 grades. Their behaviour is similar to the investigated materials. Hardmetal WC10 was chosen as a reference material because it is well studied and there is a lot of information available about it.

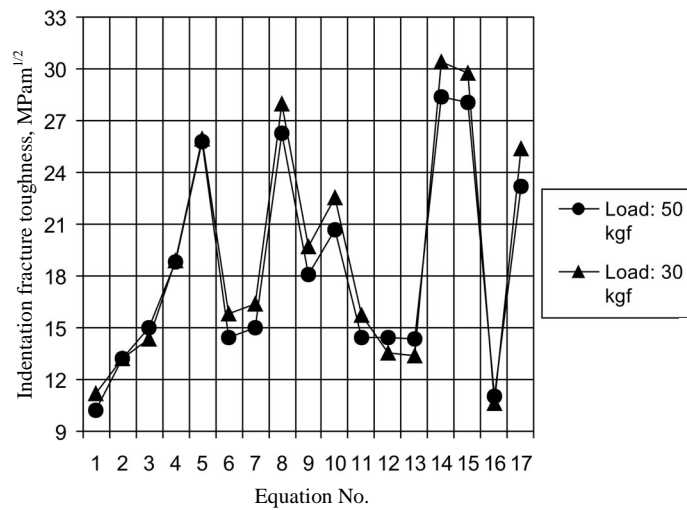


Fig. 5. Comparison of IFT values of the WC10 hardmetal, measured at 30 and 50 kgf and calculated using Eqs. (1)–(17).

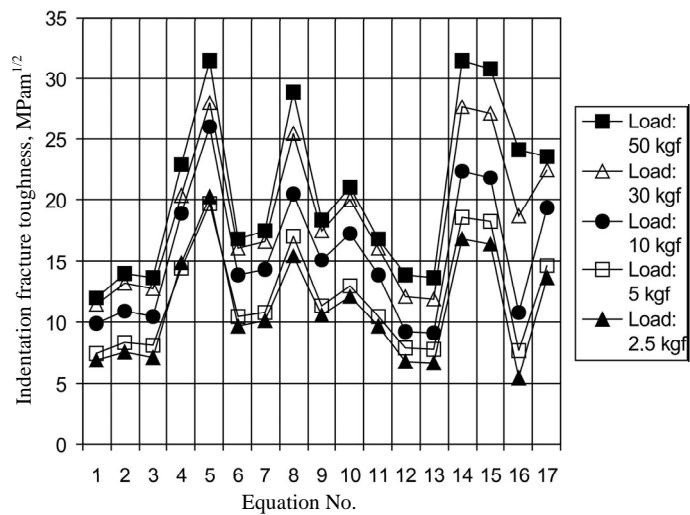


Fig. 6. Comparison of IFT values of the TiC70/14 cermet, measured at 2.5–50 kgf and calculated using Eqs. (1)–(17).

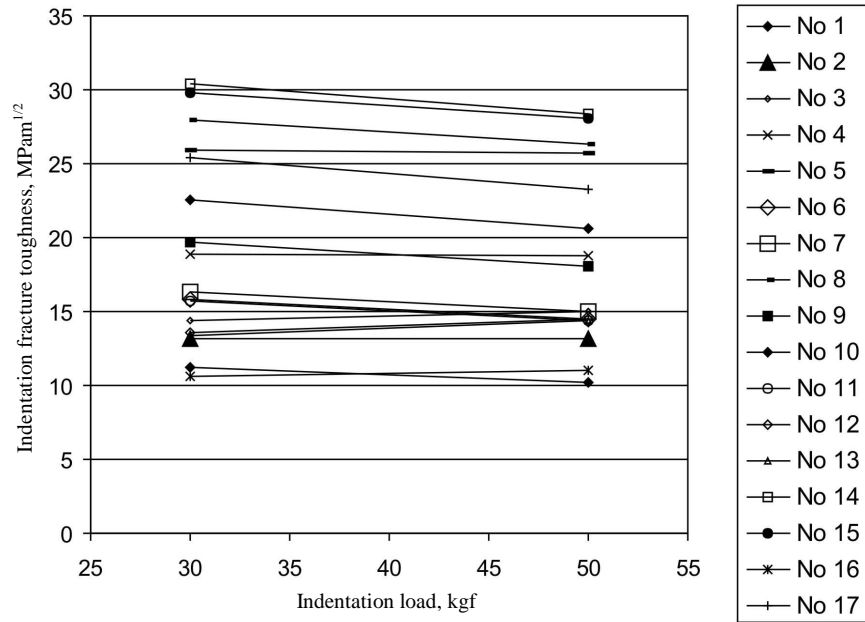


Fig. 7. Dependence of the calculated IFT values on the indentation load for WC10 hardmetal.

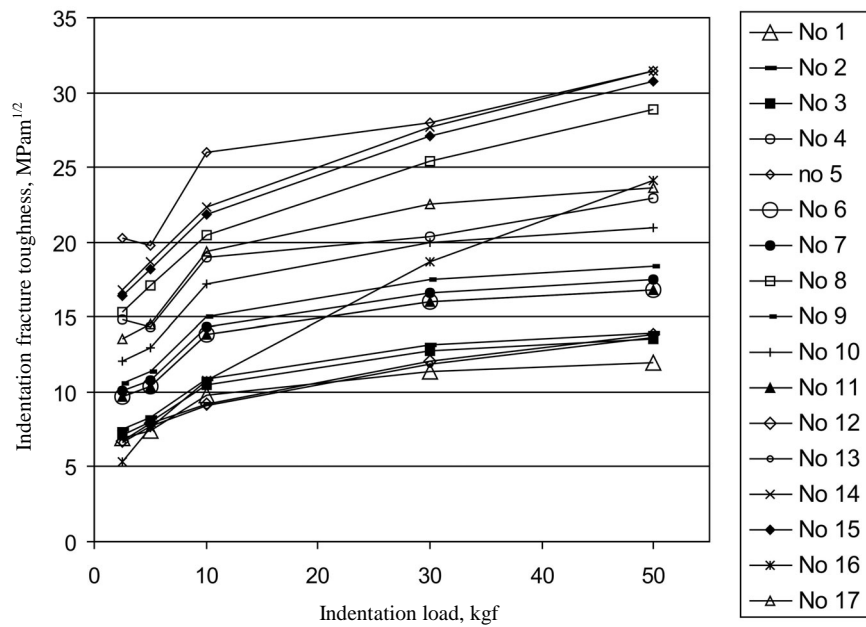


Fig. 8. Dependence of the calculated IFT values on the indentation load for TiC70/14 cermet.

Table 3. Comparison of fracture toughness K_{Ic} (MPa·m^{1/2}) values for WC10

Testing method	Schubert et al. [5]		Rosa et al. [22]		Torres et al. [4]		Scieszka [23]		Current study	
	min	max	min	max	min	max	min	max	min	max
SENB (single edge notched beam)	–	–	–	–	8.6	10.5	–	–	13.4*	14.7*
SEVNB (single edge V-notched beam)	–	–	–	–	15.2	28.3	–	–	–	–
SCF (surface crack in flexure)	–	–	–	–	7.8	11.1	–	–	–	–
CNB (Chevron notched beam)	–	–	–	–	–	–	11.61	13.78	–	–
IFT (indentation fracture toughness)	9.8	14.0	12.3	14.2	10.5	19.5	10.5	16.1	10.3	30.4

Values marked * are estimates. Source: CES 2005 Edupack.

4. CONCLUSIONS

Most of the IFT equations, used in the present work, can be used by elaborating fracture toughness measurement data for WC- and TiC-based cemented carbides, with the exception of “extreme” equations (Eqs. (1), (5), (8), (14), (15), (16) and (17)). The equations, which are in a good agreement with fracture toughness data, received using the conventional testing methods (Chevron notched beam, SEVNB etc.) are: Eqs. (2), (6) and (12) by Evans, Charles and Wilshaw, Eqs. (3), (4) and (7) by Niihara, Eq. (9) by Anstis, Eq. (10) by Tanaka, Eq. (11) by Blendell and Eq. (13) by Lankford. Equation (17) by Japanese Standards Association can be used for TiC-based cermets only. Instrumented indentation testing is a sterling technique for the determination of mechanical characteristics of hardmetals (hardness, elastic modulus, yield stress etc.). TiC-based cermets are promising materials with reference to the fracture toughness compared with WC-based hardmetals; they tend to behave more plastically in spite of higher brittleness of the titanium carbide and increase of K_{Ic} with the rise of the indentation load.

ACKNOWLEDGEMENT

This research was supported by Estonian Science Foundation (grant No. 6163).

REFERENCES

1. Ray, K. K. and Dutta, A. K. Comparative study on indentation fracture toughness evaluations of soda-lime-silica glass. *Brit. Ceram. Trans.*, 1999, **98**, 165–171.
2. Li, Z., Ghosh, A., Kobayashi, A. S. and Bradt, R. C. Indentation fracture toughness of sintered silicon carbide in the Palmqvist crack regime. *J. Am. Ceram. Soc.*, 1989, **72**, 904–911.
3. Vullo, P. and Davis, M. J. Comparative study of micro-indentation and Chevron notch fracture toughness measurements of silicate and phosphate glasses. *J. Non-Crystall. Solids*, 2004, **349**, 180–184.
4. Torres, Y., Casellas, D., Anglada, M. and Llanes, L. Fracture toughness evaluation of hardmetals: influence of testing procedure. *Int. J. Refract. Met. Hard Mater.*, 2001, **19**, 27–34.
5. Schubert, W. D., Neumeister, H., Kinger, G. and Lux, B. Hardness to toughness relationship of fine-grained WC-Co hardmetals. *Int. J. Refract. Met. Hard Mater.*, 1998, **16**, 133–142.
6. Cook, R. F. and Pharr, G. M. Direct observation and analysis of indentation cracking in glasses and ceramics. *J. Am. Ceram. Soc.*, 1990, **73**, 787–817.
7. Smith, S. M. and Scattergood, R. O. Crack-shape effects for indentation fracture toughness measurements. *J. Am. Ceram. Soc.*, 1992, **75**, 305–315.
8. Gong, J., Wang, J. and Guan, Z. Indentation toughness of ceramics: a modified approach. *J. Mater. Sci.*, 2002, **37**, 865–869.
9. Lawn, H. R. and Fuller, E. R. Equilibrium penny-like cracks in indentation fracture. *J. Mater. Sci.*, 1975, **10**, 2016–2024.
10. Evans, A. G. and Wilshaw, T. R. Quasi-static solid particle damage in brittle solids – I. Observations, analysis and implications. *Acta Metall.*, 1976, **24**, 939–956.
11. Niihara, K., Morena, R. and Hasselman, D. P. H. Evaluation of K_{Ic} of brittle solids by the indentation method with low crack-to-indent ratios. *J. Mater. Sci. Lett.*, 1982, **1**, 13–16.
12. Niihara, K. A fracture mechanics analysis of indentation-induced Palmqvist crack in ceramics. *J. Mater. Sci. Lett.*, 1983, **2**, 221–223.
13. Evans, A. G. and Charles, E. A. Fracture toughness determinations by indentation. *J. Am. Ceram. Soc.*, 1976, **59**, 371–372.
14. Lawn, B. R., Evans, A. G. and Marshall, D. B. Elastic/plastic indentation damage in ceramics: the median/radial crack system. *J. Am. Ceram. Soc.*, 1980, **63**, 574–581.
15. Anstis, G. R., Chantikul, P., Lawn, B. R. and Marshall, D. B. A critical evaluation of indentation techniques for measuring fracture toughness – I. Direct crack measurements. *J. Am. Ceram. Soc.*, 1981, **64**, 533–538.
16. Tanaka, K. Elastic/plastic indentation hardness and indentation fracture toughness: the inclusion core model. *J. Mater. Sci.*, 1987, **22**, 1501–1508.
17. Blendell, J. E. *The origins of internal stresses in polycrystalline alumina and their effects on mechanical properties*. PhD Thesis. MTI Press, Cambridge, MA, 1979.
18. Evans, A. G. Fracture toughness: the role of indentation techniques. In *Fracture Mechanics Applied to Brittle Materials* (Freiman, W., ed.). ASTM STP 678, West Conshohocken, PA, 1979, 112–135.
19. Lankford, J. Indentation microfracture in the Palmqvist crack regime: implications for fracture toughness evaluation by the indentation method. *J. Mater. Sci. Lett.*, 1982, **1**, 493–495.
20. Shetty, D. K., Wright, I. G., Mincer, P. N. and Clauer, A. H. Indentation fracture of WC-Co cermets. *J. Mater. Sci.*, 1985, **20**, 1873–1882.
21. Testing method for fracture toughness of high performance ceramics. JIS R-1607, Japanese Standards Association, 1990.
22. Rosa, L. G., Amaral, P. M., Anjinho, C., Fernandes, J. C. and Shohoji, N. Fracture toughness of solar-sintered WC with Co additive. *Ceram. Int.*, 2002, **28**, 345–348.
23. Scieszka, S. F. Wear transition as a means of fracture toughness evaluation of hardmetals. *Tribol. Lett.*, 2001, **11**, 185–194.

Kermiste purunemissitkuse määramise indenteerimismeetodite võrdlev analüüs

Fjodor Sergejev ja Maksim Antonov

Metallmaterjalide purunemissitkuse (K_{Ic}) määramiseks kasutatakse valdavalt nn Chevroni sälguga ja kompaktheid katsekehi, ümarsälguga tõmbeteimikuid jne. Kõik need meetodid on töömahukad katsekehade keeruka geomeetria ja kõrgete täpsusnõuete tõttu pingekontsentraatorile. Karbiidse faasi äärmise hapruse tõttu on ainult mõnda neist meetoditest võimalik kermiste puhul rakendada. Seetõttu on välja töötatud mitmeid indenteerimise purunemissitkuse (IPS) määramise meetodeid [^{1,2}]. IPS seisneb teemantindentori surumises materjali pinda ja tekkinud pragude pikkuse ja geomeetria põhjal materjali K_{Ic} väärtuse määramises. Eeliseks on meetodi lihtsus ja katse teostamise kiirus. Sel meetodil saadud tulemused sõltuvad oluliselt indenteerimise käigus tekkivate pragude eeldatavast tüübist (nn Palmqvisti või mediaan- ja radiaalpraod), arvutustes kasutatud valemite ja veel mitmest tegurist [³]. Artiklis on standardites ning varasemates uurimustes olevaid IPS-arvutusvalemeid kasutatud kermiste WC-Co ja TiC-Fe/Ni purunemissitkuse määramiseks ja saadud tulemusi on võrreldud teiste meetodite abil määratud K_{Ic} väärtustega. On näidatud, et kermiste puhul saadakse vaid mõnede IPS arvutusteks soovitatud valemite abil usaldusväärseid tulemusi.

Paper IV

Sergejev, F., Preis, I., Kūbarsepp, J., Antonov, M.

Correlation between surface fatigue and microstructural defects of cemented carbides. *Wear* (Article in press. Available online 15 june 2007).



Correlation between surface fatigue and microstructural defects of cemented carbides

Fjodor Sergejev*, Irina Preis¹, Jakob Kübarsepp², Maksim Antonov³

Department of Materials Engineering, Tallinn University of Technology, Ehitajate tee 5, 19086 Tallinn, Estonia

Accepted 13 February 2007

Abstract

The main aim of the present theoretical work is to determine numerical dependence between the geometrical parameter of maximum area of structural defect $\sqrt{\text{area}_{\text{max}}}$ (proposed by Y. Murakami, 1983) and surface fatigue of cemented carbides. The proposed relations allow making predictions of surface fatigue properties of cemented carbides (WC-Co hardmetals—with 10 wt% Co and 15 wt% Co binder; TiC-based cermets—with 32 wt% Fe/8 wt% Ni and 16 wt% Fe/14 wt% Ni binder) in conditions of sliding, rolling contact and impact cycling loading.

Pores are considered being equivalent to small defects. Three comparative defects conditions are distinguished: surface pores, pores just below free surface and interior pores. The Vickers hardness of the binder (as mainly responsible for the fracture mechanism of hardmetals and cermets, due to porosity) is presumed to be the basis of such an assumption.

The estimate of this prediction has been done by analyzing the pore sizes using the statistics of extremes. The lower limit of fatigue strength and surface fatigue life can be correctly predicted by estimating the maximum occurring pore size in a critical material volume.

© 2007 Elsevier B.V. All rights reserved.

Keywords: Cermets; Hardmetals; Surface fatigue; Murakami model

1. Introduction

Surface cracks and defects, which are most likely to be found in many structures in service such as pressure vessels, pipeline systems, off-shore structures and aircraft components, have been recognized as a major origin of potential failure for such components. The study of fatigue crack propagation from such defects has been an important subject during recent decades.

Powder metallurgy materials such as hardmetals and cermets are most widely used as tool materials in machining and forming applications. These materials are best known for their excellent strength-wear resistance combination. Wear resistant cemented carbides tend to contain inward and superficial natural structural

defects, pores, non-metallic inclusions or inhomogenities, etc. Their existence is crucial for most mechanical properties and material selection, and unfortunately cannot be totally excluded by current technologies.

Based on the experimental fact that the crack shape of propagating surface cracks in a plate under cyclic tension, bending or combined loading is approximately semi-elliptical, a theoretical model with two degrees of freedom is proposed for prediction of the fatigue crack growth [1,2]. This model permits to conjecture the size and location of the surface and subsurface cracks that occur during cyclic loading.

Present work is based on these assumptions and aimed at linking the geometrical parameter of maximum area of structural defect $\sqrt{\text{area}_{\text{max}}}$ (proposed by Y. Murakami, 1983) [3], and surface fatigue parameters for cemented carbides. Hertzian contact theory and Palmqvist model for indentation surface cracks were applied for numerical evaluation of subsurface crack location (depth) and number of impact cycles to failure (N_f , fatigue life).

The proposed equations are hypothetical and have not been proved experimentally so far, but are based on the previously published studies on steels, ceramic materials and glasses [4–7].

* Corresponding author. Tel.: +372 620 3355; fax: +372 620 3196.

E-mail addresses: fjodor.sergejev@ttu.ee (F. Sergejev), ipreis@ttu.ee (I. Preis), Jakob.Kubarsepp@ttu.ee (J. Kübarsepp), Maksim.Antonov@ttu.ee (M. Antonov).

¹ Tel.: +372 620 33 55; fax: +372 620 31 96.

² Tel.: +372 620 20 07; fax: +372 620 31 96.

³ Tel.: +372 620 33 58; fax: +372 620 31 96.

2. Theoretical backgrounds

Contact between two solid bodies under cyclic stressing and rolling with impacts is described with Hertz theory of fracture mechanics. This method can be used for evaluations of surface residual stress levels in brittle materials like WC-Co and TiC-Fe/Ni also. This gave an idea to combine Hertzian contact approach with the Palmqvist indentation theory. As a result we obtained a computational technique for surface crack geometry evaluation and surface fatigue life prediction for heterogeneous materials, containing hard phases (WC, TiC).

The Murakami approach for microstructure analysis with a proposed geometrical parameter of maximum area of structural defect $\sqrt{\text{area}_{\text{max}}}$ and extreme value statistics were incorporated to make the prediction more precise and correct. This method can be used for prediction of fracture toughness also. No additional fatigue or other tests are required.

2.1. Fracture by Hertzian contact (indentation)

The problems of contact between two non-conforming bodies with circular shape (rolling bearings, gears, wheel-on-rail, etc.) were first solved by Hertz and generally referred to as Hertzian contacts [8]. One of the uses of Hertzian indentation is to determine number and sizes of surface flaws. Here we consider the surface with large number of small cracks then the stress field around contact area (in our case indentation) will encompass a large number of ring cracks, outside the contact path, of radius d , see Fig. 1. Then d can be found as [5]

$$d = \left(\frac{3PR}{4E^*} \right)^{1/3}, \tag{1}$$

where P is the load on the indenter, R the indenter radius and E^* is the equivalent Young's modulus.

As we know ν_1, ν_2 and E_1, E_2 are the Poisson's and Young's moduli for the indenter and substrate, respectively, then E^* can be determine from

$$\frac{1}{E^*} = \frac{1 - \nu_1^2}{E_1} + \frac{1 - \nu_2^2}{E_2}. \tag{2}$$

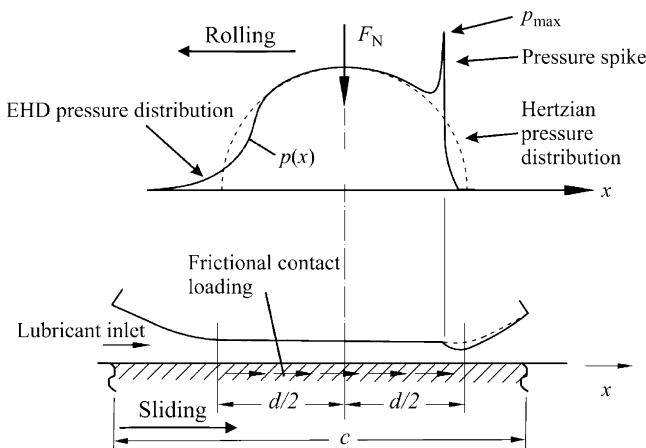


Fig. 1. EHD contact pressure distribution [9,10].

Then the maximum pressure under the contact p_{max} is [5]

$$p_{\text{max}} = \frac{3P}{2\pi d^2} = \left(\frac{3}{2\pi} \right) (P)^{1/3} \left(\frac{4E^*}{3R} \right)^{2/3}. \tag{3}$$

On the other hand, the mean contact pressure p_{mean} during the impact of an indenter in the Hertzian region [8] is equal to

$$p_{\text{mean}} = \frac{F_N}{\pi c^2}, \tag{4}$$

where F_N is the maximum normal force and c is the maximal scar that corresponds to the elastic and plastic deformation ($c = c_{el} + c_{pl}$) [6].

This is the normal condition for mechanical elements (gears, bearings) when the contacting surfaces are separated by a thin lubricant film (Elastohydrodynamic lubrication:EHD or EHL).

2.2. Fatigue life prediction

Fatigue limit was defined by Murakami as the threshold stress for crack propagation and not the critical stress for crack initiation [3].

This leads to the fact that cracks/defects are present in the microstructure of the hardmetals or cermets. Several relationships are available for prediction of the lower bound of scatter of fatigue limit (σ_f) and fracture toughness (K_{Ic}) which are based on the Vickers hardness (H_V) and maximum inclusion area (geometrical parameter of maximum area of structural defect $\sqrt{\text{area}_{\text{max}}}$) and uniform tensile/compressive stress (σ_0) values:

$$\sigma_f = 1.43 \frac{H_V + 120}{(\sqrt{\text{area}})^{1/6}}, \quad \Delta K_{th} = 1.43(H_V + 120)(\sqrt{\text{area}})^{1/3},$$

$$K_{Ic} = 0.5\sigma_0 \sqrt{\pi \sqrt{\text{area}}}. \tag{5}$$

These equations are proposed for surface defects. For other defects, just below surface and interior defect, the coefficient 1.43 must be replaced by 1.41 and 1.56 correspondently [3].

Then for surface defects with previously evaluated Murakami parameter $\sqrt{\text{area}_{\text{max}}}$ (defect size) [3] and fatigue limit lower bound (σ_f) values [11,12]. It is possible to find the total accumulated energy E_i in the material as a function of the number of impact cycles, calculated from

$$E_i = 3\sigma_f \pi R^3 \left[\frac{2}{3} - \left(\frac{c}{R} \right)^2 \sqrt{1 - \left(\frac{c}{R} \right)^2} + \frac{2}{3} \left(1 - \frac{c}{R} \right)^2 \right], \tag{6}$$

The strain energy release rate (G) for the propagation of the crack with given parameters to the controlled dimensions can be found from

$$K_{Ic} = \sqrt{\frac{E \times G}{1 - \nu^2}}. \tag{7}$$

Finally, the surface fatigue life N_{fs} (number of impact cycles to failure) can be predicted by extracting the strain energy release rate G from the total accumulated energy E_i , while the fracture

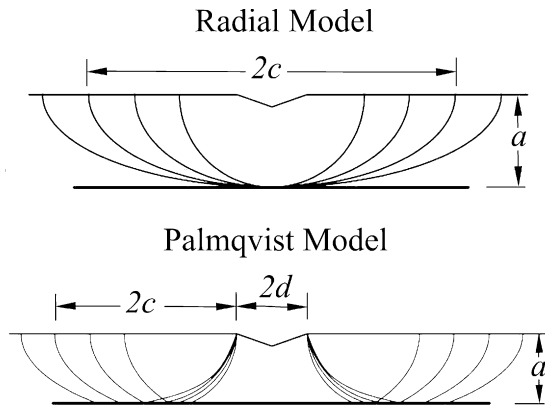


Fig. 2. Geometry for elliptic-crack models [13].

of surface is in the elasto-plastic deformation regime

$$N_{fs} = \frac{E_i}{G} \quad (8)$$

Prediction of number of cycles to failure in the cyclic impact regime gives us the practical knowledge (critical in material selection in conditions of rolling contact and impact cyclic loading) about material surface behavior at prescribed conditions.

2.3. Indentation crack geometry

Fracture toughness analyses for brittle materials generally assume that indentation precracks have the classic half-penny and radial/median geometries. However, there is no compelling evidence that this is universal. Serial sectioning of indentation cracks often reveals a surface-localized, Palmqvist crack geometry [7,13].

Fig. 2 shows a schematic of the radial/median and Palmqvist crack limiting geometries, which were produced by Vickers indentation.

The subsurface lateral cracks are orthogonal to the radial and Palmqvist cracks and can intersect them. Usually two lateral cracks can be observed—primary and secondary (in the case of glasses and ceramics, see Fig. 3) [13].

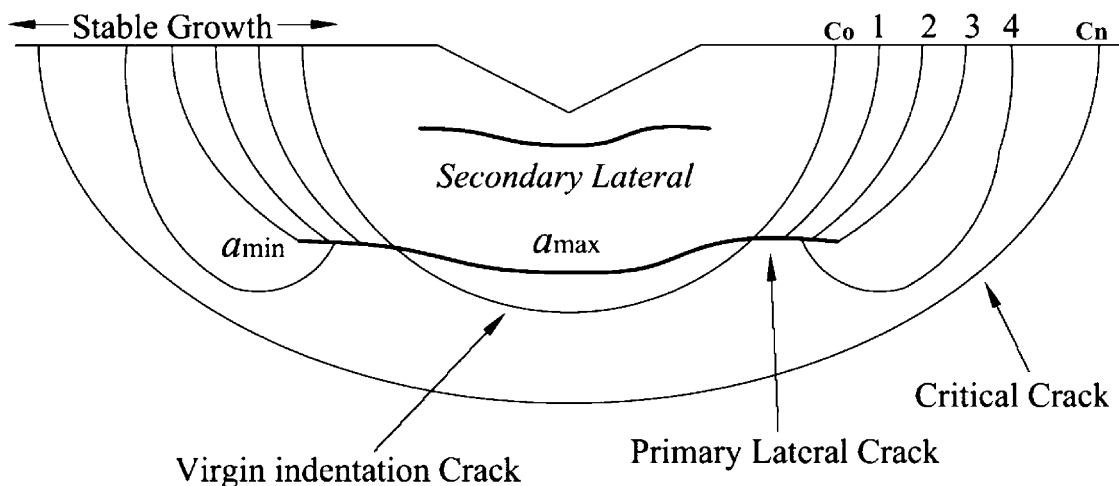


Fig. 3. The schematic representation of the shapes for subsurface indentation cracks for different indentation loads (1, 2, 3, 4, ..., n, are the test number) [13].

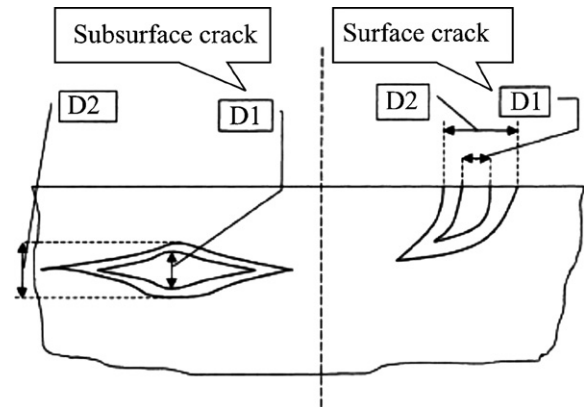


Fig. 4. Schematical drawing showing the evaluation of surface and subsurface crack configuration development with time [7].

Secondary lateral cracks cannot be taken into consideration. The primary lateral cracks are the only ones that can cause critical damage of the surface. Their propagation gives way for surface fatigue debris formation. The mechanism of such failure is schematically shown in Fig. 4. This situation is general for rolling contacts. Crack openings at early (D1) and later (D2) stages of crack propagation are indicated.

The increase of number of fatigue cycles as compared to crack growth depths has shown that indentation cracks not only change their geometries (preserving their elliptical behavior), but also tend to grow into the substrate material, increasing radically [14].

In the further investigation we assume that cracks propagate from surface and subsurface defects, and are elliptical.

3. Results and discussion

Specimens used for application of Murakami approach were produced through conventional press and sinter powder technology, according to ASTM B406. The main structural characteristics and mechanical properties are given in Table 1.

Table 1
Chemical composition and mechanical properties (Vickers hardness H_V , transverse rupture strength R_{TZ} , Young's modulus E , Poisson's ratio ν) of cemented carbides

No.	Grade	Carbide (wt%)	Binder (wt%)	Binder composition structure	H_V (GPa)	R_{TZ} (GPa)	E (GPa)	ν
1	H10	90	10	Co (W)	1.31	2.2	540	0.23
2	H15	85	15	Co (W)	1.13	2.9	600	0.23
3	T70/14	70	30	Fe + 14Ni austenite	1.27	2.4	410	0.23
4	T60/8	60	40	Fe + 8Ni martensite-bainite	1.11	2.3	395	0.22

Table 2
Calculated surface fatigue life results and employed parameters of cemented carbides

No	Grade	Total accumulated energy, E_i (J)	Surface fatigue life, N_{fs} cycles	Maximum pressure p_{max} (N/mm ²)	Mean pressure p_{mean} (N/mm ²)
1	H10	27,093	1.069×10^7	26.79	11.94
2	H15	35,636	1.291×10^7	21.92	12.05
3	T70/14	27,085	7.063×10^6	26.00	11.07
4	T60/8	28,269	8.089×10^6	22.33	10.04

All materials were produced at the Powder Metallurgy Laboratory of Tallinn University of Technology.

3.1. Computation of surface fatigue life

According to the evaluation method described in Section 2.2 and taking into consideration results of the Murakami model application for the same materials for prediction of the lower limit of the fatigue strength it can be proposed that the surface fatigue life of WC-hardmetals and TiC-Fe/Ni cermets can be equated as

$$N_{fs} = \frac{EE_i}{0.25(1 - \nu^2)\sigma_0^2 \sqrt{\pi \sqrt{\text{area}}}} \quad (9)$$

Calculated results for the studied materials are given in Table 2. The radius of indenter R is equal to 10 mm, and indentation load F is 10 N for every material. The surface fatigue life means that at the given loads, with an indenter of given radius, crack propagation up to the maximum size (critical size) for wear debris formation will be achieved after the predicted number of cycles.

The combination of knowledge about surface fatigue crack growth and debris formation will allow prediction of the service life of hardmetals and cermets in conditions of cyclic loading and rolling contact, like in metal forming and blanking applications.

3.2. Surface fatigue crack geometry

The predicted crack profile almost perfectly overlaps with a semi-ellipse crack shape (see Fig. 5), as it was shown by Lin and Smith [1,2,14]. For all four materials we got very similar surface crack depths and geometries ($c = 0.199\text{--}0.212$ mm) for conditions described above.

That is why we assume that the primary lateral crack will be located at almost the same depth, around 0.125–0.128 mm from the contact surface. This prediction cannot be accurate if other subsurface defects are present that are closer to the contact area. In case of “pure” conditions the depth of the crack has to be within the prediction limits.

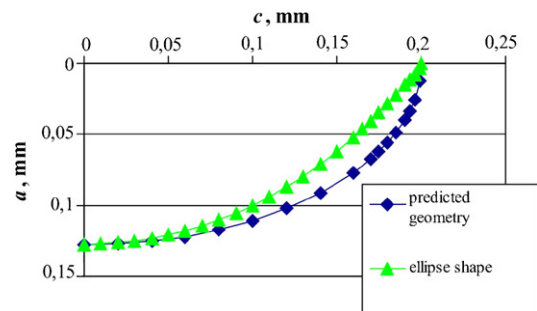


Fig. 5. Comparison of typical semi-ellipse crack with predicted crack shape (H10).

As mentioned above, several lateral cracks can appear under cyclic loading. This condition gives a reason to predict more than two lateral cracks, but in this case the number of cracks will be dependent on the loading force.

4. Conclusions

1. A new numerical technique is developed for the prediction of surface fatigue properties of cemented carbides. The proposed equation for evaluation of the surface fatigue life N_f which correlates with geometrical parameter of maximum area of structural defect $\sqrt{\text{area}}$, is in the agreement with previously reported results.
2. This numerical technique can be used for cemented carbides for prediction of the surface fatigue life and crack geometry.
3. The proposed method does not need additional fatigue tests. Only few mechanical properties and structure parameters must be known.
4. To obtain correct and reliable results: loading force (F), indenter radius (R), mechanical properties (E , ν , H_V), geometry of contacting parts and the size of structural defects (pores) must be taken into consideration.
5. Unfortunately, this method is not yet proved by experiments, but is based on surface fatigue observations and studies of WC-Co, ceramic and glass, described in literature. These materials behave very similar to cermets, as they are very brittle.

Acknowledgments

This work was supported by The Estonian Ministry of Science and Education and The Estonian Science Foundation grant T-505.

References

- [1] X.B. Lin, R.A. Smith, Finite element modeling of fatigue crack growth of surface cracked plates. Part I: The numerical technique, *Eng. Fract. Mech.* 63 (1999) 503–522.
- [2] X.B. Lin, R.A. Smith, Finite element modeling of fatigue crack growth of surface cracked plates. Part II: Crack shape change, *Eng. Fract. Mech.* 63 (1999) 523–540.
- [3] Y. Murakami, *Metal Fatigue: Effects of Small Defects and Non-metallic Inclusions*, Elsevier Science Ltd., Oxford, UK, 2002, p. 380.
- [4] M.-O. Guillou, J.L. Henshall, R.M. Hooper, The measurements of surface contact fatigue and its application to engineering ceramics, *Mater. Sci. Eng. A-Struct. A* 209 (1996) 116–127.
- [5] S.G. Roberts, C.W. Lawrence, Y. Bisrat, P.D. Warren, D.A. Hills, Determination of surface residual stresses in brittle materials by Hertzian indentation: Theory and experiment, *J. Am. Ceram. Soc.* 82 (7) (1999) 1809–1816.
- [6] A.C. Sekkal, C. Langlade, A.B. Vannes, Tribologically transformed structure of titanium alloy (TiAl_6V_4) in surface fatigue induced by repeated impacts, *Mater. Sci. Eng. A-Struct. A* 393 (2005) 140–146.
- [7] M. Terheci, Microscopic investigation on the origin of wear by surface fatigue in dry sliding, *Mater. Charact.* 45 (2000) 1–15.
- [8] K. Holmberg, A. Matthews, *Coatings Tribology: Properties, Techniques and Surface Engineering*, Elsevier Science Ltd, London, UK, 1994, p. 442.
- [9] J. Flašker, G. Fajdiga, S. Glodež, T.K. Hellen, Numerical simulation of surface pitting due to contact loading, *Int. J. Fatigue* 23 (2001) 599–605.
- [10] J. Flašker, G. Fajdiga, S. Glodež, The influence of different parameters on surface pitting of contacting mechanical elements, *Eng. Fract. Mech.* 71 (2004) 747–758.
- [11] F. Sergejev, I. Preis, H. Klaasen, J. Kübarsepp, Murakami approach: fatigue strength prediction of cemented carbides by considering pores to be equivalent to small defects, in: *Proceedings of the European Congress and Exhibition on Powder Metallurgy, EuroPM, Prague, 2005*, pp. 335–340.
- [12] I. Preis, G. Marquis, F. Sergejev, Estimation of the endurance limit of cemented carbides based on pore size, in: *Proceedings of the 9th International Fatigue Congress, Fatigue 2006, Atlanta, 2006*, pp. 1–9.
- [13] M. Stanley, Smith, O. Ronald, Scattergood, Crack-shape effects for indentation fracture toughness measurements, *J. Am. Ceram. Soc.* 75 (2) (1992) 305–315.
- [14] X.B. Lin, R.A. Smith, Finite element modeling of fatigue crack growth of surface cracked plates. Part III: Stress intensity factor and fatigue crack growth life, *Eng. Fract. Mech.* 63 (1999) 541–556.

CURRICULUM VITAE

1. Personal data

Name Fjodor Sergejev
Date and place of birth 25.08.1978, Tallinn, Estonia

2. Contact information

Address 19086 Tallinn, Ehitajate tee 5, Estonia
Phone +372 6203355, +372 55677290
E-mail Fjodor.Sergejev@ttu.ee

3. Education

Educational institution	Graduation year	Education (field of study/degree)
Tallinn University of Technology	2000	Department of Mechanical Engineering/ BSc.
Tallinn University of Technology	2003	Department of Mechanical Engineering/MSc.
Tallinn University of Technology	2007	Department of Mechanical Engineering/PhD.

4. Language competence/skills (fluent, average, basic skills)

Language	Level
Estonian	Fluent
English	Fluent
Russian	Mother tongue
German	Basic skills
Finnish	Basic skills

5. Special courses

Period	Educational or other organisation
27.10.2004	Research in Europe: National and European Funding Possibilities for Graduates and Post-Docs, DoWe
23-24.11.2004	E-education collaboration and quality workshop, Tartu University
06.03-11.05.2006	Online Course Design, Tartu University
20-21.10.2005	Engineering Teachers Course, Federation of Estonian Engineering Industry (EML)
03-11.09.2005	Powder Metallurgy Training Courses, European Powder Metallurgy Association (EPMA)
16.12.2005-16.02.2006	E-course (online) construction, Tallinn University of Technology - Open University

01.12.2005-26.02.2006	Pedagogic and teaching techniques training, Centre of personnel development, Tallinn University of Technology
08.05.2006	Course on self-expression skills, Centre of personnel development, Tallinn University of Technology
11.09-15.12.2006	Business English course, Centre of personnel development, Tallinn University of Technology

6. Professional employment

Period	Organisation	Position
2000-2000	Loksa Shipyard	Engineer-designer
2001-2003	Baltic Ship Repairers	Engineer-technologist
2004-present	Tallinn University of Technology	Teaching assistant

7. Scientific work

Powder metallurgy, fatigue properties of cermets and composites, fracture mechanics, mechanical reliability

8. Defended theses

T. Dantševa, *BSc.* Elaboration of manufacturing process of the reducer closure head, TUT, 2005

O. Aleksandrova, *MSc.* Research on recycling possibilities of plastics of end-of-life vehicles, TUT, 2007

D. Dubov, *BSc.* Offshore containers design and manufacturing, TUT, 2007

9. Main areas of scientific work/Current research topics

T 505, Wear resistant materials and wear. 2003-2007.

ETF 6163, Nanostructural design of advanced materials. 2005-2008.

ETF 5882, Technology of cemented carbides for complicated wear conditions. 2004-2007.

ETF 5878, The technology and properties of nanocrystalline deformable rare metals. 2004-2005.

10. Other research projects

V 313, Euroweld. 2005-2007.

ELULOOKIRJELDUS

1. Isikuandmed

Ees- ja perekonnanimi Fjodor Sergejev
Sünniaeg ja -koht 25.08.1978, Tallinn, Eesti

2. Kontaktandmed

Aadress 19086 Tallinn, Ehitajate tee 5, Eesti
Telefon +372 6203355, +372 55677290
E-posti aadress Fjodor.Sergejev@ttu.ee

3. Hariduskäik

Õppeasutus (nimetus lõpetamise ajal)	Lõpetamise aeg	Haridus (eriala/kraad)
Tallinna Tehnikaülikool	2000	Mehaanikateaduskond/tehnikateaduste bakalaureus
Tallinna Tehnikaülikool	2003	Mehaanikateaduskond/tehnikateaduste magister
Tallinna Tehnikaülikool	2007	Mehaanikateaduskond/filosoofia doktor

4. Keelteoskus (alg-, kesk- või kõrgtase)

Keel	Tase
Eesti	Kõrgtase
Inglise	Kõrgtase
Vene	Emakeel
Saksa	Algtase
Soome	Algtase

5. Täiendusõpe

Õppimise aeg	Täiendusõppe läbiviija nimetus
27.10.2004	Research in Europe: National and European Funding Possibilities for Graduates and PostDocs, DoWe
23-24.11.2004	E-õppe koostöö ja kvaliteet seminar, Tartu Ülikool
06.03-11.05.2006	Veebipõhise kursuse disain, Tartu Ülikool
20-21.10.2005	Masinaehituserialade õppejõudude koolitus, Eesti Masinatööstuse Liit (EML)
03-11.09.2005	Koolituskursus Pulbermetallurgias, European Powder Metallurgy Association (EPMA)

16.12.2005-16.02.2006	E-kursuse loomine, Tallinna Tehnikaülikool, Avatud ülikool
01.12.2005-26.02.2006	Pedagoogika ja õppemetoodika koolitus, Tallinna Tehnikaülikooli Personaliosakond
08.05.2006	Eneseväljendus kunsti kursus, Tallinna Tehnikaülikooli Personaliosakond
11.09-15.12.2006	Inglise ärikeeles kursus, Tallinna Tehnikaülikooli Personaliosakond

6. Teenistuskäik

Töötamise aeg	Tööandja nimetus	Ametikoht
2000-2000	Loksa Laevatehas	Insener-konstruktor
2001-2003	Balti Laevaremonditehas	Insener-tehnoloog
2004-k.a.	Tallinna Tehnikaülikool	Assistent

7. Teadustegevus

Pulbermetallurgia, kermiste ja komposiit materjalide väsimusomadused, purunemismehaanika, tööiga

8. Kaitstud lõputööd

T. Dantševa, *BSc.* Redukti korpuse kaane valmistamise tehnoloogilise protsessi väljatöötamine, TTÜ, 2005

O. Aleksandrova, *MSc.* Romusõidukites sisalduvate plastikute taaskasutuse võimaluste uurimine, TTÜ, 2007

D. Dubov, *BSc.*, Offshore konteinerite projekteerimine ja valmistamine, TTÜ, 2007

9. Teadustöö põhisuunad

T 505, Kulumiskindlad materjalid ja kulumine. 2003-2007.

ETF 6163, Kaasaegsete materjalide nanostruktuuri disain. 2005-2008.

ETF 5882, Komplitseeritud töötingimustes töötavate karbiidkermiste tehnoloogia. 2004-2007.

ETF 5878, Deformeeritavate nanostruktuursete haruldaste metallide tehnoloogia ja omadused. 2004-2005.

10. Teised uurimisprojektid

V 313, Euroweld. 2005-2007.